ΕΘΝΙΚΟ ΜΕΤΣΟΒΙΟ ΠΟΛΥΤΕΧΝΕΙΟ
ΔΙΠΜΣ: ΥΠΟΛΟΓΙΣΤΙΚΗ ΜΗΧΑΝΙΚΗ
ΚΑΤΕΥΘΥΝΣΗ ΜΗΧΑΝΙΚΗ ΤΩΝ ΡΕΥΣΤΩΝ

# Εμβιομηχανική του μηριαίου οστού κονίκλου: Τρισδιάστατη ανακατασκευή του μηριαίου οστού και συγκριτική αξιολόγηση των πειραματικών διατάξεων κάμψεως

Μεταπτυχιακή Εργασία

**Κανάρη Λήδα**

Επιβλέποντες Καθηγητές : Ιωάννης Δαφαλιάς, Σταύρος Κουρκουλής

Αθήνα, Οκτώβρης 2012

ΕΘΝΙΚΟ ΜΕΤΣΟΒΙΟ ΠΟΛΥΤΕΧΝΕΙΟ
ΔΠΜΣ: ΥΠΟΛΟΓΙΣΤΙΚΗΣ ΜΗΧΑΝΙΚΗΣ
ΚΑΤΕΥΘΥΝΣΗ ΜΗΧΑΝΙΚΗ ΤΩΝ ΡΕΥΣΤΩΝ

# Εμβιομηχανική του μηριαίου οστού κονίκλου: Τρισδιάστατη ανακατασκευή του μηριαίου οστού και συγκριτική αξιολόγηση των πειραματικών διατάξεων κάμψεως

Μεταπτυχιάκή Εργασία

**Κανάρη Λήδα**

Επιβλέποντες Καθηγητές : Ιωάννης Δαφαλιάς, Σταύρος Κουρκουλής

Εγκρίθηκε από την τριμελή εξεταστική επιτροπή, την Τρίτη 23 Οκτώβρη 2012

| | | |
|---|---|---|
| ..... | ..... | ..... |
| Ι. Φ. Δαφαλιάς | Σ. Κ. Κουρκουλής | Δ. Ευταξιόπουλος |

Αθήνα, 2012

NATIONAL TECHNICAL UNIVERSITY
OF ATHENS
DPMS: COMPUTATIONAL MECHANICS
FLUID MECHANICS

# Biomechanics of rabbit femur bone: 3D reconstruction of femur bone and comparative evaluation of bending experimental setups

Master thesis

**Kanari Lida**

Supervisors : Ioannis Dafalias, Stavros Kourkoulis

Approved by the three-member examination committee, Tuesday 23 October 2012

| | | |
|---|---|---|
| ..... | ..... | ..... |
| I. F. Dafalias | S. K. Kourkoulis | D. A. Eftaxiopoulos |

Athens, 2012

.....

Κανάρη Λήδα

Διπλωματούχος Εφαρμοσμένων Μαθηματικών και
Φυσικών Επιστημών Ε.Μ.Π.

*Fig. 0.1:* Fetus representation by Leonardo da Vinci

# ΠΕΡΙΛΗΨΗ

Η παρούσα εργασία εξετάζει την αποτελεσματικότητα τόσο καινοτόμων όσο και παραδοσιακών πειραματικών τεχνικών στον τομέα της εμβιομηχανικής των οστών, με την κατασκευή των αντίστοιχων υπολογιστικών μοντέλων. Θα χρησιμοποιηθούν υπολογιστικές μέθοδοι για την σύγκριση και την αξιολόγηση διαφορετικών πειραματικών τεχνικών, που αποσκοπούν στον προσδιορισμό των μηχανικών ιδιοτήτων των οστών, με βασικό στόχο την ανάδειξη των προτερημάτων και των αδυναμιών της εκάστοτε τεχνικής.

Η επιστήμη της εμβιομηχανικής καταλαμβάνει όλο και μεγαλύτερο τμήμα της κλινικής πραγματικότητας με έμφαση στον τομέα της ορθοπεδικής διάγνωσης και της ορθοπεδικής χειρουργικής. Η εισαγωγή νέων τεχνικών συμβάλει στη βελτίωση των διαγνωστικών μεθόδων και των θεραπευτικών αγωγών, έτσι ώστε να περιορίζονται οι μετεγχειρητικές επιπλοκές και η πιθανότητα αποτυχίας της θεραπευτικής μεθόδου. Με την ανάπτυξη αποτελεσματικότερων και δραστικότερων θεραπευτικών τεχνικών ελαχιστοποιείται ο χρόνος παραμονής του ασθενή σε ακινησία αλλά και ο πραγματικός χρόνος ανάρρωσης, με πολλαπλά οφέλη.

Το βασικό πρόβλημα στην παραπάνω ενδιαφέρουσα προσέγγιση, εντοπίζεται στους περιορισμούς της πειραματικής εμβιομηχανικής που καθιστούν όλο και δυσκολότερη την αξιοποίηση και την εφαρμογή των νεότερων μεθόδων στην κλινική πραγματικότητα. Οι περιορισμοί αυτοί αφορούν, αρχικά, στην αδυναμία εντοπισμού κατάλληλων δοκιμίων για την εξαγωγή αξιόπιστων αποτελεσμάτων, που ανταποκρίνονται στην πραγματική κατάσταση και όχι σε ελλιπείς προσεγγίσεις. Το βασικότερο όμως ζήτημα εισάγεται από την αδυναμία εφαρμογής των κυριότερων μεθόδων της εμβιομηχανικής σε ασθενείς, εξαιτίας της καταστροφής των δοκιμίων και της αδυναμίας επαναληψιμότητας των πειραματικών διαδικασιών.

Τις παραπάνω αδυναμίες των πειραματικών μεθόδων της εμβιομηχανικής επιχειρεί να επιλύσει η εισαγωγή υπολογιστικών μοντέλων που αντικαθιστούν την μη αξιοποιήσιμη πειραματική διαδικασία ή καλύπτουν τα κενά που αδυνατεί να πληρώσει η εφαρμογή της στους ασθενείς. Οι υπολογιστικές προσομοιώσεις,

αξιοποιώντας τα δεδομένα της πειραματικής διαδικασίας, οδηγούν στην εξαγωγή σημαντικών συμπερασμάτων για τις μηχανικές ιδιότητες των οστών και την απόκριση τους σε διάφορες καταπονήσεις, που δεν είναι δυνατό να διεξαχθούν πειραματικά.

Η παρούσα εργασία εξετάζει την απόκριση ενός μηριαίου οστού κονίκλου σε διαφορετικά είδη φορτίσεων. Αρχικά, θα χρησιμοποιηθεί η αξονική τομογραφία ως απεικονιστικό μέσο για την εύρεση της ακριβούς γεωμετρίας του οστού. Από τις τομογραφικές εικόνες θα εξαχθεί το τρισδιάστατο μοντέλο της γεωμετρίας του οστού, το οποίο θα συγκριθεί με πειραματικά δεδομένα.

Το επόμενο στάδιο περιλαμβάνει την υποβολή του παραπάνω μοντέλου σε υπολογιστικές διαδικασίες που προσομοιώνουν τα εργαστηριακά πειράματα. Οι βασικές περιπτώσεις που μελετώνται είναι η κάμψη τριών και τεσσάρων σημείων, για την περίπτωση εγκιβωτισμένων και ελεύθερων δοκιμίων. Τα υπολογιστικά αποτελέσματα θα συγκριθούν με τα πειραματικά αποτελέσματα αντίστοιχων δοκιμών και θα αξιοποιηθούν για την αξιολόγιση των παραπάνω μεθόδων. Στόχος της εργασίας είναι η ανάδειξη των προτερημάτων της κάθε μεθόδου ανάλογα με το μηχανικό πρόβλημα. Το επιθυμητό αποτέλεσμα είναι η συμβολή της παρούσας εργασίας στην επιλογή της πειραματικής διαδικασίας που θα ακολουθείται ανάλογα με το υποβαλλόμενο ερώτημα, με σκοπό την βέλτιστη αξιοποίηση των πειραματικών πόρων για την εξαγωγή όσο το δυνατόν πιο αξιόπιστων αποτελεσμάτων.

**Λέξεις Κλειδιά :** μηριαίο οστό, εμβιομηχανική κονίκλων, κάμψη τριών σημείων, κάμψη τεσσάρων σημείων, εγκιβωτισμός

# ABSTRACT

The current thesis studies the effectiveness of innovative but also traditional experimental techniques in the field of bone biomechanics, through the construction of computational models. Computational methods will be used for the comparison and the evaluation of different experimental methods, which are used for the determination of bone mechanical properties, in order to illustrate the benefits and the difficulties of each method.

The science of biomechanics is becoming more and more part of the clinical practice, especially in the field of orthopaedics. The introduction of modern techniques, contributes to the improvement of the diagnostic methods as well as of the therapeutic procedure, in order to eliminate the postoperative complications and the possibility of a failure of the clinical treatment. The development of more effective and radical treatment techniques leads to the decrease of the recovery time, when the patience should stay immobilized, with multiple benefits.

However, the major problem of the above convenient approach, is the imposed restrictions of experimental biomechanical techniques, which render the application of those techniques in clinical practice unattainable. Those restrictions concern, first of all, the weakness of utilizing the appropriate specimen, for example human bones, in order to export results corresponding to reality rather than to insufficient approaches. The major problem of experimental methods is introduced by the inability of their direct application in patients during the clinical procedure, due to the destruction of experimental specimen and the lack of reproducibility of the procedure.

The computational methods attempt to solve the above weaknesses of the experimental biomechanical methods, by substituting the parts of the procedure, which cannot be transferred in the clinical practice. The computational simulations use the information of the experimental data, in order to extract important results concerning the bone's mechanical properties and their response to certain loadings. Those results would require the application of biomechanical techniques in patients in order to be collected experimentally.

In the current thesis, a femur rabbit bone is tested under different loading procedures. The first step of the procedure, contains the use of computed tomography in order to receive accurate data for the bone geometry. Those information will be used for the construction of the three dimensional model of the femur bone. The computational model will be compared with experimental data for the confirmation of its accuracy.

In the next step, the created model will be subjected in computational tests that simulate the experimental procedure. The study contains three and four point bending tests applied in both free and embedded bone specimen. The computational results will be compared with respective experimental results and will be used for the evaluation of each experimental technique. The purpose of the study is to illustrate the advantages of each test in different cases, in order to contribute to the optimization of the experimental techniques for the optimum use of the resources.

**Key Words :** rabbit biomechanics, femur bone, three point bending, four point bending

Ολοκληρώνοντας αυτή τη μεταπτυχιακή εργασία νοιώθω την ανάγκη να ευχαριστήσω όλους όσους με στήριξαν κατά τη διεξαγωγή της και συνέβαλαν με κάθε μέσο στην ολοκλήρωσή της. Θα ήθελα να ευχαριστήσω τους γονείς μου την εμπιστοσύνη που μου έδειξαν όλα αυτά τα χρόνια και για την αμέριστη υποστήριξη τους.

Θα ήθελα αρχικά να ευχαριστήσω τον καθηγητή Ι. Δαφαλιά για την ανάθεση της διπλωματικής εργασίας και την επίβλεψή της. Θα ήθελα επίσης να ευχαριστήσω τον αναπληρωτή καθηγητή Σ. Κουρκουλή για την επιλογή του θέματος, την ενθάρυνσή του καθ΄ όλη τη διάρκεια της διεξαγωγής της μεταπτυχιακής εργασίας καθώς και για τις γνώσεις που μου έδωσε την ευκαιρία να αποκτήσω κατά τη διάρκεια της συνεργασίας μας. Θα ήθελα να ευχαριστήσω τον κ. Βαγγέλη Μαγνήσαλη και την εταιρία εμβιομηχανικής BIOXEHAGON , για την παροχή κάθε δυνατής υποστήριξης για την διεξαγωγή της παρούσας εργασίας, τόσο για την πρόσβαση στα πειραματικά δεδομένα και τις χρησιμοποιούμενες πειραματικές διατάξεις, όσο και για το προγραμματιστικό περιβάλλον το οποίο μου δόθηκε η ευκαιρία να αξιοποιήσω στα πλαίσια της παρούσας εργασίας.

Είναι επίσης, πολύ σημαντικό για μένα να ευχαριστήσω τον διδακτορικό φοιτητή Παναγιώτη Χατζηστέργο για την πολύτιμη συμβολή του για την διεξαγωγή και την ολοκλήρωση της παρούσας εργασίας. Χωρίς τις πολύτιμες γνώσεις του και την πληθώρα των ωρών που αφιέρωσε δεν θα καθίστατο δυνατή η ολοκλήρωσή της. Τέλος, ένα μεγάλο ευχαριστώ στον Ζήση Ελευθέριο για την αμέριστη υποστήριξη του και τις ιδέες του που είχα συχνά την ευκαιρία να αξιοποιήσω.

This project is being carried out in the context of the postgraduate course (MSc), and is co-sponsored by the European Programme "Education and Lifelong Learning", the European Social Fund (ESF) and national funds (NSRF 2007-2013) through the operational programme "Postgraduate scholarships to students by the Greek State Scholarships Foundation (IKY) for the academic year 2011-2012".

# CONTENTS

# LIST OF FIGURES

# 1. BACKGROUND

## *1.1 Medical background*

### *1.1.1 Biomechanics*

Biomechanical engineering is the science that studies the structure and functioning of biological systems by means of the methods of mechanical sciences. Biomechanics applies mechanical methods, traditionally used in engineering, in medicine, in order to explain the mechanical and physical procedures, which occur in biological systems. The biomechanical studies are important for the deeper comprehension of the microstructure and functioning of each part of a body, as well as the intercommunication of those parts. Those results are useful for the interpretation of the dysfunction of the body that causes certain diseases and could lead to possible treatments. Therefore, the results of the biomechanical studies are used in the rehabilitation of the functionality of the human body, either by supporting the structural members in need, or by replacing the dysfunctional members with mechanical ones.

The term 'Biomechanics' dates back to the seventies, although the actual first practice of the science dates a lot of centuries earlier, at the age of Aristotle. In his books 'On the motion of Animals' and 'On the parts of Animals' he describes the physiology and the properties of the motion of animal's parts. However, the first biomechanics is considered to be Leonardo da Vinci, who was the first to study the anatomy of the human body from the perspective of the mechanical engineering. He formulated theorems describing the mechanical properties of the different parts of the human body and the mechanical motion of each separated part, establishing a complete theory for the human motion. He is therefore considered to be the first scientist which has approached the medicine through the mechanical perspective.

Contemporary biomechanics studies a variety of medical subjects through the perspective of engineering. The broad range of biomechanical applica-

tions contains the microstructure of the biological systems, such as the mechanical functioning of cells, as well as the macrostructure of the internal organs and the skeletal system. Important progress has been achieved in the domain of soft tissues studies and in the domain of orthopedics. Biomechanics plays an important role in the study of the mechanical properties of the bones and has made a significant contribution in clinical practice of orthopedics.

The contribution of the modern biomechanical techniques could be illustrated from the high progress in the domain of rehabilitation of limb mobility as well as the invention of new techniques of spine fusion and bone support which have been introduced in medicine the last years. As a result, the domain of biomechanics, which is concentrated in the study of bones, plays a leading role in modern research. The skeletal system itself plays an important role in the conservation of the normal functioning of the whole body and its study is of major importance.

### *1.1.2 Bone structure*

The current study is concentrated in the biomechanical study of the bone tissue -or osseus tissue-. In particular, a New Zealand White rabbit's femur osseus tissue is studied. The New Zealand White is a large rabbit with an average weight of $4 - 5\ kg$ and have a substantial build: the New Zealand White rabbit's body is broad with rounded haunches and short, powerful legs. The rabbit's skeleton has similar mechanical properties to the human skeleton, although it is subjected to different loading environment. The biomechanical study concentrates to the mechanical study of the bones, examining their mechanical properties and their response to different loading tests.

The importance of the study of the osseous tissue is illustrated by the multifunctional role of the skeleton system in the mammal body. The bone, the main structural support of the mammal body, has a leading role in various aspects of the mammal's life. The skeleton supports the softer tissues and provides the points of attachment for most muscles. The attachment of the skeletal muscles to the bones assists the movement of the body, through the procedure of muscle contraction. The skeletal system also provides mechanical protection for the vulnerable internal organs of the body, preserving the integrity of the body. Another important role of the skeletal system is the storage of several minerals such as Calcium and Phosphorous in the bone

tissues, which are released in the blood, when needed, in order to maintain the balance of minerals. The production of blood cells is also attributed in the skeletal system, since blood cells are produced in the red bone marrow. Finally, the bones of the mammal body consist an important chemical energy deposit, through the formation of the yellow bone marrow.

The bone is, in biological terms, a connective tissue, which is characterized by high hardness. In mechanical terms, the bone tissue is considered as a complex material, with separated solid and liquid phases. It contains polymer chains of collagen enriched with an inorganic phase of mineral components. The hardness of the bone is attributed to the extracellular template of collagen, which is enriched by the inorganic mineral phase forming hydroxyapatite crystals $(Ca)_{10}(PO_4)_6\ (OH)_2$.

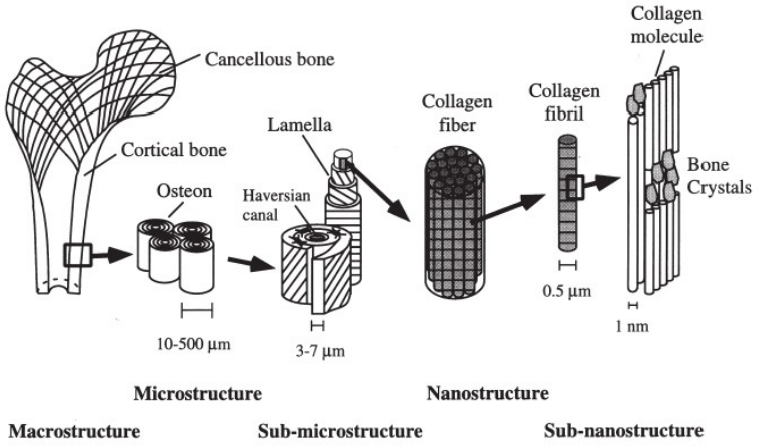


*Fig. 1.1:* Structure of the bone: Formation of osteons

The bone's structure is highly complicated and can be separated in hierarchical levels of organization, according to the different length scale, in which various bone entities occur. As mentioned above, the main structural components of the bone are polymer chains, water and mineral components. The first form collagen fibrils of type I, mineralized by the carbonate apatite crystals formed by the later ones. Those components of the bones are organized into layers. At the nanostructural level, these fibrils gather into bundles commonly referred to as fibril arrays. The typical length of the fibril arrays varies from 100 $nm$ to $1\mu m$. Those arrays are typically organized in an anisotropic way, forming bunches of parallel fibrils called collagen fibers.

As a result, the bone acquire unique directional structural and mechanical properties.

At the submicrostructural level, discrete layers of parallel fibers are formed, commonly known as lamellae. Their thickness is approximately a couple of micrometers $(4 - 7\mu m)$. Alongside the bone, lamellae orientation alternates, causing the different directional mechanical properties described. Since the individual collagen is characterized as isotropic, the anisotropy is attributed to the mineral components of the system, as well as the parallel orientation of the collagen fibrils of the precedent level.

At the microstructural scale, layers of lamellae surround a central hole, named Haversian canal, forming the osteon. A typical osteon is several millimeters long and around $0.1 - 0.2mm$ in diameter. The Haversian canals surround the blood vessels and the nerve cells of the bone. The unique feature of lamellae sheets to slide between each other, which causes an elongation of the osteon, when longitudinal loads are applied, provides greater resilience alongside the osteons. The cement line defines the boundary of the osteon. The space between adjoining osteons is occupied by interstitial lamellae. Near the external surface of the compact bone, lamellae are directed parallel to the surface, constituting the circumferential lamellae. A system of connection between the osteons is established, known as Volkmann's canals. Through the Volkmann's canals, osteons exchange blood supplies between each other and with the outer surface of the bone, the periosteum.

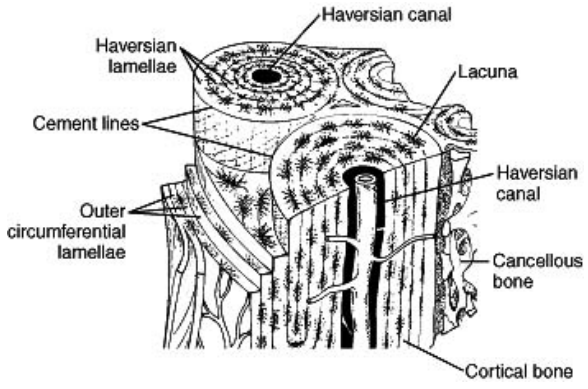


*Fig. 1.2:* Microstructure of the bone: Typical osteon

The Haversian canals communicate with osteocytes, in lacunae, through canaliculi, a network that facilitates the exchange of nutrients and metabolic

waste. Osteocytes are involved in the routine turnover of bony matrix and are responsible for the bone deconstruction through a mechanism called osteocytic osteolysis. Respectively, osteoblasts, often developed into osteocytes, are responsible for bone formation. They produce the collagen matrix and mineralize it. The system of osteoblasts and osteocytes constantly reshape the bone, rendering the bone a dynamic tissue.

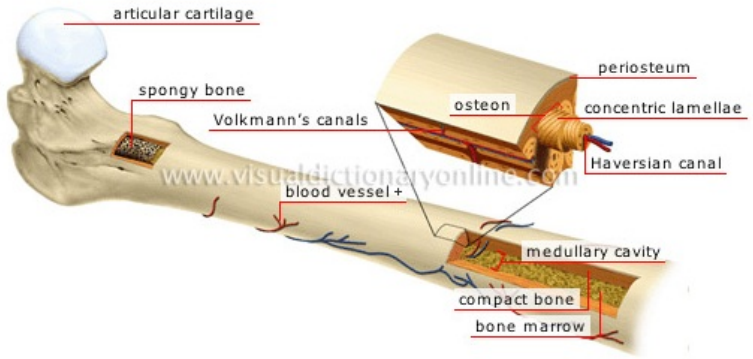


*Fig. 1.3:* Microstructure of the bone

At the macrostructural level, two distinct types of osseus tissue can be defined: the cortical bone, also known as compact bone, and the cancelous bone, also known as trabecular bone. The main difference between those osseous tissue types is the differences in porosity and in density. The cancelous tissue is characterized by much higher porosity and lower density, forming large vacuum cavities in the lattice, at the interior region of the bone, which wipe out at external cross-sections of the bone, where the cortical tissue starts to form. Cortical bone forms the cortex, the outer shell, of most bones, contributing about 80% of the skeleton's weight. The primary anatomical and functional unit of cortical bone is the osteon.

The cancelous bone typically occurs at the ends of long bones, proximal to joints and within the interior of vertebrae. It contains the majority of bone blood vessels, forming the red bone marrow, where the blood cell's production, hematopoiesis, occurs. The bone tissue is formed by tiny lattice-shaped spicules, which renders the cancelous bone to weight much lesser than the cortical bone. The primary anatomical and functional unit of cancelous bone is the trabecula. A trabecula is a small microscopic tissue element

composed of dense collagenous tissue. Trabecula has a similar shape of a septum, but in three dimensions it is usually roughly rod or pillar shaped.

According to the described features, the cancelous bone occupy higher surface area, but is less dense than the cortical bone. As a consequence, the main metabolic activities of the bone occurs in the cancelous region. On the other hand, the cortical bone is much denser, harder, stronger and stiffer. As a result, the mechanical properties of the bone are defined by the cortical bone. The load carrying capacity of the bone is determined by the mechanical properties of the cortical bone, since the yield strength and the ultimate strength of the cortical bone is higher than of the cancelous bone. The elasticity modulus of the cancelous bone is significantly less than that of the cortical bone. This observation illustrates the ability of the cancelous bone to deposit higher amounts of energy than the cortical. The application of the same force causes a higher displacement in the case of the cancelous bone, due to its ability of higher deformation.

The macroscopic fracture of the bone frequently occurs due to the mechanical failure of the cortex, as the cortical bone cannot deposit the amounts of energy that can be stored in the cancelous bone. However, small fractures which occur more often in the cancelous bone, do not affect the global functioning of the bone, owing to the high self-repairing ability of the cancelous bone due to its high metabolic ability. However, those fractures are commonly the major cause of degenerative diseases, such as osteoporosis, in greater ages, when the self-repairing ability is no longer so strong. Small fractures in the cancelous bone violate the mechanical balance of the bone and could produce secondary fractures. If those fractures cause a discontinuity in the cortical bone, they could lead in an observable fracture in the region of the bone.

Three main regions can be identified alongside the long bones of mammals, with different geometric features: the epiphysis, the metaphysis and the diaphysis. Epiphysis is separated in distal and proximal epiphysis and contains the terminal parts of the bone. The outer shell of the bone, at the terminal parts, consists of cortical bone and the internal region consists of cancelous bone. Diaphysis is the longest part of the bone, between the two regions of epiphysis. Diaphysis contains compact tissues in the outer rings of the cross-section and encloses the medullary cavity in the center. Metaphysis is the small part of the bone between the epiphysis edges and

the diaphysis. The interior of metaphysis contains a percentage of cancelous bone that reduces closer to the diaphysis, to create the medullary cavity. A clearer structure of a long bone is illustrated by the next figure:

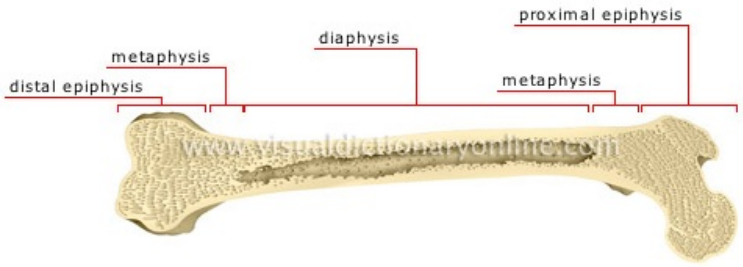


*Fig. 1.4:* Macrostructure of the bone: Epiphysis, Metaphysis, Diaphysis

The current study concentrates on the mechanical properties of a left New Zealand White rabbit femur bone. The femur is the longest and strongest bone in the skeleton. Its cross- section does not diverge significantly from a cylinder in the greatest part of its extend and as a result, it is convenient for mechanical studies. The femur bone consists of the body and of two extremities.

The upper extremity of the femur consists of a head, a neck, a greater and a lesser trochanter. At the upper extremity (proximal extremity), the head articulates with the acetabulum, the cup shaped socket of the pelvis. The head is globular and is directed upward, medialward, and a little forward, the greater part of its convexity being above and in front. Its surface is smooth, coated with cartilage in the fresh state, except over an ovoid depression, the fovea capitis femoris,that gives attachment to the ligamentum teres. The neck is a flattened pyramidal process of bone, connecting the head with the body, and forming with the latter a wide angle opening medialward. The trochanters have an important role in muscle's functioning, as they afford leverage to the muscles that rotate the thigh on its axis. The Greater Trochanter is a large, irregular, quadrilateral eminence, situated at the intersection of the neck with the upper part of the body. It is directed a little lateralward and backward, and, is approximately about $1cm$ lower than the head. The Lesser Trochanter is a conical eminence, which varies in size in different subjects and projects from the lower and back part of the base of the neck. A prominence, occurs at the intersection of the upper part

of the neck with the greater trochanter, known as the tubercle of the femur. It is the point of meeting of five muscles: the Glutus minimus, the Vastus lateralis, the tendon of the Obturator internus and two Gemelli.

The lower extremity, is wider than the upper and consists of two oblong eminences known as condyles. The lower extremity (distal extremity) articulates with the patella and the tibia. Its shape is cuboid and its transverse diameter is greater than its antero-posterior. In the front surface, the condyles are slightly prominent, and are separated from one another by a smooth shallow articular depression called the patellar surface. At the back surface, they project considerably, and the interval between them forms a deep notch, known as the intercondyloid fossa.

The Body or Shaft (corpus femoris)is almost cylindrical in form, a little broader above than in the center and broadest and flattened from before backward below. It is slightly arched, so as to be convex in front, and concave behind, where it is strengthened by a prominent longitudinal ridge, the linea aspera. The linea aspera is a prominent longitudinal ridge, on the middle of the bone, presenting a medial and a lateral lip, and a narrow rough, intermediate line.

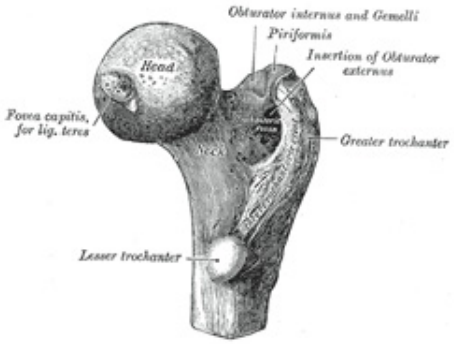


*Fig. 1.5:* Upper extremity

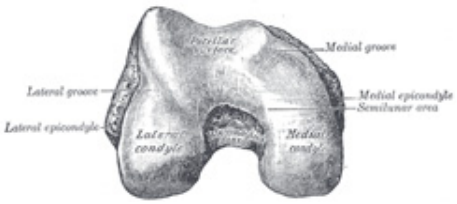


*Fig. 1.6:* Lower extremity

The bone tissue development is proportional to the external loading, according to the Wolff theorem. For instance, in cases of long term immobilization, the bones became less dense and lose part of their bone mass. As a result, bones of long term immobilized patients become unable to carry higher loadings. Koch, through a mathematical approach, has shown that "in every part of the femur there is a remarkable adaptation of the inner

structure of the bone to the mechanical requirements due to the load on the femur-head." The different parts of the femur form a mechanical structure which optimizes the transmission of the loads from the acetabulum to the tibia, with the most efficient and economical way. Every element is properly distributed in the internal structure of the femur, so that it contributes its modicum of strength, which occurs due to the load of the femur head, in a way of maximum efficiency. From the microscopic point of view, the bony material is arranged in paths where the maximum internal stresses are developed, achieving optimum use of the material. The above observations lead to the conclusion that the structure of the bone is formed in order to optimally carry the preponderant load of the body's weigh transmitted to the femur head through the acetabulum. The femur appears to obey the theoretical mechanical laws imposed in mechanical constructions in order to achieve maximum economy and efficiency. Those laws could be summarized as follows:

- The mechanical conditions at every point of the bone define the inner structure and the external form of the bone.
- The inner architecture of the bone is determined by mathematical and mechanical requirements, in order to produce maximum strength with the minimum material.

An example of this typical behavior of the bone structure could be given through the the description of the inner structure of the femur. The trabeculae of the upper femur are arranged in two general systems, a compressive and a tensile system, in correspondence with the potential lines of maximum and minimum stresses in the femur. Their thickness and the spacing between them varies according to the distribution of maximum stresses, in order to achieve the greatest strength with the minimal material in regions where maximum stresses occur.

The amount of bony material in the cancelous bone, varies according to the intensity of the shearing forces developed. Shear stress presents a minimum near the neutral plane and is most efficiently resisted by material placed closer to the neutral axis. Since, alongside the shaft, the neutral plane passes through the central cross-section, the material in the central space is minimized. This arrangement is also efficient for optimally resisting bending stresses, since in order to resist bending moment stresses most effectively

the material should be as far from the neutral axis as possible. The inner architecture of the shaft is also adapted to resist in the most efficient way the combined action of minimal shearing forces and the axial and maximum bending stresses occurred.

The important role of the skeleton as well as its weakness for rapid self-healing in numerous pathological situations, a feature that leads to frequent fractures, render the need for the improvement of biomechanical treatments increasingly important. The mechanical tests applied in bone specimens, extract important information on the effectiveness of the medication, of the surgery procedure or the mechanical support used during a treatment. In various cases, such as osteoporosis, simple mechanical tests can evaluate the effectiveness of the treatment, by the identification of the bone's mechanical properties, before and after the clinical procedure. Mechanical tests even during the treatment provide information of its effectiveness and are used for the medical surveillance of the patience.

However, the limitations of mechanical tests in clinical applications has led to the necessity of the development of alternative techniques in order to extract the necessary mechanical information. The development of new imaging techniques, which reconstruct the internal structure of the body, without the need of surgical operations, has contributed the most to the development of non-invasive clinical techniques with various applications. Therefore, the utilization of non-invasive imaging techniques in combination with the construction of computational models suggest new methods for the determination of the mechanical properties of bones.

### *1.1.3 CT imaging*

Computed Tomography, also known as Computed Axial Tomography is a non invasive technique for image reconstruction, typically used for medical reasons. As illustrated by the term 'Tomography', the CT scanner reproduces images through different slices of the biological tissue in test. The basic operating principle of CT imaging is the ability of biological tissues to absorb X-ray photons, according to their density. The CT scanner generates an X-ray beam, which passes through a selected cross-section of the biological tissue. A proportion of the beam's photons is absorbed by the tissue, depending on the path length traveled within it. The remaining photons, which are detected by the CT scanner, demonstrate the density of the material. As

a result, the generated images compose a two dimensional reconstruction of the linear attenuation coefficient of X-rays, in each slice of the tissue.

A photon beam traveling through a material with constant density attenuates according to the exponential law:

$$I = I_0 * \exp(-\mu\Delta\chi) \tag{1.1}$$

Where $I$ is the remainder beam's intensity, $I_0$ is the initial intensity, $\mu$ is the linear X-ray attenuation coefficient and $\Delta\chi$ is the path length covered within the material.

Respectively, in the case of complex materials of different thickness, the attenuation is defined by the sum of the independent attenuation coefficients as follows:

$$I = I_0 * \exp[-(\mu_1 * \Delta\chi_1 + \mu_2 * \Delta\chi_2 + \mu_3 * \Delta\chi_3 + \dots)] \tag{1.2}$$

In the CT imaging, the intensity of the initial beam and of the final beam are defined. By using the above formula, the density and the length of each material are determined, during the image reconstruction procedure. The intensity of the initial beam is selected by the CT scan operator, according to the biological tissue that is required to be visualized. The intensity of the final beam is detected by the detecting system of the CT scanner. As a result, the image of each slice is created according to the collected information and corresponds to the absorption of the photons through each cross-section.

The different CT technologies depend on the arrangement of components (the source and the detector of the X-rays) and the mechanical motion required to collect the data. They are divided into five generations. The term generation has been applied because of the order in which the CT scanner designs have been introduced.

The CT scanner of the first generation consists of a single X-ray source and a single X-ray detector situated in a diametrically opposite position. The system of the source and the detector, which are rigidly coupled, first is translated across the patient to obtain a set of parallel projection measurements at one angle. Then it is rotated around the patient in order to cover the different angles of each slice. The translation and rotation motions are repeated until the scan covers 180° degrees.

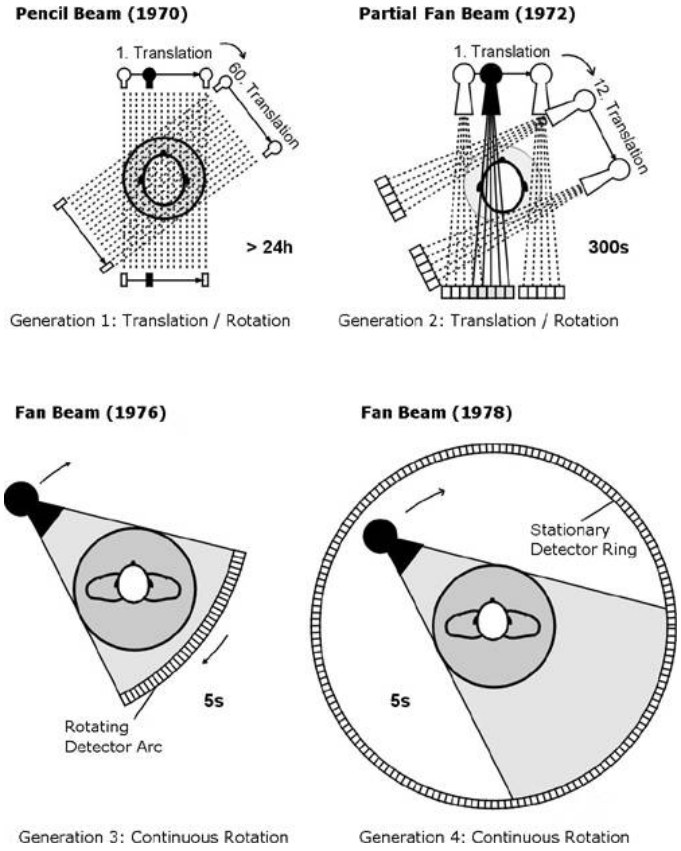


*Fig. 1.7:* CT generations

In order to reduce the time of the examination as well as the time of the exposure of the patient in radiation, the source of the X-rays beam of the second generation scanner becomes divergent. Multiple detectors are distributed within the scan plane improving the efficiency of measuring projections. The system of the source and the detectors performs a translational and rotational movement, respectively to the first generation's scanner, but each translation step generates multiple parallel projections, reducing significantly the duration of the procedure.

In the third generation CT, the divergence of the beam allows to avoid the translational movement. A detector array is designed with enough, high spatial resolution cells to allow the simultaneous measurement of a fan-beam projection of the entire patient cross-section. The assembly does not longer needs to be translated past the patient and only rotates around him. The

imaging process is significantly faster than the previous generations. However, very high performance detectors are needed in order to avoid ring artifacts.

The innovation introduced in the fourth generation in order to reduce the sensitivity in ring artifacts, is the design of a stationary detecting system and a rotating X-ray source. The detectors are distributed in the whole circular area, covering all the angles, consisting a ring detector, placed outside the circular path of the X-ray source. The data of each slice are collected, after the activation of the detecting system by the rotating beam of the X-rays. The ring artifacts are eliminated by the automated calibration of the detecting system during the examination. However, the detector is more sensitive to scattered radiation since a larger acceptance angle for radiation is required. Fourth generation geometries also require a larger number of detector cells to achieve the same spatial resolution and dose efficiency.

Fifth generation CT scanner has no mechanical scanning motion and consists of a high energy beam of electrons which is moved around the circular path of the previous generation and is led in a semicircular tungsten anode, producing the X-rays beam. The detectors remain distributed along the ring area, as in fourth generation. The only moving part of the scan is the beam of electrons that produces the X-rays, but the side effects of the moving parts are almost completely eliminated from the image reconstruction. The fifth generation scans are significantly rapid, reducing the time of a slice scan in $50msec$.

A typical CT scanner comprises several components.These basically include:

- The scanning unit, containing the gantry, the tube and the detector system
- The patient table
- The image processor
- The console

The console is the computational system which contains the control unit for the examination procedure. The examination parameters are controlled by an operator that handles the console. The console is a multifunctional device, which is also used for the evaluation of the examination's results. The

reconstructed images are projected to the console screen for offline image processing and evaluation.

The patient table represents the position of the patient in the CT scanner. The patient table can be moved vertically to the ring of the scanner in order to facilitate the placement of the patient. The latest technology scanners contain an automatic system of table movement which creates a spiral path during the examination eliminating further its duration.

The image processor contains the major computational system which is responsible for the image reconstruction of the collected data. Image reconstruction in CT is a mathematical process that generates images from X-ray projection data acquired during the examination procedure. The primordial image from the data acquisition system, of the gantry, is transferred to image processor for further processing and conversion in a suitable form for examination. Image reconstruction has a fundamental impact on image quality and therefore on radiation dose. For a given radiation dose it is desirable to reconstruct images with the lowest possible noise without sacrificing image accuracy and spatial resolution.

The scanning unit consists of the X-ray generator unit and the data acquisition unit. The X-ray source functions as a transmitter and respectively the data acquisition system as a receiver. Those two components are placed in a ring shaped unit, commonly referred to as the gantry system. The ring shaped unit also contains the detecting system.

An X-ray tube anode reaches high temperatures, which are reduced by the integrated cooling system of the scanner, that maintain continuous operational capabilities. The focal spot size of the X-ray tube is determined by the size of the filament and cathode and a CT scanner usually contains multiple focal spot sizes. The tube or source collimators are located in the x-ray tube and determine the section thickness that will be utilized for a particular CT scanning procedure.

The CT detector system relies on collecting attenuated photon energy and converting it to an electrical signal, which will then be converted to a digital signal for computer reconstruction. The detectors used are scintillation crystals (solid state detector) or ionizing gases (such as xenon gas) that when struck by an x-ray photon produce light or electrical signal. The strength of the detector signal is proportional to the number of attenuated photons that are successfully converted to light energy or to an electrical signal.

Once the detector generates the analog or electrical signal it is directed to

the data acquisition system. The signal is amplified, converted into digital signal, in order to be recognized by the computational system, and transferred to an array processor for the mathematical algorithms to be applied, for the image reconstruction.

Each CT scanner is equipped with a system of grids, collimators and filters. This system provides shielding against scattered radiation, in order to preserve the scan slices undisturbed and to reduce the radiation dose received by the patient and the examiner. There are two types of filtration commonly used: mathematical algorithms included in the CT reconstruction process and inherent tube filtration of aluminium or teflon in order to shape beam intensity by by filtering out low energy photons that contribute to the production of scatter.

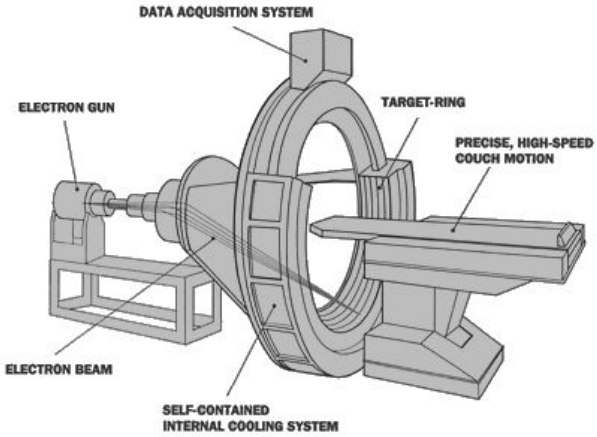


*Fig. 1.8:* Fifth generation CT scanner parts

## 1.2 Mechanical Background

Mechanical tests of bone provide valuable information about the material and the structural properties, important for understanding bone pathology and function in both clinical and research cases of study. Mechanical properties of bone are basic parameters which can be measured by testing whole anatomical units or specimens properly prepared to isolate particular structural components. The mechanical response of bone in normal loading is similar to that of an elastic material. However, bone can be degraded and still retain its morphological features for an indefinite period of time. Bone tissue contains adaptive mechanisms which have the ability to repair itself in case of a fracture, altering its mechanical properties and morphology. The repair mechanisms they need a certain period of time in order to be activated, which exceeds the experimental duration. Along with the fact that the specimens in test contain in majority deceased tissue, the materials in test respond similarly to elastic materials with non-organic properties rather than organic.

The most commonly used techniques of mechanical tests which are applied in bone biomechanics contain bone tensile and compression methods, and bending and torsional tests. The torsion and bending techniques become more and more popular among the engineering community due to the introduction of technological innovations which render the experimental procedure easier and capable to collect important information for the mechanical properties of the specimen.

The mechanical tests applied in bone specimens provide useful information for the identification of the macrostructure and the mechanical properties of the bones. The most important results extracted from mechanical tests concern the characteristics of the stress- strain curve (or force- deformation curve respectively), which characterize the mechanical system in study. The main information that can be extracted from the stress- strain curve contain:

- The elastic range, in which the stress is directly proportional to the strain of the specimen.
- The elastic limit, which represents the greatest stress which can be applied without leaving permanent deformation upon removal of the load.

- The yield strength, which is the threshold of loading applied after which permanent deformation occurs in the specimen.
- The range of plastic deformation, the section of the curve from the yield point to the failure point.
- The failure point, determining the ultimate strength after which the failure of the specimen is observed.
- The amount of energy absorbed by the specimen prior to failure, given by the area determined from the stress- strain curve.

An example of the above characteristics is given in the sample stress-strain curve below:

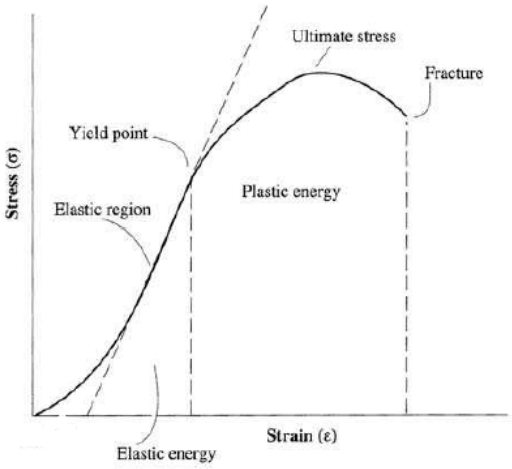


*Fig. 1.9:* Example of stress- strain curve

### *1.2.1 Basic Principles of Bending*

Bones are frequently modeled as beams, although the geometry of the beams differ significantly from the geometry of the cylindrical specimen. Due to the general curvature of long bones they are subjected to axial and bending forces in vivo. Bending loads on bones can be represented by tests such as three point bending and four- point bending. Bending loading causes the appearance of tensile forces on the convex side of the bone, which causes

lengthening, and compressive forces on the concave side, which causes shortening respectively. Stress and strains are achieving their maximum at the surfaces of the beam and are zero at the neutral axis. Bending forces can be represented by the action of a coupled loading containing axial and transverse components. Because of the bone best resistance in compressive loads, muscle contraction favors the attenuation of the tensile forces, reducing the danger of fracture in high loadings.

The purpose of bending tests is to apply a pair of forces that causes the bone to bend about an axis. A bone is subjected to a combination of tension and compression force when it is loaded in bending. Compressive stresses and strains act on one side of the neutral axis while tensile stresses and strains act on the other. The neutral axis remains unloaded during the bending experiment. The distance from the neutral axis determine the magnitude of the applied stresses. Due to lack of symmetry in the bone cross-section, the tensile and compressive stresses may not be equal. Since the bone's resistance in tension is lower, the fractures propagate from the tensile surface of the bone to the compressive surface. When the shear forces, acting on the 45° plane become high enough, they result in a fracture appearing in the compressive side of the bone.

The bending test consist of the specimen loading and the measurement of the emerging displacement. From the collected data the stress- strain curve is designed. The applied load can be controlled either by load control with feedback from the load cell or through displacement control with feedback from the crosshead. In bending test the load is typically applied during a single- cycle loading with sequential load increase, except in cases of fatigue tests. The rate of load application depends on the nature of the experiment. In tests of normal bone activity a physiological rate is selected, when for trauma fracture studies a higher rate is selected.

### *Bernouli- Euler technical beam theory*

The first complete methodology for the mathematical description of beam bending was introduced by Bernoulli and Euler, known as the Bernoulli-Euler technical beam theory. The theory is a simplification of the linear theory of elasticity, which provides a mathematical model of the load- carrying and deflection behavior of beams. A number of practical assumptions is made in order to simplify the problem and suggest a useful and practical solution. The first assumption concerns the beam material, which is consid-

ered as a linear elastic material that obeys Hooke's law. In Bernoulli- Euler beam theory, the deflection of the beam is considered as significantly small and shear deformations are neglected. The plane sections remain plane and perpendicular to the neural axis, or normal to the longitudinal axis.

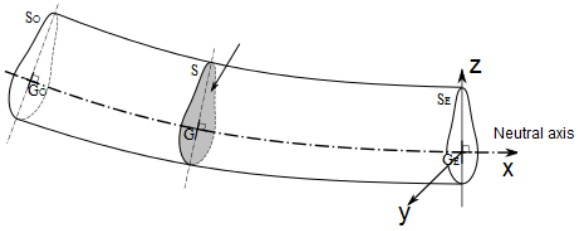


*Fig. 1.10:* Bernoulli-Euler theory: plane sections

The theoretical study requires the examination of equilibrium equations in an infinitesimal beam element. The test element could be defined by the following sketch.

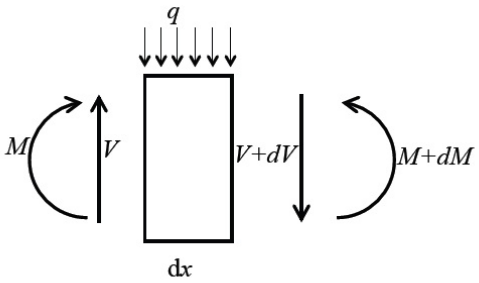


*Fig. 1.11:* Infinitesimal element

The equilibrium equations in the x- axis result in the relations for vertical equilibrium and moment equilibrium:

$$q = -\frac{dV}{dx} \tag{1.3}$$

$$V = -\frac{dM}{dx} \tag{1.4}$$

The moment is given as the product of the applied force and the corresponding distance from the point of the force application. From the definition of stress, the integration of the axial stress over the cross- section gives the moment:

$$M = -\int_A \sigma z dA \tag{1.5}$$

The minus sign in the above expression is due to the direction of the stress, which is by convention less than zero, when it is compressive. If the elastic property of the material is taken into account, the relation between stress and strain is:

$$\sigma = E \cdot \epsilon \tag{1.6}$$

However, since the mechanical problem is defined by a two- dimensional element, and the equilibrium equations apply for two dimensions, the exact elastic relation is given :

$$\sigma_{xx} = \epsilon_{xx} \frac{E}{1-\nu^2} \tag{1.7}$$

The axial displacement is related to the strain as follows:

$$\epsilon = \frac{du}{dx} \tag{1.8}$$

In an elementary cross- section, the geometry is given by the following sketch and the basic geometric relations between the defined quantities result to the following relations.

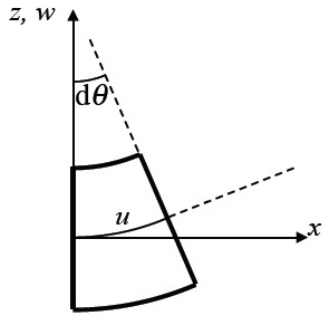


*Fig. 1.12:* Elementary cross- section

$$du = -d\theta z \tag{1.9}$$

The infinitesimal angle $\theta$ relates the transversal displacement $dw$ to the $dx$ displacement.

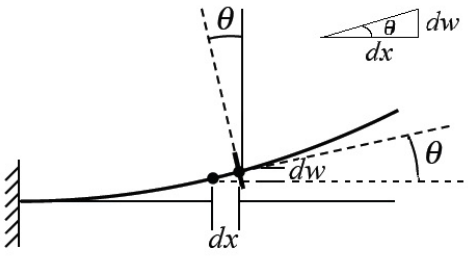


*Fig. 1.13:* Deflection of the beam

$$\tan\theta = \frac{dw}{dx} = \theta \tag{1.10}$$

$$d\theta = \frac{d^2w}{dx} = \theta \tag{1.11}$$

$$\epsilon = \frac{du}{dx} = -\frac{d\theta}{dx}z = -\frac{d^2w}{dx^2}z \tag{1.12}$$

The curvature of the beam $\kappa$ is defined as a function of the radius of the curvature of the beam $R$:

$$\kappa = \frac{1}{R} \tag{1.13}$$

$$\kappa = \frac{d\theta}{dx} = \frac{d^2w}{dx^2} \tag{1.14}$$

From the definition of $\tan\theta$:

$$\theta = \tan^{-1}\left(\frac{dw}{dx}\right) \tag{1.15}$$

As a result, the curvature is given as:

$$\kappa = \frac{d}{dx}\left(\tan^{-1}\left(\frac{dw}{dx}\right)\right) \tag{1.16}$$

$$\kappa = \frac{\frac{d^2w}{dx^2}}{1 + \left(\frac{dw}{dx}\right)} \tag{1.17}$$

The differential equation for the beam deformation is then given:

$$\begin{aligned} q &= -\frac{dV}{dx} = -\frac{d^2M}{dx^2} = \frac{d^2}{dx^2}\int_A \sigma_{xx} z dA \\ &= -\frac{d^2}{dx^2}\int_A -\epsilon_{xx} E z dA = \frac{d^2}{dx^2}\int_A E\left(-\frac{d^2w}{dx^2}\right) z^2 dA \\ &= \frac{d^2}{dx^2}\left(-\frac{d^2w}{dx^2}\right)\int_A E z^2 dA \end{aligned} \tag{1.18}$$

If the modulus of elasticity is constant and the moment of inertia is defined as:

$$I = \int_A z^2 dA \tag{1.19}$$

Then the differential equation is:

$$q = -EI\left(\frac{d^4w}{dx^4}\right) \tag{1.20}$$

*Timoshenko beam theory*

The Bernoulli- Euler theory describes with sufficient accuracy simple bending problems. However, because of the numeral assumptions a large number of practical problems cannot be described by the above theory. The shear forces, neglected in the Bernoulli- Euler approach, are in reality causing serious deformation to the cross- section of the beam. Timoshenko theory suggested a more practical approach, including on the solution the effect of shear forces on the beam. In the Timoshenko beam theory, plane sections still remain plane but are no longer normal to the longitudinal axis due to shear deformation, which is not considered as null.

The deformation of the cross- sections, due to shear forces, is particularly important when the area of the cross- section is comparable with the beam length. As a result, Timoshenko theory is useful for the study of real problems, where typical beams are characterized as deep, and the shear forces cannot be taken as negligible. The shear forces are highest around the neural axis, where the largest shear deformation occurs.

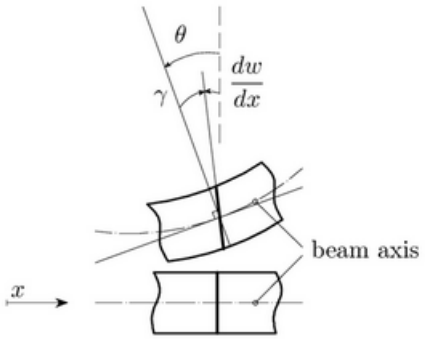


*Fig. 1.14:* Timoshenko theory: shear effect

The actual deformation of the cross- section, from the action of shear forces is shown in the left sketch. The Timoshenko theory retains the assumption that the cross- sections remains plane. As a result, the deformation of each cross- section is simplified as shown in the right sketch.

*Fig. 1.15:* Real deformation

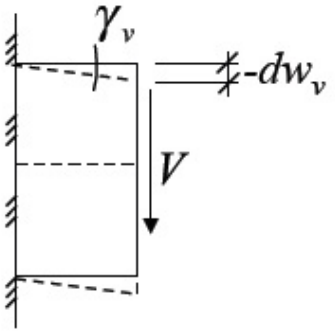


*Fig. 1.16:* Timoshenko deformation

The requirement of the total work, carried out in the average deformation, to equal the sum of the work carried out by all the separated fibres deforming results in the relation:

$$\int_A dw \cdot \tau dA = dw_\nu \cdot V \tag{1.21}$$

According to the geometry illustrated in the deformed shape for Timoshenko theory, the transversal displacement is $dw = \gamma \cdot dx$. This kinematic relation, inserted in the above formula results:

$$\int_A (\gamma dx) \cdot \tau dA = \gamma_\nu \cdot dx \cdot V \tag{1.22}$$

If the shear modulus $G$ is defined by $G = E/(2(1+\nu))$, substitution of the material law $\tau = G \cdot \gamma$ yields:

$$\int_A \left(\frac{\tau}{G}\right) dx \cdot \tau dA = \frac{\tau_\nu}{G} \cdot dx \cdot V \tag{1.23}$$

The average shear stress can be expressed in terms of the shear force $V$ through the auxiliary shear area $A_\nu$

$$\tau_\nu = \frac{V}{A_\nu} \tag{1.24}$$

And therefore

$$\int_A \left(\frac{\tau}{G}\right) dx \cdot \tau dA = \frac{V}{A_\nu}\frac{1}{G} \cdot dx \cdot V \tag{1.25}$$

The shear angle contribution from each infinitesimal element of the beam is given by the expression:

$$\gamma_\nu = \frac{\tau_\nu}{G} = \frac{V}{GA_\nu} \tag{1.26}$$

The kinematic relation between the angle $\theta$ and the transversal displacement, calculated in the Bernoulli- Euler theory, is not valid if the shear forces are included. The relation is transformed in order to include the shear deformation. The total cross- section rotation is given :

$$\theta = -\frac{dw}{dx} + \gamma_\nu \tag{1.27}$$

Substitution in the strain relation as extracted in the Bernoulli- Euler beam theory yields:

$$\epsilon = \frac{du}{dx} \tag{1.28}$$

$$du = -d\theta z \tag{1.29}$$

$$\epsilon = \left(-\frac{d^2w}{dx^2} + \frac{d\gamma_\nu}{dx}\right) \cdot z \tag{1.30}$$

The classical equation of equilibrium results in the modified differential equation for the beam bending:

$$q = \frac{d^2}{dx^2} \int_A E \cdot \left( -\frac{d^2 w}{dx^2} + \frac{d\gamma_\nu}{dx} \right) z^2 dA \tag{1.31}$$

Therefore, the differential equation for the Timoshenko theory is:

$$q = EI \left( \frac{d^4 w}{dx^4} - \frac{d^3 \gamma_\nu}{dx^3} \right) \tag{1.32}$$

If the shear angle contribution is substituted from equation (1.26):

$$q = EI \left( \frac{d^4 w}{dx^4} - \frac{1}{GA_\nu} \frac{d^3 V}{dx^3} \right) \tag{1.33}$$

The introduction of the equilibrium equation $q = -dV/dx$ results in the main differential equation of Timoshenko beam theory:

$$\frac{d^4 w}{dx^4} = -\frac{q}{EI} + \frac{1}{GA_\nu} \frac{d^2 q}{dx^2} \tag{1.34}$$

### *1.2.2 Three point bending experiment*

The mechanical test during which three forces applied on a specimen produce two equal moments is characterized as three- point bending test. Each moment is the product of one of the two peripheral forces and its perpendicular distance from the axis of rotation, which coincides with the point of application of the middle force. If the bone is considered as homogenous and symmetrical, the fracture will occur at the application point of the middle force. A typical example of three- point bending fracture is the "boot-top" tibial fracture sustained by snow skiers. The general experimental setup for a three- point bending test can be given by the following sketch, where the support and loading points are illustrated by the arrows.

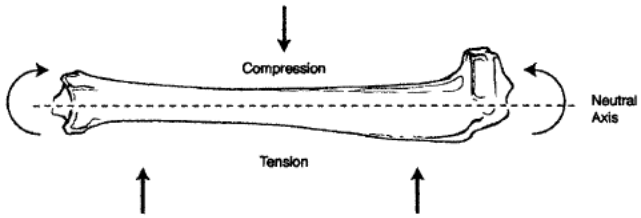


*Fig. 1.17:* Three- point bending experiment

The experimental setup, described, results in the development of a shear force on both sides of the applied force. The diagram of the shear force developed is given in the next sketch.

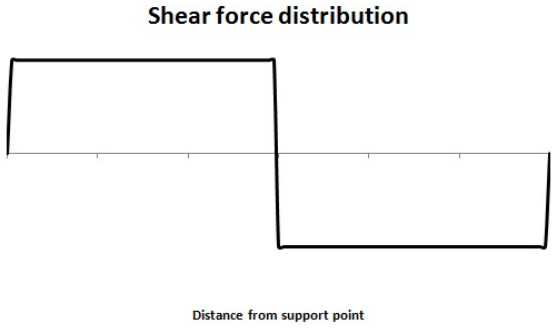


*Fig. 1.18:* Three- point bending shear force diagram

The described system results also in the development of a linear moment on both sides of the applied force. The moment diagram is given in the next sketch.

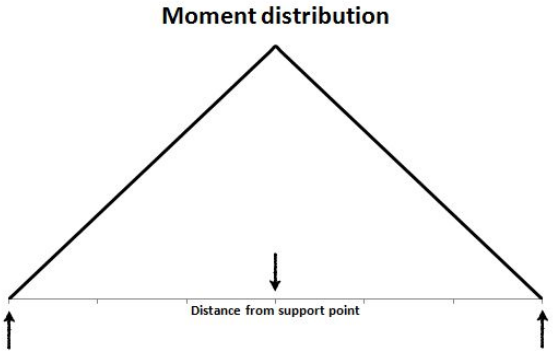


*Fig. 1.19:* Three- point bending moment diagram

From those diagrams two important observations can be made. The shear force is given by the derivative of the bending moment, as illustrated by the relation:

$$\frac{dM}{dx} = V \tag{1.35}$$

The development of a shear force illustrates the demand of the study of the three point bending experiment through a more advanced model than the Bernoulli- Euler approach, which assumes that the shear force is null at the bending area.

### *1.2.3 Four point bending experiment*

Respectively, the mechanical test during which two force couples applied on a specimen produce a pair of equal moments is characterized as four- point bending. A force couple contains a pair of parallel forces of equal magnitude and opposite directions. The moment magnitude is stable in the area between the forces couples. The major problem of the test is the inability to predict the point of the fracture, which depends on the microscopic structure of the specimen which is not actually symmetrical or homogenous, since the each cross- section is equally loaded. However, this inability of prediction of the fracture point, illustrates a more realistic approach closer to the clinical reality of bone fractures. A typical example of four- point bending clinical fracture is the femoral fracture resulting from one force couple formed by the

posterior knee joint capsule and tibia and the other by the femoral head and hip joint capsule.

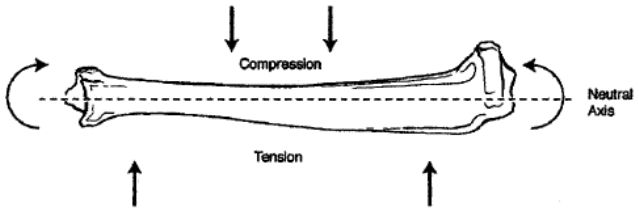


*Fig. 1.20:* Four- point bending experiment

The experimental setup, described, results in the development of a shear force only at the extremities of the bone. The region of interest is free of shear force, as illustrated by the diagram of the shear force developed, as given in the next sketch.

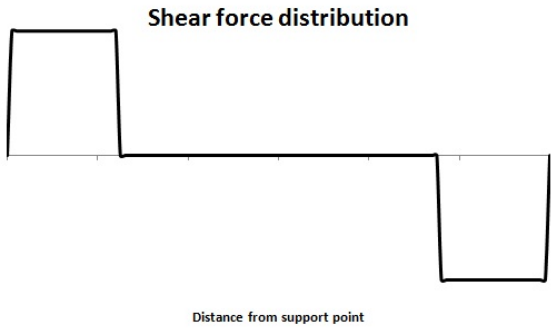


*Fig. 1.21:* Four- point bending shear force diagram

The described system results also in the development of a moment between the points of the load application. The resulting moment is stable within the area of interest. The moment diagram is given in the next sketch.

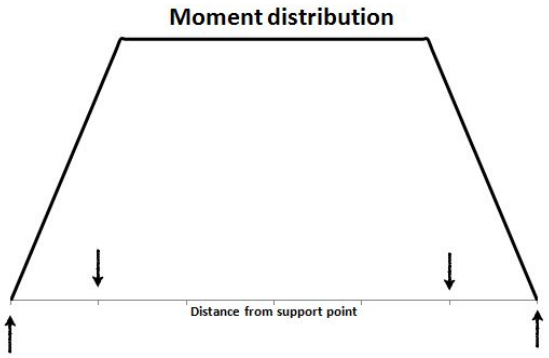


*Fig. 1.22:* Four- point bending moment diagram

The shear force is given by the derivative of the bending moment, as in the case of the three- point bending experiment, satisfying the relation:

$$\frac{dM}{dx} = V \tag{1.36}$$

The lack of a shear force in the area of interest illustrates the high accuracy of the study of the four- point bending experiment, through the Bernoulli- Euler theory, since the basic assumption of the theory is satisfied. As a result, the four- point bending experiment is superior from the three-point bending experiment, since it can be analytically studied through the suggested theories with high consistency between the experimental and the predicted results.

## 1.3 Computational Methods Background

The experimental methods, described above are broadly used not only in mechanical engineering, but also in biomedical engineering. The results exported from those experimental methods evaluate various important parameters, such as the disease assessment and the effectiveness of the treatment. However, the experimental procedure introduces important difficulties that cannot be surpassed in many situations. The major problem of experimental techniques is the destruction of the specimen, which causes the inability of reproduction of the experiment and renders the method not applicable in patients.

The mathematical study along with the computational advances, which have been significantly improved the last years, could insert in the biomechanical research a new perspective which imparts reproducibility and broad applicability of the method. The computational model, which has to obey the theoretical laws of mechanics, simulates the experimental procedure. Based on the experimental details, an accurate computational model could provide computational results which are as close as possible to the results, that would have been obtained by the experimental procedure. The advantages of the above method are numerous and will be discussed in detail at the next chapter.

However, the main problem of the computational techniques is the complexity of the mathematical model, due to the microscopic anisotropy of the biological tissues. The complete mathematical problem cannot be solved analytically, if all the parameters are taken into account. The translation of this model into a computational one, would also be difficult if not impossible to be solved, due to computational limitation, such as memory and time inadequacy of the computational means. An important computational technique has been introduced at the decade of 50, the Finite Element Method, known as 'FEM', in order to deal with many of those difficulties. Finite Element Methods consist a category of approximate techniques which converts the continuous problem into a discrete problem, simplifying the computational solution.

### 1.3.1 Basic Principles of Finite Element Methods

The approximate computational techniques, based on energy theorems, are becoming more effective, providing a solution in cases where other meth-

ods are inadequate. Those methods are based on the determination of a field (for example the displacement field) through auxiliary functions, defined in the body in test. Those functions must obey a set of initial and boundary conditions. The initial problem of the determination of the field in every point of the body, which is infinite, is transformed in a discrete problem, where a set of parameters, characterizing the field, should be determined. The substitute simplified problem determines an approximate solution, close to the real solution, that wouldn't be measurable in the case of the exact problem.

The construction of the auxiliary functions, however simple in the case of a plain geometry, can become rather complex in more difficult geometries. This is the reason the finite element methods are introduced. The basic principle of FEM methods is the separation of those complex geometries into elements, elementary areas of more simple geometries, such as triangular or quadrilateral elements. After this separation, a system of simple auxiliary functions, often polynomial functions, is used, determined in each element and in correspondence with the global geometry.

When the number of the elements used is sufficiently large the initial geometry is accurately represented by the finite elements. The resulting solution approaches the exact solution and the problem is once again reduced in an approximation of the initial problem with finite degrees of freedom. The divergence of the exact solution is inverse of the element number and proportional to the element size. The finite element method consists one of the most efficient methods to deal with a boundary condition problem.

Assuming an elastic material that occupies a certain volume, the first phase of the finite element analysis contains the separation of the volume in elements. The mesh is realized through selected areas or lines that separate the different elements. The dimension of the elements differ according to the dimension of the space in study. In biomechanics, the common space of study is a $3D$ volume and the elements are triangular or quadrilateral $3D$ elements.

The elements are joined together with common nodes, in which the basic functions of the study are measured. The nodes are finite and their number is proportional to the number of elements. The nodes could be distributed in the boundary areas between the elements or, in cases of complex auxiliary functions, could be also placed in the inertial area of the elements such as

the center of the element. The degrees of freedom are defined in the nodes of the construction, so that the model is consistent with the mechanical theory and with the actual experimental problem.

Every finite element is characterized by the same mechanical features that characterize the initial construction. The gain of this method is the simplification of the complex geometries and the finite number of the elements, that limits the analysis in a length scale where the solution is approachable. The functions are measured in every node of the construction and consequently the results of the determining field are also measured on the nodes. The estimation of the field in every other point of the construction is made through interference, either linear or more complex, depending on the auxiliary functions used.

The next phase of the finite element analysis, contains the determination of the parameters of the mechanical problem, which have not been calculated. For instance, in case of a problem in which the displacement field is determined, the strain and the stress fields should also be defined in each node. Those quantities are determined through basic mechanical equations. When determined for the finite number of the nodes, the fields could be measured in every point through the method of interpolation described. The relation between the displacement and the strain could be included in the general form:

$$\epsilon = L \cdot u \tag{1.37}$$

Where $\epsilon$ is the strain matrix, $u$ the displacement matrix and $L$ the operator matrix. Respectively, the stress matrix, $\sigma$ is defined by the elastic formula:

$$\sigma = E \cdot \epsilon \tag{1.38}$$

Where $E$ is the elasticity matrix, which contains the elasticity modulus at each direction. From the above analysis and the conservation of the energy laws, the solution is determined at each node. If the number of the nodes is N and the degree of freedom of each node is k, $k \cdot N$ equations should be solved to reach the solution.

The solution of the problem depends on the method that is used. A widespread method that achieves important accuracy is the Galerkin method. Galerkin method constitutes a technique of approximate solution of a differential equation or a system of differential equations. This technique does not base the solution on energy theorems, but uses the system of differential equations obtained by the design of the project in order to reach the solution.

If a linear differential equation with homogeneous boundary conditions is given:

$$L \cdot u = f \text{ in the interval } D \tag{1.39}$$

$$D \cdot u = g \text{ in the boundary } \partial D \tag{1.40}$$

The differential operators $L, D$ depend on the design of the problem. For example, in a linear beam under bending the most simple differential operator that could be used is $L = EI\frac{d^4}{dx^4}$. The solution $u$ could be expressed by the form of a finite function series based on a selected basis functions $\phi$, in order to convert the problem in a discrete form:

$$\tilde{u} = \sum_{j=1}^{N} u_j \phi^j \tag{1.41}$$

The solution is discretized in $N$ nodes, according to the problem discretization. It represents the approximate solution, denoted by $\tilde{u}$. The number of the basis functions is also N. Each basis function is non zero only in a partition of the interval and is usually defined as unit in a certain node. The basis functions are orthogonal so that the following relations applies:

$$\begin{aligned} \int \phi_j \phi^j dv &= 1 \\ \int \phi_j \phi^i dv &= 0 \end{aligned} \tag{1.42}$$

The approximate solution differs from the exact solution by the term:

$$L \cdot \tilde{u} - L \cdot u = \epsilon \tag{1.43}$$

$$L \cdot \tilde{u} - f = \epsilon \tag{1.44}$$

The optimal approach of the solution requires the minimalization of the remainder $\epsilon$. The integration of the fundamental differential equation multiplied by the basis function results in the relation:

$$\int [L \cdot \tilde{u} - f]\phi_i dv = \int \epsilon \phi_i dv \tag{1.45}$$

The requirement of the remainder minimalization results in the equalization of the second term with zero. Since the remainder, as defined above, should equal zero the weighted residual could be defined as follows:

$$R_i = \int (L\tilde{u} - f)\phi^i dv \tag{1.46}$$

And should also equal zero, for each $i = 1, 2, \ldots, N$. The number of the weighted remainders is equal to the number of the basis functions and as a result to the number of the nodes of the grid. Replacing the value of u by the discretized form, the residuals are transformed:

$$R_i = \int (L \sum_{j=1}^{N} u_j \phi^j - f)\phi^i dv \tag{1.47}$$

$$R_i = \int \phi^i L \sum_{j=1}^{N} u_j \phi^j dv - \int f \phi^i dv \tag{1.48}$$

Provided that the differential operator is linear, it is only applied in the basis functions and does not affect the solution's coefficients $u_j$.

$$L \sum_{j=1}^{N} u_j \phi^j = \sum_{j=1}^{N} u_j \left(L\phi^j\right) \tag{1.49}$$

Applying this formula to the weighted remainders, the system of equations is transformed to an algebraic problem of N differential equations:

$$R_i = \int \phi^i \sum_{j=1}^{N} u_j \left(L\phi^j\right) dv - \int f\phi^i dv \tag{1.50}$$

$$R_i = \sum_{j=1}^{N} u_j \int \phi^i \left(L\phi^j\right) dv - \int f\phi^i dv \tag{1.51}$$

Therefore the system becomes an algebraic problem of N differential equations, where the solution is given by the identification of the solution's coefficients $u_j$ and the integrals can be computed from the given basis functions. Those equations can be easily solved through various computational methods. The solution takes the form of a vector solution $\vec{u}$, representing the N nodal unknowns $u_j$, the N independent numbers which give the value of the requested field at each node, provided the basis functions. The general form of the equivalent problem is:

$$R_i = \sum_{j=1}^{N} a_{ij} u_j - b_i = 0 \tag{1.52}$$

where,

$$\begin{aligned} a_{ij} &= \int \phi^i L\phi^j dv \\ b_i &= \int f\phi^i dv \end{aligned} \tag{1.53}$$

The solution can be generalized by interpolation in every spatial position, and specially in the positions which are not represented by nodes and the results are not directly given. If the position vector is defined by $\vec{x} = \sum_{i=1}^{n} x_i e_i$, the solution in each position $\vec{x}$ is given by the formula:

$$u(\vec{x}) = \sum_{j=1}^{N} u_j \phi^j(\vec{x}) \tag{1.54}$$

The above procedure is used in order to convert a mathematical problem with the infinite degrees of freedom, which cannot be solved analytically, into a discrete problem, which can be solved computationally. The common procedure of a program which uses the finite element method, is the construction of the matrix $a_{ij}$, and the vector $b_i$. Those quantities are obtained through the described procedure, which depends on the system of equations of each problem. The next steps consists of the solution of the system with a selected computational method.

The computational methods used are either direct, such as the gauss elimination or iterative such as Newton- Raphson method. The first category of solvers, approaches the real solution without significant deviations. The procedure is typically completed in a number of steps proportional to the number of the equations. However, those methods are not always rapid enough. This problem is solved by the use of an iterative method, which approaches the solution within a number of selected iterations. The number of the iteration determines the deviation from the actual solution. The resulting solution is a vector $u_j$, which represents the requested function in the position of each node. The solution can then be generalized as described above, in order to cover the whole volume of the problem.

# 2. PROBLEM DESCRIPTION

The current study focuses in four different experimental setups. The first experiment concerns the three- point bending test and is performed for both free and embedded specimen. The second experiment concerns the four-point bending test, which is also performed for free and embedded specimen. The purpose of the experiments is the measurement of the pairs of loading and deformation at every timepoint, so that the stress- strain curve can be constructed. The important information extracted from the stress- strain curve concern the yield strength, the ultimate strength, the total energy absorbed and other mechanical features.

Those data are used either for clinical or for research causes. One of the most important application of bending tests in biomechanics concerns the evaluation of therapeutic methods, used in orthopedics and the suggestion of their improvement. The further purpose of those tests, is the research for optimized techniques that would be more effective in pathological cases that cannot be treated properly. The results of those tests are of significant importance for clinical practice, since little improvement can be substantial. An example of the experimental procedure, commonly followed in mechanical tests of bones, is described in details in the next section.

## *2.1 Description of experimental procedure*

Bone specimen are harvest immediately postmortem. The articulation and surrounding joints are carefully removed and the bones are wrapped in saline-soaked towers and placed in appropriately configured tubes. They are then frozen at $-20^{\circ}$ until testing. The tests should be performed in average temperature, $20^{\circ}$ to $22^{\circ}$. After removal from the freezer, the specimen should be kept wet and in saline, during the testing procedure. In order to simulate as closely as possible fresh bone conditions, the time between thawing and testing should be kept to a minimum.

### 2.1.1 Three-Point Bending

*Experimental setup*

The typical support span for the bending tests extends from metaphysis to metaphysis, in order to ensure stable contact. The area of interest is contained within the diaphysis area which is characterized by more regular geometry and can be consider as a cylindrical structure. As a result, mechanical studies focus on the mechanical properties of diaphysis. The support should follow certain rules in order to maintain the independence of the tests from the experimental setup. Therefore, the support is strong enough to withstand the developed forces, wide enough to contain the bone width and sufficiently long to contain the area of interest within the support span. The end supports, which contain the area of contact with the specimen, should be smooth to prevent stress concentration. They should also be flat and perpendicular to the horizontal axis in order to avoid preload and for the test to be independent of the inclination of the ends.

Three- point bending is performed through an actuator, which has a single point of application, the contact point with the specimen. The application point is located in the midline between the two end supports. The load can be applied to the anterior or the posterior surface of the bone according to which side the actuator will be applied.

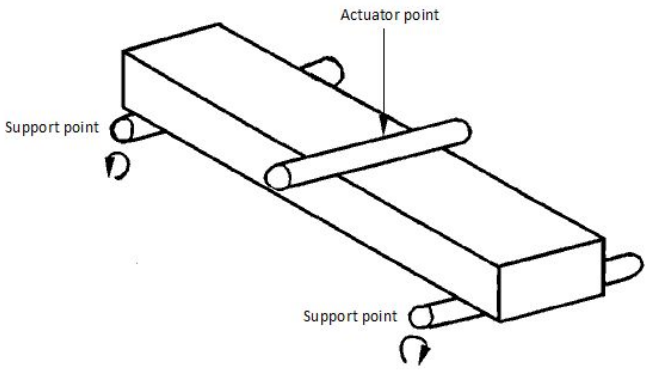


*Fig. 2.1:* Typical three- point bending experimental setup

The loading rate depends on the study. The rate of the loading defines whether the experiment concerns a dynamic or a static test. Within the current study, the performed tests are static. The load is applied over a single cycle with a stable rate. The respective constant displacement rate that does not exceed the $1mm/min$. The specimen are tested to failure. As a result the maximum displacement is not specified before the experiment, but depends on each test. It is commonly determined as a proportion of the displacement reached right after the failure load is applied. The failure point coincide with the contact point of the specimen with the actuator.

*Experimental procedure and data*

During testing, the force and crosshead displacement are recorded at each timepoint. The rate of data saving is selected at the beginning of the test and is stable throughout the procedure. The frequency of data collection should be chosen carefully, in order to preserve the continuity of the collection. The data are directly saved on a computer storage system linked with the experimental setup and can be processed after the end of the testing procedure in order to extract the required information. Typically, a load-deformation curve is created, which should be translated into a stress- strain curve. For bending tests the loading is represented by the bending moment. Stiffness value is calculated from the gradient of the curve in the linear section. The failure load is defined as the maximum load applied, without the occurrence of discontinuities in the bone cortex.

### *2.1.2 Four-Point Bending*

*Experimental setup*

The specimen preparation does not depend on the applied test and is the same as described for the three- point bending procedure. After the preparation of the specimen, they are submitted in a loading procedure through a similar support span as in the three- point bending test. The size and the material of the support span and the actuator depend on the experiment. However, the main rules followed in the three- point bending, also apply in the four- point bending test. The difference lies in the application of the displacement. In the four- point bending test, the displacement is applied by a pair of actuators instead of a single one. The area of interest, which is commonly the diaphysis, is contained between the two points of the actuator

pair. This setup ensures that the bending moment is uniform within the area of interest. The four- point bending test is a test of pure bending.

Due to irregular surface shape of bone specimen, the span between the actuator pair may be limited. In order to obtain accurate results, the two points of load application must contact the bone at the same time. For the same reason, the complete loading procedure should be synchronized. The points of contact should be smooth to eliminate stress concentration. The rate of the loading is once again stable and at the same level as in the case of three- point bending. Since the specimen are tested to failure, the maximum displacement cannot be specified before the experiment. It is commonly selected as a proportion of the displacement reached after the failure load is applied. The factor that should be determined in the four- point bending test, is the region of the failure point. It is located in the area between the actuator pair, but the exact point depends on the microstructure of the bone and cannot be defined before the experiment.

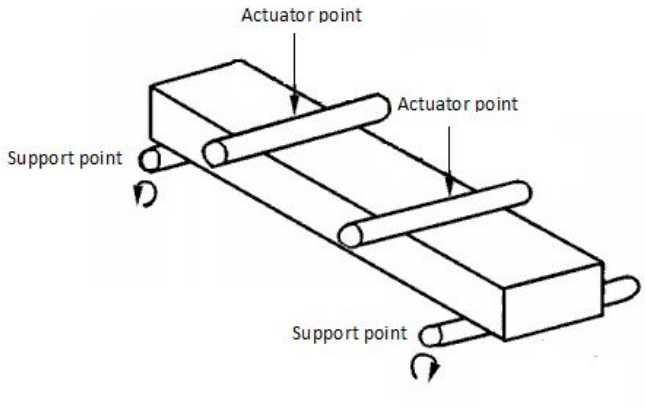


*Fig. 2.2:* Typical four- point bending experimental setup

*Experimental procedure and data*

The quantities that should be measured are once again the force applied and the corresponding displacement at each timepoint. Therefore, the loading is calculated through the measurement of the forces applied on the crossheads. Since the velocity of the motor that applies the deformation of the pair actuator is constant and the procedure is synchronized, the moment

developed is expected to be uniform in the area of interest. Deviations are mainly caused due to bone anisotropies and the deviation of the geometry from the cylindrical cross- section. The identification of the failure point is commonly performed after the experimental process is completed, by the mechanical study of the ruptured specimen. The discontinuities occurring on the bone surface indicate the mechanical failure and define the failure load, as described in the three- point bending test.

Respectively to the three- point bending technique, the data saving rate is stable and pre- selected. The frequency of data collection should be chosen carefully, in order to preserve the continuity of the collection and in the case of four- point bending is usually higher in order to identify the failure point with higher accuracy. The data are also directly saved on a computer storage system and can be processed after the end of the testing procedure in order to extract the required information. Typically, a load- deformation curve is created.

## *2.2 Embedding of specimen*

The three- point and four- point bending tests can also be applied in specimen, specially configured. A common configuration with important advantages is the embedding of the specimen in a resin material. The embedding consists of two basis of resin constructed at the extremities of the bone. The basis extend till the metaphysis surface and only the area of interest, within the diaphysis region remains unbound. The principal utility of the embedded specimen is the stabilization of the placement in the experimental setup. The embedding procedure eliminates rotation and slip occurrence during the experimental procedure, reassuring the stability of the specimen. If the procedure is properly done, it can assure reproducibility and consistency of the method.

The embedding of the specimen requires the placemen of the bone in two molding cups. The molds are orthogonal parallelepipeds and of exactly the same size. The magnitude of the molds is chosen properly in order to contain the total volume of the extremities, but occupy the minimum possible volume. The procedure of the embedding should be carefully performed in order to avoid preloading and secondary mechanical effects that would affect the mechanical properties of the bone. The experimental conditions, such as the temperature and the pressure, are precisely controlled, and remain stable

throughout the procedure of embedding.

The material used for the embedding procedure is significantly important, in order to maintain close mechanical properties to the specimen and eliminate secondary mechanical effects. The principal material used for the construction of the embedded structure is the resin. Resin is a composite polymer based material. The most common polymer- based composite materials include at least two parts, the substrate and the resin. The resin based materials are commonly used in biomechanics, because of their elasticity modulus, which is close to the elasticity modulus of the bone and are therefore convenient for showing similar mechanical properties to the bone tissue.

## 2.3 Problems of experimental procedure

The described experimental procedures consist the most widespread techniques for determination of the mechanical properties of various specimen. They are accurate and easily applied techniques, used not only for mechanical but also for medical purposes. However, in the case of bone biomechanics, those methods cannot be easily and effectively applied. The weakness of the methods lies in the lack of applicability in clinical cases. The specimen cannot be subjected in common experimental tests as vivid tissues.

### 2.3.1 Experimental limitations

An important problem which questions the liability of the biomechanical tests is the specimen used. There are two main sources of bone specimen used, specimen from artificial material, which simulates bone properties, and specimen from necrotic tissue. However, these materials are significantly different from the real bone tissue, functioning in a biological organism. Moreover, the necrotic tissue typically used in biomechanical tests is from mammals with similar bone properties as human's, as human specimen are not easily accessible for experiments. The experiment, corresponding to the actual response of bones in loading, should be held in vivo. A simple example that illustrates this flaw of the method, is the action of repair mechanisms. In the case of a bone tissue inside an active organism, the repair mechanisms would resist on a bone fracture. In a necrotic tissue, those mechanisms are deactivated. The reality of the bone functioning could be tested only with in- vivo experiments, which is not an option in bone biomechanics.

Consequently, the experimental results depend on the parameters of the specimen used. The recent experiments follow an oblate protocol for the use of bone specimen. This protocol describes the optimal conditions of the sample, in order to simulate as accurately as possible the actual bone functioning. The latest results from similar experiments show high consistency and accuracy, corresponding as close as possible to experimental results that would be received from in- vivo experiments. However, they still differ from the results, that would be obtained from in- vivo experiments.

Another important problem of mechanical tests is the destruction of the specimen. In order to determine the failure point, the specimen should be loaded to its failure. As a result, the same tissue cannot be used for confirmation of the results. Similar tissues are used to reproduce the experimental process, but in experiments which study live processes two specimen can never have the exact same response. In studies where the failure point does not need to be determined, the tissue is loaded with minimum deformation. However, due to secondary effects those experiment cannot be reproducible either.

A necrotic tissue subjected to a loading, even if it has not reached its failure point, does not have the same load- carrying ability in a second experimental procedure. This behavior can be described by the fatigue tests applied in bones. The most commonly used fatigue test is the application of a stable loading in various cycles at the same specimen. Even if the load is not hight enough to cause a mechanical failure, small bone damages are eventually developed over time, causing an observable failure. Fractures resulting from continued repetitive loading rather than extreme trauma are commonly known as stress fractures.

According to those difficulties described, a variety of secondary problems arises. Because of the irreversibility of the testing system, the experiments cannot be reproduced under the exact same conditions in the case of necrotic tissue. On the other hand, the experiments held with artificial materials, simulating the real bone can be reproduced, since the specimen used are identical. However, in the case of artificial materials, the mechanical properties determined, differ significantly from the bone's properties, as the microstructure and the anisotropy of the material are not taken into account. Consequently, the obtained results do not represent the actual situation.

The disadvantage of the three- point bending test in particular, is the deviation of the loading field from the stable field to which the theoretical predictions correspond. The moment occurred is not stable in the area of

interest, but is instead represented by a linear function. This leads to the occurrence of secondary effects, introducing an additional factor of deviation from the mathematical predictions of the model. Another important problem in the three- point bending test is the support of the specimen. In case of a free specimen, the support system is not sufficient to eliminate rotation of the specimen, during the loading procedure. As a result, the failure surface cannot be easily determined.

At the four- point bending test, the moment is stable between the points of load application, which renders the technique consistent with the theoretical approach of the problem. However, in contrast with the three- point test, where the failure point is precisely determined as the point of load application and the strain can be accurately measured in the failure region, in the four- point test the failure point cannot be easily located. This is the major disadvantage of the method, which is highly accurate compared to different experimental setups. This practical problem is of major importance, as it introduces a supplementary factor of vagueness in the experiment. The difficulty of the determination of the failure point renders the technique impractical, since the stress and strain distribution are difficult to be measured in the exact region of the fracture.

The support problem of the experimental techniques can be solved by the embedding of the specimen. In that case, the rotation of the system is excluded and the failure surface is well defined. However, in the case of the embedded sample, secondary effects cause a possible inconsistency between the theoretical and the practical approach. In the contact surfaces of the system, secondary stresses may occur that cannot be measured. Moreover, if the embedding procedure is not performed with prudence pre- loading effects may also affect the results. Those practical problems of each method illustrate the lack of a dominant technique, since every setup has its own disadvantages.

Because of the destruction of the specimen, the mechanical experiments cannot be transferred in clinical practice. In reality, this is the major problem of common mechanical tests. The fundamental utility of biomechanical tests can be separated in two major categories: research studies and clinical practice. The research studies can be realized with specimen that would be destroyed, even if a couple of problems arise by this practice. However, the specimen destruction in combination with the experimental procedure, which have not be designed to be applied in- vivo, exclude the application of those methods in patients. Similar alternative methods can be used clinically, but

the received results do not correspond to the required outcome.

The major need for a practical and accurate test for the determination of the bone properties is related to the clinical use. The application of a mechanical test is of significant importance for diagnostic, therapeutic and operational uses. If those techniques cannot be transferred in the clinical reality they cannot be useful for the most important part of the clinical community: the patients. A modern method should be introduced in order to utilize the advantages of the mechanical tests, overcoming the problems of the current techniques.

### *2.3.2 Limitations in mathematical approach*

The major weakness of the theoretical approach in the biomechanical study of the bone is the inability to attain an analytical solution which includes the complete model. The limitation of the mathematical model is introduced by the complicated nature of biological tissues. The bone tissue is highly anisotropic, due to the directional mechanical properties of osteons, especially when the microscopical level of structure is studied. The differential equations that would describe more accurately the real situation, could not be solved, due to high complexity. This is the main reason for the inadequacy of any mathematical model to describe the actual situation. As a result, the methods proposed for the biomechanical description of the bone exclude various procedures occurring in the bone micro- processes, which are important for the further comprehension of the actual model.

Contemporary studies have contributed important improvements in the traditional mechanical theories, in order to include secondary effects that describe the actual situation and render the theoretical approach as accurate as possible. The macrostructure of the bony tissue is successfully described by numerous mechanical models. If only higher hierarchical levels of structure are taken into account, the results obtained are adequately accurate. However, important secondary effects are not included in those models, causing important deficiencies in certain cases. A typical example of the significant importance of the microstructure, is the inability of current theories to predict the failure point, in the four- point bending test.

The exact distribution of stress, in a beam subjected to the action of a concentrated force is not closely defined, even in the case of the simpler cross-section of a prismatic beam. The three- point bending problem obtains an accurate solution as long as the length of the beam exceeds the dimensions

of each cross- section and the planes far from the central one are studied. In practical problems, such as biomechanical studies, the beam cross- section is comparable to its length and the solution is therefore highly divergent.

As the aperture of the beam (length over height) becomes smaller than ten, the perturbation effects in the central area become more dominant and cannot be neglected. A detailed elastic solution that includes the punch-effect is then indispensable in order to avoid solutions that do not correspond to the actual situation. A couple of modern solutions have been proposed by Stokes, Timoshenko and Goodier, and later by Crouch and Starfield in an attempt to define the central solution more accurately. However, the stress and strain distribution in the central region of the beam cannot be predicted with strict precision, as the microstructure of the bone should be taken into account for further correction of the solution.

The exact distribution of stress can be expressed in the study of the four-point bending. However, a similar problem arises due to the microstructure of the bone, already mentioned in the experimental limitations of the test. The inability of identification of the failure point, when the moment is uniformly distributed in the length of the beam, introduces an important indeterminacy in the theoretical approach. Equally important as in the experimental technique, the microstructure of the bone should be studied in the attempt to suggest a consistent result.

As well as in the experimental methods, the mathematical limitations exclude important factors from the solution which eliminates the integrity of the solution. A more accurate method is indispensable to be developed in order to correspond to the reality of the problem. The currently developed computational techniques represent the most prominent possibility for the improvement of the current biomechanical techniques.

## *2.4 Utility of Computational Methods*

The described problems occur either from the practical limitations of experimental techniques or from the mathematical inability to achieve the required accuracy. A solution to the majority of those problems can be achieved by the use of computational methods.The available computational tools give the opportunity to study complex problems, through simplifications. The computational methods use simple assumptions to generalize the nature of a problem and translate an infinite problem into a discrete one.

The finite element methods ensure the simplicity of the discretization and the utilization of rapid solvers. A finite element method designed for a bending experiment can be used for similar problems with simple modifications. In this way, the procedure is optimized and is becoming as rapid as possible. Those techniques eliminate the problem of accuracy in the theoretical approach of the study, since they are applicable in every geometry. The discretization of the surface assures convergence of the method even in the case of complex geometries that cannot be studied mathematically.

The computational methods allow regional anisotropy, since each element can be characterized by different material. As a result, structures of different materials can be conveniently modeled, as in the case of the embedded specimen. The accuracy problem introduced by the theoretical approach is eliminated in the computational modeling. The accuracy can be improved by increasing the number of elements used. The grading of the mesh results in the elimination of deviation and achievement of the desired accuracy. The increment of the number of elements is a simple way to control the velocity of convergence over the accuracy of the solution.

The practical limitations of an experimental setup could be appropriately treated by a computational method, that would recreate the experiment with the use of a virtual specimen. If the specimen and the experimental setup description correspond to the studied test, the obtained results could reproduce the experiment with high accuracy. The use of a computational model is offering the ability of reproducibility, since the created model specimen can be preserved for further experiments. The loading and boundary conditions are not restricted and can be applied in any region of the body. As a result, the exact experimental procedure can be simulated, when the adverse effects of not efficient support occurring during experimental techniques, are eliminated.

The computational methods offer important improvement from both the experimental and the theoretical approach. Even though they cannot be applied as an individual method, combined with traditional techniques they can overcome the main difficulties and produce important results. In the current study a geometry model will be created for the bone specimen. This model will be imported in a computational model of experimental setups and subjected in different experimental procedures.

# 3. COMPUTATIONAL MODEL: 3D RECONSTRUCTION OF RABBIT FEMUR BONE

## *3.1 CT reconstruction*

The CT scanner is the most suitable technique for non invasive bone examination. Opposite to techniques that utilize the hydrogen concentration in tissues, such as the MRI, or their metabolic activity, such as the PET scanner, the CT scanner separates different tissues according to density differences. Due to the high density of bone tissue, the bones are highly distinguishable from other tissues and the CT scanner can effectively reveal osseus regions.

The CT images represent a $2-D$ distribution of the attenuation coefficient for each slice of the tissue. The image reconstructed from the CT data represents a distribution of the tissue's density, in different shades of grey. The primary image received from the detectors is of limited diagnostic use, since important artifacts render the image blurred and it does not correspond to actual tissue structure. The image reconstruction procedure is crucial for the creation of an accurate image which illustrates the anatomy of the body in test. The final image reconstruction is achieved after various steps of image processing.

### *3.1.1 Image Generation*

The reconstruction methods can be separated in two major categories: the analytical reconstruction and the iterative reconstruction. The analytical methods typically implement some analytical inversion formula in order to transform collected data into an image corresponding to the actual anatomical structure. On the other hand, the iterative methods generate a sequence of estimates that eventually converge towards a real solution, so that the collected data would be reproduced. Although analytical reconstruction methods require much less computational effort and are broadly

used in most image reconstruction devices, iterative methods allows to easily model constraints and to incorporate prior knowledge, so that the radiation dose could be significantly reduced (even to 50% of the initial value).

One type of analytical reconstruction methods that is currently widely used on clinical CT scanners, is the methods based on filtered backprojection (FBP) because of their computational efficiency and numerical stability. The basic principle of the backprojection methods, the simplest analytical methods used, is the use of fourier transformation in order to project the data to fourier space. The fourier transformation can be defined by the terms:

Forward fourier transformation:

$$f(x) = \int_{-\infty}^{\infty} F(u) \exp[-2i\pi ux] du \tag{3.1}$$

Inverse fourier transformation:

$$F(u) = \int_{-\infty}^{\infty} f(x) \exp[2i\pi ux] dx \tag{3.2}$$

One of the most fundamental concepts in CT image reconstruction if the "Central-slice" theorem. The central-slice theorem states that the one dimensional fourier transformation of a projection, measured at a certain angle $\phi$, is equal to the radical slice (a profile through a line drawn through the center of the fourier plane, at a certain angle) taken from the two dimensional fourier domain of the object at the same angle.

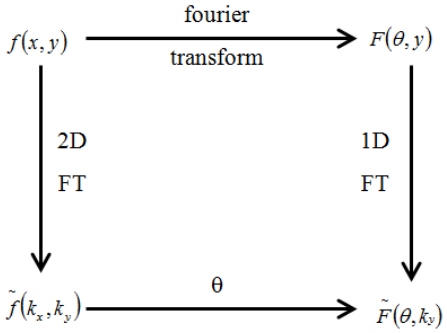


*Fig. 3.1:* Central slice theorem

The central slice theorem plays an important role in image reconstruction techniques, as it relates the two dimensional fourier transformation of an image to the one dimensional fourier transformation of its projection. If all the projections of the object, from every angle, are transformed as described and interpolated into a two dimensional fourier plane, then the full two dimensional fourier transformation of the object will be reconstructed. The next step requires the inverse fourier transformation to be applied in the two dimensional fourier representation that has been created. Then, the object will be reconstructed in the normal plane.

However effective this technique might seem, the backprojection method results in a blurred image because of the biased data received from the detectors. Due to the angular data collection, the central region of the object is favored since the projection lines are denser in the center. As a result, there is a need for a filter application in order to eliminate the favoritism of the central area and reconstruct an image corresponding to the actual anatomy of the testing body. This optimized technique is called filtered backprojection.

In the method of filtered backprojection the same procedure is followed in order to create the two dimensional representation of the image in the fourier space. Then a filter is applied in order to eliminate artifacts created either by the detecting system or by the reconstruction procedure. Those filters depend on the generation of the scanner as well as the exact geometry of the scanning system. Since the system, subjected to fourier transformations, is linear, the filter is equivalently applied in the normal and the fourier space. In common de-blurring image techniques the filter is applied prior to the backprojection procedure.

In fourier space the filter that needs to be applied has the form of $|r|$. The spatial form of the filter is the inverse fourier transformation of the fourier form. The projection of each cross-section is subjected in one of the following processes : fourier transformation, multiplication with $|r|$ and inverse fourier transformation, or convolving the projection with the inverse fourier transformation of the filter to be applied, in this case $|r|$. This procedures, which are equivalent, transform the projection of each spot into a filtered projection, with negative side lobes. It is therefore, a spatial-frequency optimization of the original projection. The high-frequency boost is exactly equal to the high-frequency attenuation that is applied during the process of backprojection.

If all the projections of the object are transformed as described and interpolated into a two dimensional fourier plane, then the full two dimen-

sional fourier transformation of the object will be reconstructed, exactly as in the case of backprojection. The positive parts of the image re-enforce each other, as well as the negative components. The positive and negative components though, tend to cancel each other. After numerous back-projection operations, everything is canceling, except for the intensities at the original position of each spot of the image. If generalized for a real image, which is the sum of numerous single spots in case of an arbitrary projection, and since the system is linear, the above results could be generalized respectively. The repetition of this operation for a large number of arbitrary projections would results in the reconstruction of the entire cross-section. The last step requires the application of the inverse fourier transformation in the two dimensional fourier representation that has been created. The reconstruction of the cross-section is then completed.

The mathematics of the image reconstruction process, as described in the above procedure, can be expressed compactly in the equation:

$$g(r,\theta) = \int_0^{\pi} \int_{\infty}^{\infty} \left[ \int_{\infty}^{\infty} f(\xi,\phi) exp[-i\pi\rho\xi] d\xi \right] |\rho| exp[i\pi\rho r cos(\theta-\phi)] d\rho d\phi \tag{3.3}$$

Where, $g(r,\theta)$ is the function representing the reconstructed image at each point $(r,\theta)$ and is given by the filtered backprojection at each angle. The $f(\xi,\phi)$ is representing the original projection, which is subjected in a fourier transformation as illustrated by the application of the first integration. The result is multiplied by the filter $|\rho|$ and subjected to an inverse fourier transformation.

The described techniques represent the basic procedure of the most commonly used methods of image generation, through CT scanning. However, every CT scanner uses special techniques for image generation, appropriately modified for the specific features and the characteristics not only of the particular CT- scanner but also of particular case studied. The modification of the image reproduction technique aims to the optimization of the resulting images so that they correspond as accurately as possible to the actual structure of the tissue. From each specialized procedure, a set of images is obtained.

### 3.1.2 Image Processing

The CT reconstruction procedure results in a set of two- dimensional images of the scanned cross- sections of the bone, for each scanned slice. Those images represent the density distribution through different shades of grey. The denser structures are presented by lighter shades. The denser structures are typically white regions, while the darkest regions represent the vacant space, where no attenuation of the beam occurs.

For the reconstruction of the thee- dimensional model, a simple procedure will be applied. The first step contains the special treatment of each slice of the CT representation through a brightness filter in order to distinguish the density that corresponds to the bone areas. Brightness is one of the most important pixel characteristics. It is involved in many image-editing algorithms. However, there is no conventional formula for brightness calculation and the term brightness is typically used for the non- quantitative reference to physiological perceptions of light. Developers of algorithms for digital image processing should develop a method to describe brightness more strictly, but there is, currently, no conventional numerical description for this stimulus characteristic. Since the application of the same stable filter for each bone region is not quantitatively accurate, each slice will be examined separately.

The combination of those slices through polynomial curves leads to the creation of the $3-D$ model. Then a smoothing algorithm should be applied. In image processing, the smoothness of a data set corresponds to the creation of an approximate function in order to capture important patterns in the data, while leaving out noise or other fine-scale structures. The data points of a signal are modified so that individual points, caused by noise or false signal, are reduced, and points that are lower than the adjacent points are increased leading to a smoother signal. Smoothing can contribute to data analysis by extracting supplementary information from the data, and reveal the real geometry of the structure in test, as long as the assumption of the smoothing is reasonable. Many different algorithms are used for smoothing but data smoothing is typically done through the simplest density estimator, the histogram.

The CT scanning of the femur specimen resulted in 186 independent images, for each cross- section. Those images are inserted in an image processing program, $3D$- DOCTOR. The purpose of the first processing step is the creation of the three- dimensional geometry of the bone. The procedure is separated in the reconstruction of the outer and the inner surface of the

bone. The outer surface determines the boundary of the bone. The specimen is cleansed from adjacent soft tissue in the major part of its extend. The brightness- threshold applied for the identification of the outer bone surface is clearly distinguishable.

A clear cross- section is selected as a sample cross- section, typically from the diaphysis region, for the determination of an accurate threshold.

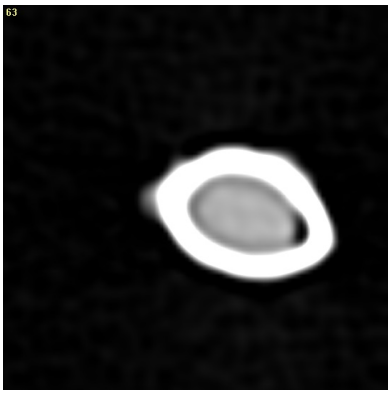


*Fig. 3.2:* A typical diaphysis CT slice

This density threshold is selected in order to include the maximum bone surface, omitting any vacant space.

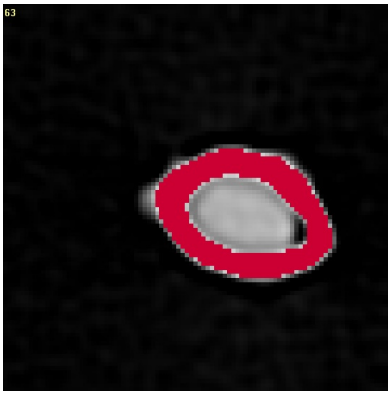


*Fig. 3.3:* Threshold application

A polynomial curve is created from the threshold application. This curve describes the boundary of the bone surface in the selected cross- section and

will be used for the creation of the $3-D$ model.

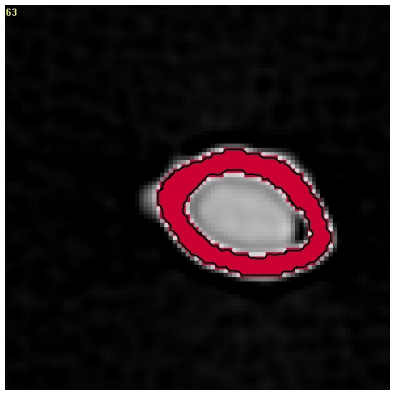


*Fig. 3.4:* Cut application

This general threshold is then applied to every cross- section, to retain consistency of the method. However, each cross- section is specially treated in order to exclude fallacious areas mistaken as bony tissue. In some cases, virtual holes should be corrected in order to include bone regions of lower density, that have been omitted by the general threshold application.

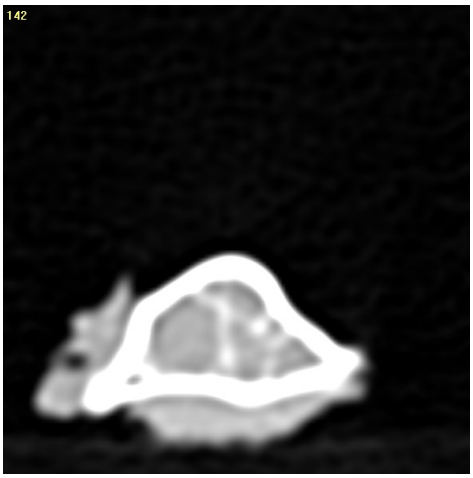


*Fig. 3.5:* Extremity CT slice

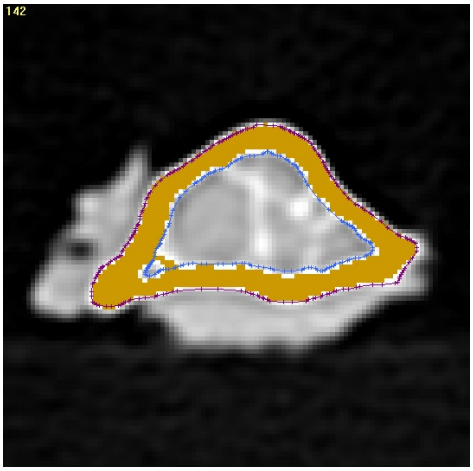


*Fig. 3.6:* Threshold application

When the procedure is completed for each slice, a connective algorithm is applied, as an interpolation between the different cross- sections in order

to create triangular elements for the determination of the three- dimensional surface. This process results in the construction of the first approximation for the outer bone surface. The application of a smoothness algorithm, as described, eliminates artifacts occurred from the internal spaces between the slices and assures continuity. The $3-D$ model of the outer surface of the bone is created, as illustrated in the following image.

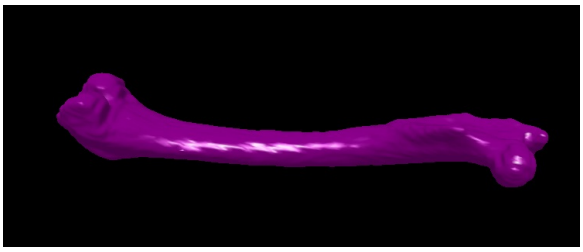

*Fig. 3.7:* 3-D model of the outer surface

The described procedure is repeated for the inner surface of the bone, which separates the cancelous from the trabecular tissue. In the diaphysis region, where the inner volume of the bone is vacant, the procedure is accomplished as described. However, in the extremities of the bone, where the trabecular and cancelous density do not differ significantly, the procedure is more complicated. Bibliographic images and anatomy documentaries have been used in order to set an accurate threshold for those regions. The further steps are performed similarly to the outer surface, resulting in the creation of a corresponding $3-D$ surface of the inner region of the bone.

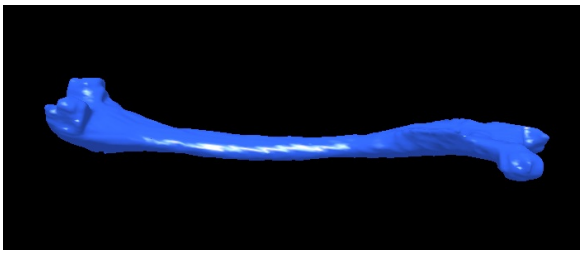

*Fig. 3.8:* 3-D model of the inner surface

This process results in the construction of two $3-D$ surfaces, which define the boundaries of the bone region. The combination of those surfaces

define the volume of the osseus tissue, as illustrated in the following picture, where the surfaces are set to the transparent mode.

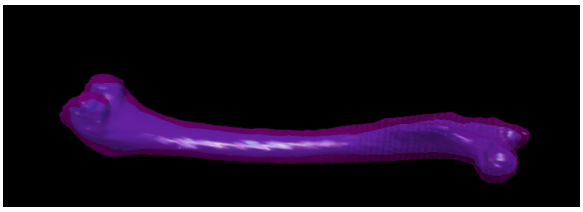

*Fig. 3.9:* Combination of surfaces resulting in the 3-D bone model

The combination of those surfaces results in the definition of the cancelous tissue, that will be used for the mechanical tests of the specimen. The created geometry, after a couple of further processing steps, will be used as the sample geometry for the bending experiments described. The geometry from the $3D$- DOCTOR is extracted in the form of triangular elements after the application of various smoothness filters. The model is extracted as a set of triangular elements, defining the created geometry, in a "ply" format file in order to be inserted in the computational program, Solid Works, for further processing.

## 3.2 Solid Works

### 3.2.1 Geometry Model: Dimensioning

The developed geometry is inserted in the form of triangular elements in the commercial program Solid- Works. The geometry contains two surfaces, which define the inner and outer boundaries of the bone tissue. Once inserted in Solid Works, polynomial curves are created, describing the section defined by the triangular elements of the model. These curves define a set of elementary surfaces that cover both of the boundary surfaces of the bone.

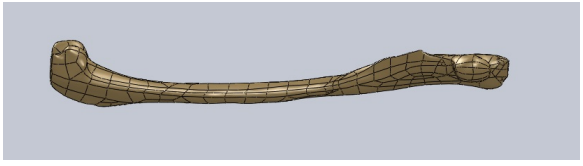

*Fig. 3.10:* Solid Works model for inner surface

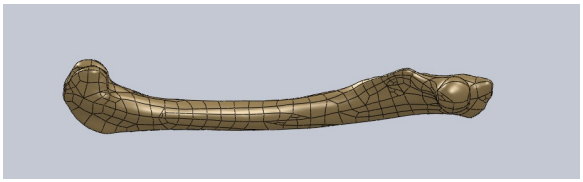

*Fig. 3.11:* Solid Works model for outer surface

When the inner defined volume is extracted from the outer volume, the resulting section represents the actual area of the bone's tissue.

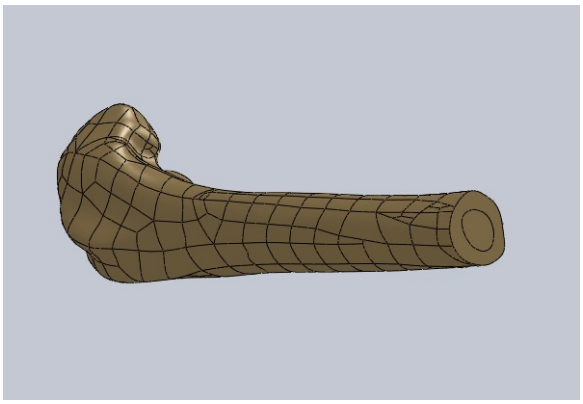

*Fig. 3.12:* Inner and outer defined volumes

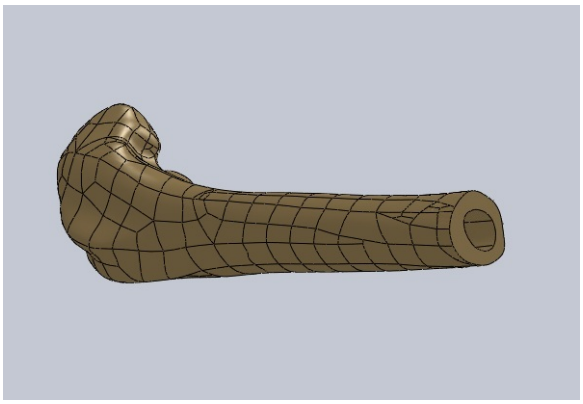

*Fig. 3.13:* Volume of the femur bone's tissue

The developed model is inserted in the Solid Works program, in the angle in which the bone would balance if placed in a horizontal surface. The geometric model created is then subjected to certain dimensioning measurements, in order to verify the agreement between the computational model and the specimen. The first measurement concerns the length of the femur specimen. A pair of auxiliary planes is created, each coinciding with the furthest points of each extremity. Subsequently, the distance between the two planes is calculated through the respective tool of Solid Works, in order to be compared to the experimental data.

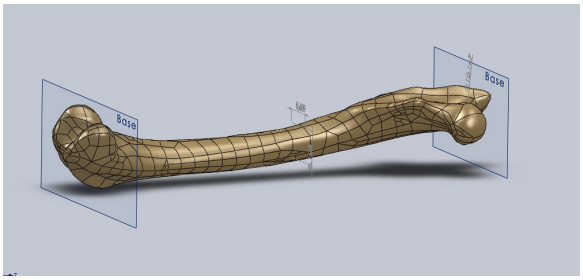


*Fig. 3.14:* Length measurement

During the experimental procedure, a set of diameters are measured, for a selected cross- section of the diaphysis region of the bone. The cylindrical assumption of the diaphysis region, indicate that all the measurements of the diameters should be equal. However, the actual geometry differs significantly from the ideal presentation and there are observable differences between the experimental measurements. The experimental procedure is reproduced with a computational technique. The selected cross- section of the artificial model is identified by locating the plane at the selected distance from the basis plane, so that it coincides with the cross- section at which the experimental measurements are performed. For the defined cross- section, a couple of measurements are performed for the identification of the diameter length. The results of the computational method are then compared with the experimental data, as described with more detail in chapter 5.

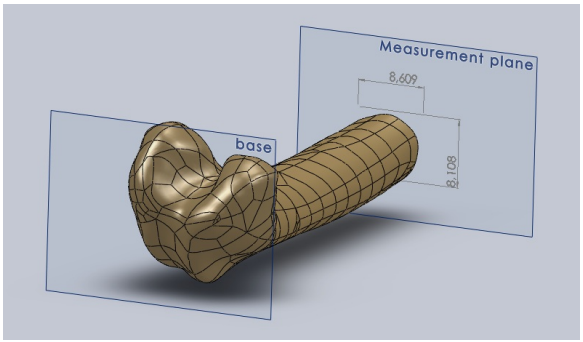


*Fig. 3.15:* Diameter measurement

The third step of the evaluation process concerns the identification of the head diameter of the femur bone. The experimental measurement is performed at the widest region of the head. In the computational model, a set of auxiliary circumcircles are designed around the head region.

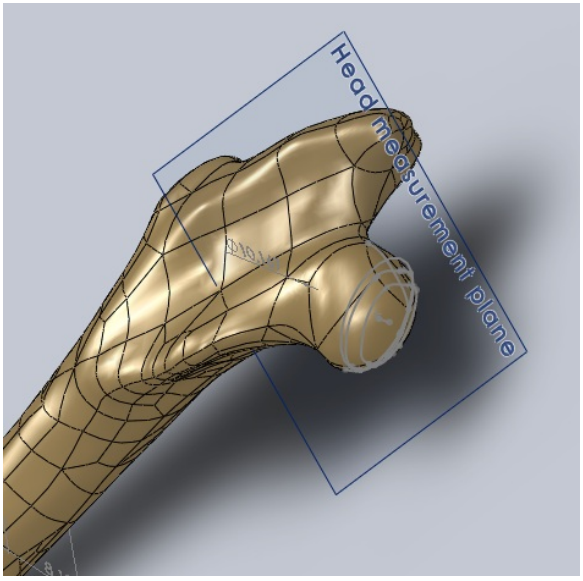


*Fig. 3.16:* Circumcircles around the head

Those circles are utilized for the creation of a sphere, which is coincident to the head. Afterward, the diameter of the sphere is calculated. The computational measurement is compared with the experimental results. A

possible deviation is expected due to the different technique applied for the measurements of the diameter.

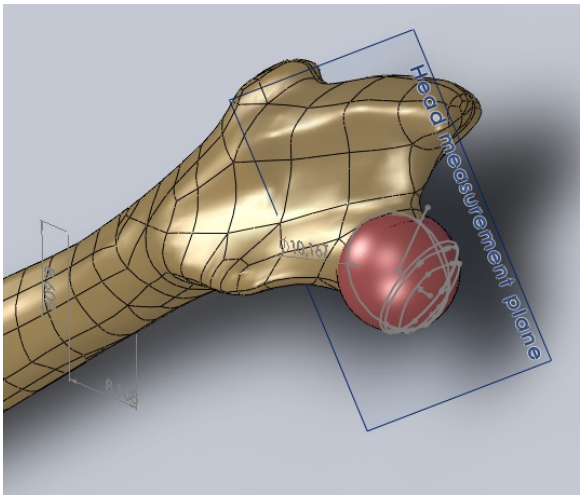


*Fig. 3.17:* Sphere construction

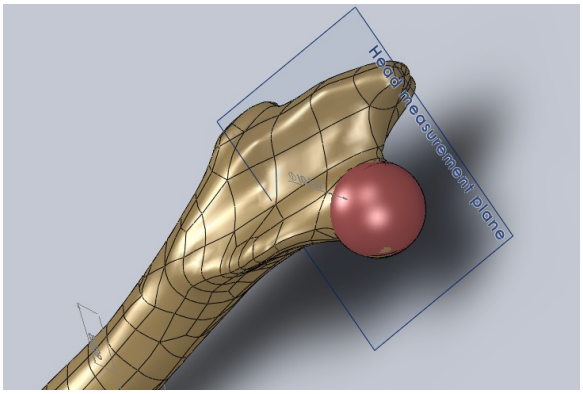


*Fig. 3.18:* Head measurement

The results of the evaluation process are cited in detail in chapter 5, where the confirmation of the model is achieved. The developed model and the actual geometry of the specimen are in satisfactory agreement. As a result, the constructed geometry is appropriate to be subjected in the mechanical tests, simulating the experimental procedure.

### 3.2.2 Geometry of Experimental setup

According to the described procedure, the model simulating the geometry of the femur bone is developed, evaluated and confirmed as consistent with the actual geometry of the specimen. The next phase consists of the conversion of the experimental setups to the computational model. The specimen is already been developed. Accordingly, the supplementary devices should be constructed and added in the mechanical assembly that will be used for the computational experiments.

In order to simulate the experimental procedure, a number of additional mechanical components should be introduced in the computational model. The main auxiliary components represent the support and the loading system, which are inserted as compartments of cylindrical shape. The material of the cylinders is selected to be of hight elasticity modulus, and is considered as non- deformable, compared to the bone's material. The surfaces of contact between the cylinders and the bone are simulated as contacts between deformable and rigid bodies. The location of the support structures should be stable for all the experimental setups, in order to retain consistency. However, since in the case of the free specimen the support system is more difficult to be selected, differences will occur between the embedded and the free specimen.

Another important component of the construction is the resin basis, which are created in the case of the experiments that are performed with the embedded specimen. The purpose of the current study is the evaluation of four different experimental techniques. Consequently, certain properties should be similar in all the experimental methods for the processes to be comparable. The basic properties of the computational experiments should also be consistent with the experimental procedure.

At first, the area of interest, within the diaphysis region has to be identified. The area of interest will be placed among the support structures and will be stable for all the experiments. It contributes significantly to the obtained results and its identification is therefore of major importance. The selected region has to satisfy a number of conditions. First of all, the selected area must belong to the diaphysis area. Hence, the cross- section of the selected area has to be as close as possible to cylindrical.

The part of the bone, that belongs to the region of interest represents almost half of the bone's extend, and is selected, according to the studied cross- sections, so that it contains the majority of the diaphysis area. The

parts outside the region of interest, do not contribute to the mechanical study and can therefore be neglected. Those parts will be at the external side of the support system. In the case of the embedded specimen, those regions will be inserted into the molds, in order to be immersed into the resin material. The next sketch shows the bone separation into the described regions, along with the corresponding dimensions.

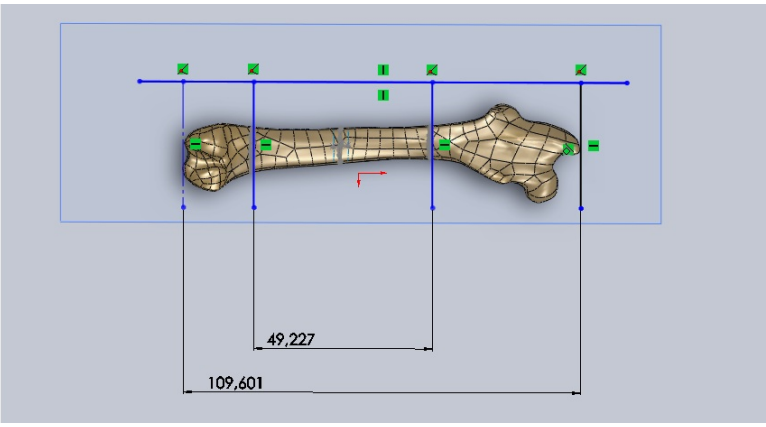


*Fig. 3.19:* Region of interest: Dimensioning

The most important step of the procedure is the selection of the main region. After the completion of this step, the embedding of the specimen can be performed. The embedding area is selected as the area that does not belong in the region of interest. The projection of the metaphysis and the epiphysis regions is sketched on the auxiliary plane that defines the lowest surface of the bone. This projection defines two rectangular areas, corresponding to the two extremities of the bone. The area of the projection of the upper extremity is wider than the area of the lower extremity. Since the embedding parts should be equal, the embedding area will be determined from the upper extremity projection.

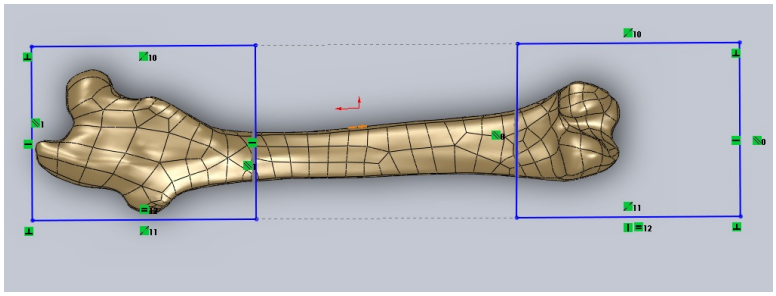

*Fig. 3.20:* Embedding procedure: Definition of projections

Therefore, the two areas are designed by equal and parallel lines that define the rectangular regions of the embedding space. Those regions contain the total projection of both extremities. The computational embedding procedure is completed by the extraction of those areas, so that they cover the entire bone volume. From the two rectangles, the two orthogonal parallelepipeds are reconstructed. The above description defines the principal process for the embedding procedure. Then, the different experimental procedures will be tested on the two specimen types developed: the free specimen and the embedded specimen. The two model specimen are shown in the following images:

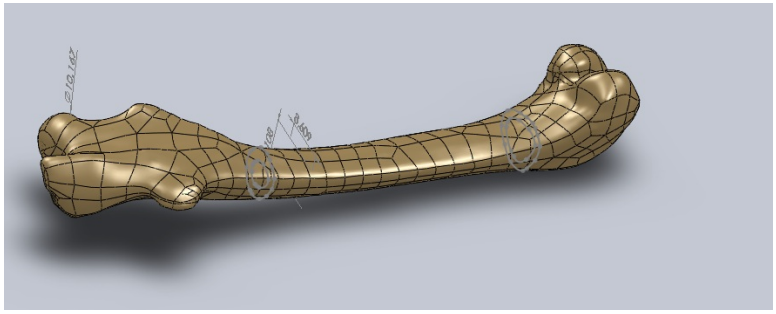

*Fig. 3.21:* Computational model: Free specimen

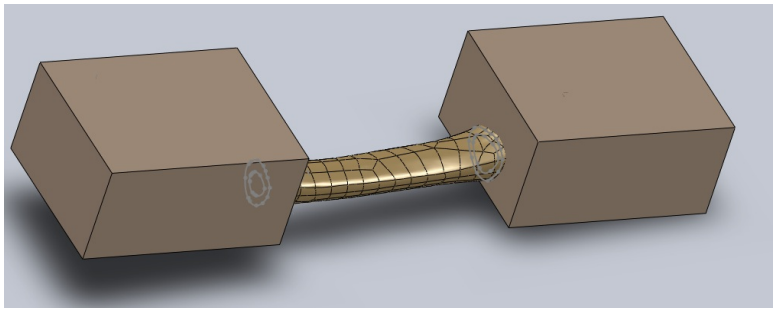

*Fig. 3.22:* Computational model: Embedded specimen

Two different experimental setups should then be applied on each model. The support system will be similar for all the experimental setups. The points of the support cylinders location should be chosen so that the diaphysis is in the region of linear moment, in the case of the three- point bending experiment, or the region of stable moment, in the case of the four- point bending experiment, respectively, as described in chapter 1. The major difference of the two experimental setups is the application of different loading systems.

The positions of the support cylinders will be defined according to the embedded region of the bone. The cylinders will be placed at a selected distance from the plane defined by the internal facets of the auxiliary orthogonal parallelepipeds of resin. In both experiments, the cylinders should be placed equidistant from the central cross- section of the diaphysis. As a result, the distance from the internal facet plane will be equal for both sides.

The central cross- section of the diaphysis is defined during the loading procedure of the three- point bending experiment. The central cross- section is identified as the region of maximum deformation of the curved region of the diaphysis. At a selected lateral view, this point is identified as the point of maximum distance from the horizontal axis of the bone. The central cross- section is placed at the middle of the distance between the embedding parallelipeds. The three- point bending experiment requires the definition of an actuator point, at which the load will be applied. The load application point is defined by a cylindric compartment, respectively to the support system. This point will be placed in the middle cross- section of the region of interest, so that it is equidistant from the parallelepipeds' facets. Both in the embedded and in the free specimen, the point of load application will remain the same, at the central cross- section of the diaphysis region.

The point of the load application is defined as the intersection point of

the diagonal lines drawn from the internal edges of the orthogonal parallelepipeds. A sketch of the central point determination is given below.

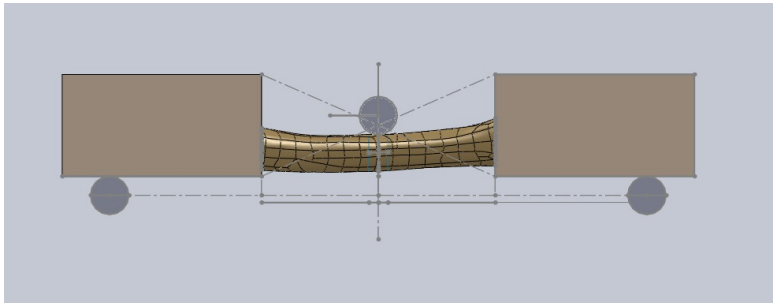

*Fig. 3.23:* Experimental design: 3 point bending, embedded specimen

This procedure cannot be reproduced in the case of the free specimen. For this reason, the central cross- section will be defined as the cross- section of the maximum deformation of the diaphysis curve, as in the case of the three- point bending experiment. Representative distances are measured for each procedure, in order to retain consistency between the different experiments.

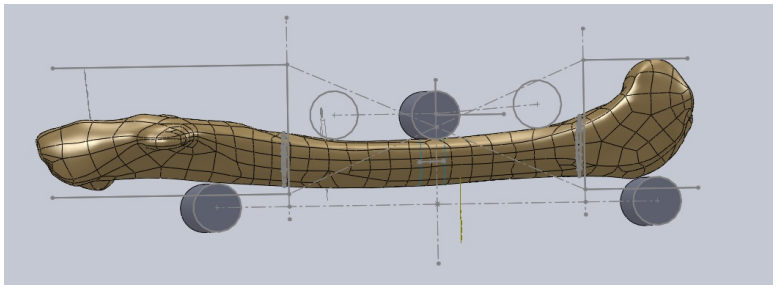

*Fig. 3.24:* Experimental design: 3 point bending, free specimen

The three- point bending experiment requires the definition of an actuator, while the four- point bending experiment requires the definition of an actuator pair. The actuator pair is defined by a pair of cylindrical compartments, so that they are equidistant from the central cross- section of the diaphysis. The location of the points, at which the actuators will be placed, is also defined by the resin orthogonal parallelepipeds internal facet. The distance of loading application from the internal facets is equal to the distance

of the support application from the external facets. As a result, the distance from the internal facets is defined through the length of the parallelepipeds and the distance of the support system from their internal facets. The sketch of the described procedure for the pair actuator determination is given below.

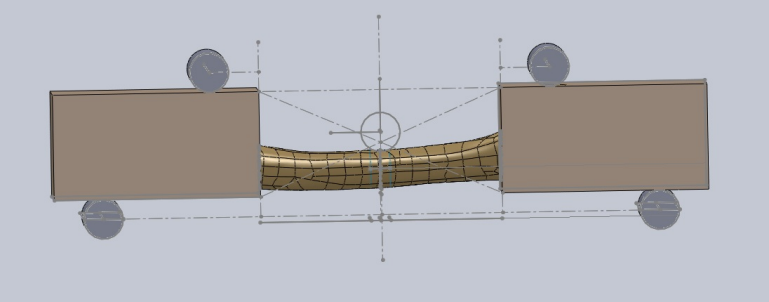

*Fig. 3.25:* Experimental design: 4 point bending, embedded specimen

In the case of the free specimen, the procedure cannot be reproduced. As described in the three- point bending construction, the central cross-section will be defined as the cross- section of the maximum draft of the diaphysis curve and will be placed in the middle of the region of interest. The support system of the bone will be based on the designed support system for the case of the three- point bending experiment of the free specimen. The loading points will be selected in order to be equidistant from the central cross- section and at the same height level. This requirement is of high significance, since the actuator pair should be synchronized. The described procedure is consistent with the experimental procedure of the support and loading systems' definition.

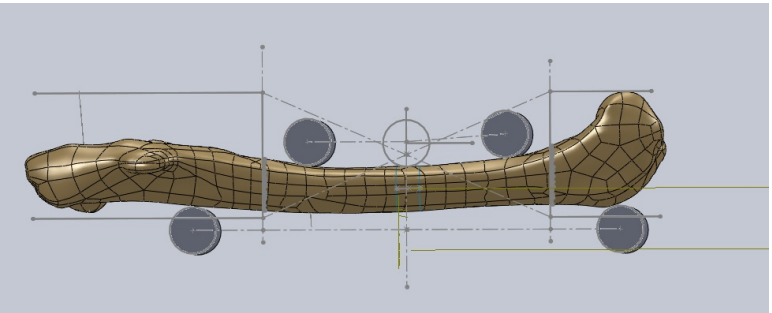

*Fig. 3.26:* Experimental design: 4 point bending, free specimen

# 4. COMPUTATIONAL MODEL: SIMULATION OF EXPERIMENTAL PROCEDURE

The simulation of the experimental procedure will be performed through the commercial program ANSYS. ANSYS is a computational program that uses finite element analysis to simulate physical processes. Different mechanical problems, described by a set of differential equations, can be solved through ANSYS analysis, as described in detail in chapter 1. More information on the solver and the finite element method of ANSYS is given in the Appendix 1.

## *4.1 Techniques used*

The computational analysis, performed through ANSYS, requires a number of steps. The first phase of the analysis contains the construction of the geometry of the model. The geometry is defined by a set of points, forming lines, areas and volumes. The typical procedure requires the determination of a coordinate system, according to which the parts of the designed geometry will be defined. The points defined will be used for the determination of the nodes of the elements, in the meshing procedure. At the current study, the geometry of the model is defined from the external file, received from the $3D$- DOCTOR and the Solid Works analysis. As a result, the first phase is carried out by defining the input file from which the geometry will be constructed.

Since ANSYS is a finite element based program, the next step requires the definition of the element properties. The type of element is first selected, according to the geometry and its separation in elementary parts. The element type should be carefully chosen for the analysis to be accurate. Different types of elements, for example two- dimensional or three- dimensional elements define different problem solutions. The number of used elements is defined during the meshing procedure.

Another important step is the material definition. The materials used are defined for each compartment of the mechanical construction. The type of the material is first chosen, according to the mechanical properties of each part. The most common materials are defined as linear elastic, or linear elastic perfectly plastic. In the current study, rigid parts are defined as non-deformable. The deformable parts are defined either as linear elastic, such as the resin parts, or as linear elastic perfectly plastic, as the bone's parts. The data used for the material definition are received from previous experimental data and bibliography.

After the definition of the materials and the elements used, the grid of the solution should be defined. Since the element type is already selected, the grid is defined by the number of elements used. The selection of this number is important for the convergence of the problem. If a high enough number is chosen the problem will not be able to be solved in a rational time period. On the other side, a selection of a small enough number will provide non- accurate results. For those reasons, a parametric study should be made for the determination of a suitable number of elements. The problem is first solved for a small number of elements. Then the procedure is repeated, with densification of the nodes used. At each solution a characteristic measurement is stored in order to verify the convergence if the solution. If the finite element analysis is accurate, densification of the nodes should result in stabilization of the characteristic measurement and accordingly stabilization of the received solution.

The next step consists of the loading and support definition. The support system should be carefully defined, for the model to be sufficiently supported in order to be mechanically consistent and solvable. The load application is an important step for the determination of a correct solution that corresponds to the actual mechanical problem. For example, in the case of the four- point bending procedure of the free specimen, the determination of the loading system is rather complex, in order to retain a synchronized loading procedure that would be consistent with the experimental process.

After the definition of the above critical properties, the mechanical model is ready to be solved. Then, the solution parameters should be selected. Depending on the nature of the mechanical problem, different solution parameters are important. Those options are important for the elimination of the duration of the solution procedure. The parametric analysis is also highly affecting this part of the process and is therefore representing a procedure of high significance for the convergence speed. The solving parameter settings

control the solving technique, whether an iterative or direct solution will be used, the steps of the solution, as well as the stored information at each step. Commonly, the important data are collected after the convergence of the solution. The convergence is defined from the difference of characteristic measurements between two iterative steps, that should be under a selected quantity.

The last phase of the ANSYS analysis consists of the data processing. The results received from the finite element analysis are stored in a general database and the valuable information should be extracted in order to be used. The most useful results concern the stress and strain concentration, from which the strain- stress curve is designed in order to be compared with the experimental results.

## 4.2 Model details

### 4.2.1 Geometry construction

As already mentioned, the geometry of the computational model is defined by an external file, created through the Solid Works program. The geometry data are introduced into the ANSYS analysis as an input file, defined in the beginning of the analysis. The input file contains the information for the geometry construction. First of all, the keypoints of the geometry are introduced, from which the geometric areas and the corresponding volumes are defined. The model contains different separated volumes, according to the experimental setup studied. Generally, the bones areas, the embedding areas and the loading- support cylinders are independently defined.

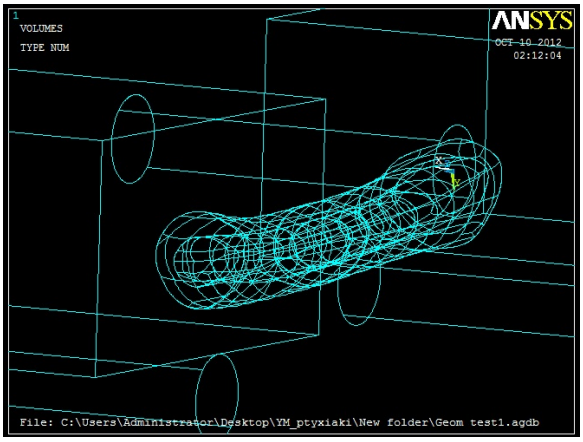


*Fig. 4.1:* Geometry structure, as inserted through Solid Works: area definition

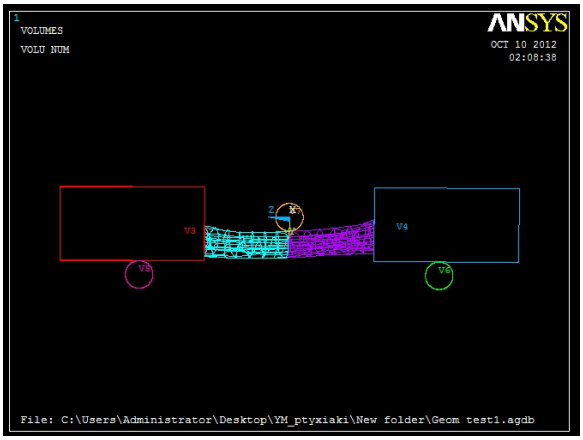


*Fig. 4.2:* Geometry structure, as inserted through Solid Works: volume definition

The bone, as well as the embedding areas should be defined as a consistent body, since they cannot be separated after the embedding procedure. For this reason, the areas which are not defined by the same volume are joined together by the following technique. Each volume is defined by a set of keypoints. Within the areas that need to be joined, the keypoints of each volume coincide with the keypoints of the corresponding volume. A function is applied to those keypoints, which replaces the pair of keypoints that are separated by a distance below a selected threshold, with a single keypoint.

Through this procedure, the required volumes are glued and are handled by the program as a united body.

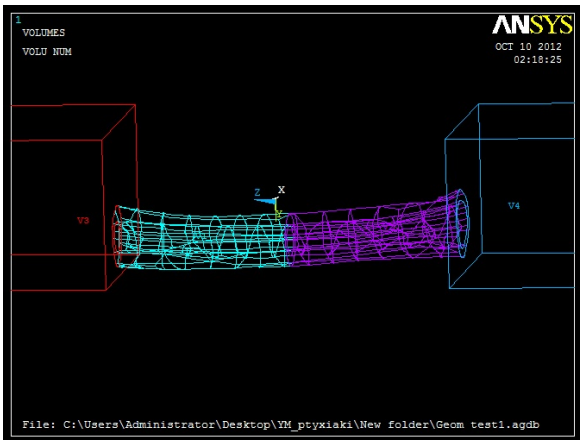


*Fig. 4.3:* Joined specimen parts

### *4.2.2 Element and material properties*

The elements selected for the separation of the volumes are the same for the finite element analysis of every experimental setup. The mechanical process is not linear. As a result, the selection of elements with midpoints are not accurate and would only cause useless delay, since it would not contribute to the result approach. Therefore, the selected elements are defined by nodes which are placed only in the edges of each element. The three- dimensional model indicates a use of three- dimensional elements. As a result, there are used elements of *Solid*183 type. The elements are chosen to be triangular three- dimensional, as illustrated by the following sketch:

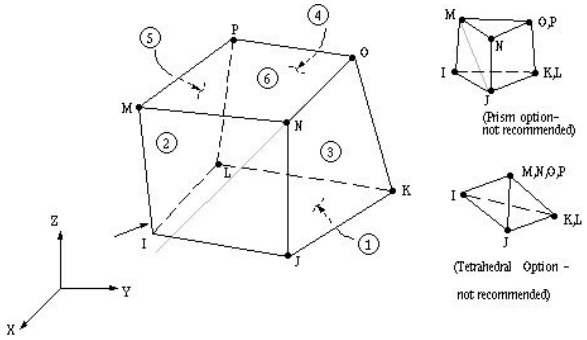


*Fig. 4.4:* Element Solid185

There will be used three types of materials in the current study: the bone material, the resin material and the cylinders' material. The simulated material of the cylinders, which are considered as rigid bodies, is steel and is defined as linear elastic, characterized by a modulus of elasticity of $110GPa$. The mechanical properties of the steel are estimated by the relative bibliography. The resin material is also defined as linear elastic. The modulus of elasticity is defined at $0,992GPa$, as derived from the experimental study of the resin material used in the experimental procedure. The bone material is simulated as linear elastic perfectly plastic material. The values of the elasticity modulus, $17GPa$, and the yield strength, $130MPa$, are also defined by the bibliographic studies.

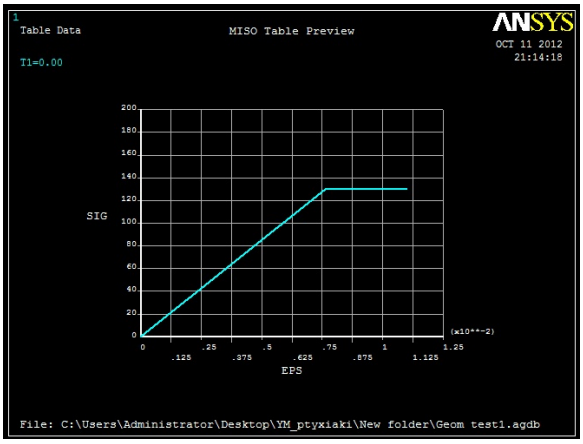


*Fig. 4.5:* Bone material definition

Then, the type of contact elements is defined, for each pair of contact area. The contact element technique, is a method used by ANSYS program in order to identify the forces developed during a mechanical procedure, between two areas of contact. The contact elements will be used in the current study for the definition of the contact behavior between the support system and the specimen and the contact behavior between the loading system and the specimen. In both cases, the cylinder volume should not penetrate in the specimen volume. At the same time, the surfaces of the cylinders and of the specimen should remain in contact and not be separated, during the experimental procedure.

The loading cylinder is meshed as an one- element contact, and more specifically as a rigid cylindrical element. The contact element technique, used for the loading cylinder simulation, requires that the distance between the specimen surface and the external cylinder surface should remain stable. This requirement is achieved by controlling the developed forces between the two surfaces element, so that this distance is allowed to remain between certain limitations. At each step of the procedure, a new force is applied, so that the model satisfies the above requirement.

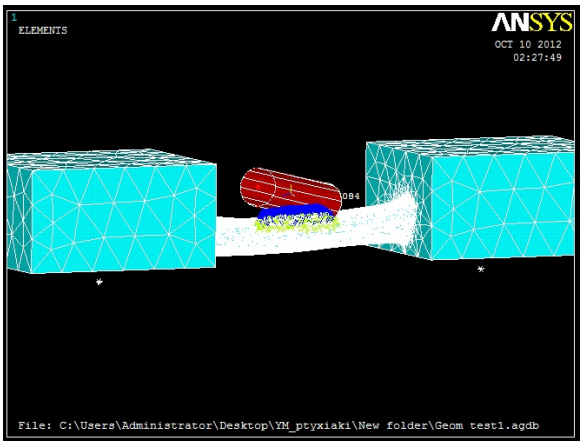


*Fig. 4.6:* Contact elements: loading cylinder

The support system is simulated by an ideal system of a spherical and roller support. The center of each support cylinder is immobilized. Then, a contact relation is imposed for each contact element surface pair, so that the mechanical requirements are satisfied. According to the type of support, all the degrees of freedom are restricted except from those that remain free

in each support system. The contact element technique imposes a developed force of the contact surfaces, which reserves the distances at the restricted degrees of freedom stable, so that the surfaces remain in contact during the experimental procedure simulation.

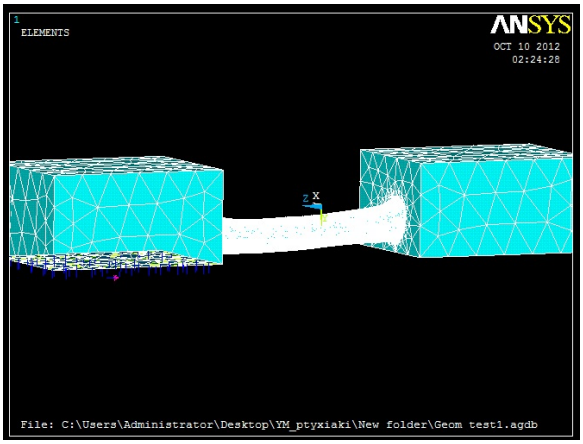


*Fig. 4.7:* Contact elements: support system

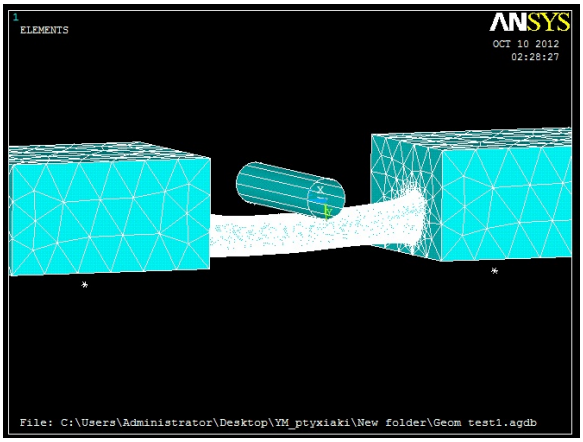


*Fig. 4.8:* Contact element general structure

### *4.2.3 Meshing of the model*

Once the element and material definitions are completed, the meshing of the model is easily performed. The number of elements is the least possible

number of elements, for which a consistent solution is obtained. The cylinders are meshed with a single element, since no deformation occurs within those regions, due to the high elasticity modulus. The resin areas are meshed with the largest elements allowed, in order to receive an accurate solution. It is important to keep the number of elements as small as possible in order to accelerate the solution procedure. However, in the bone region the elements are chosen to be much denser in order to describe the complex geometry as accurately as possible.

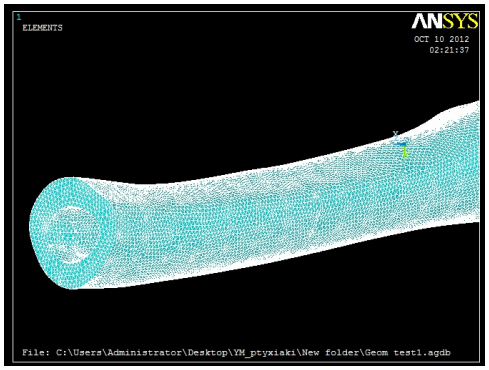


*Fig. 4.9:* Meshing of bone area

A parametric analysis is required for the definition of the most convenient number of elements. The divergence of the solution must decrease with the increase of the number of elements. Once the convergent behavior is assured, the number of elements is selected as the one that gives an absolute error lower that the required one, between two steps of element densification. The meshing procedure is completed when the number of elements is identified for the optimized convergent behavior.

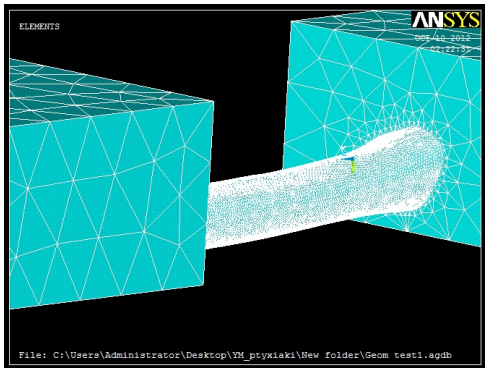


*Fig. 4.10:* Meshing of embedded parts

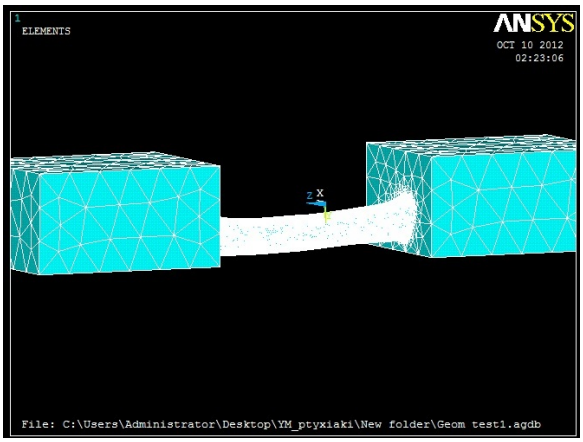


*Fig. 4.11:* Meshing of the model

### *4.2.4 Loading and support definition*

The loading and support systems are both defined through the relations imposed between the specimen and the corresponding cylinders. Both the support and the loading conditions are imposed as deformation conditions and the developed loading, or the developed stress respectively, is measured at each step of the procedure. The loading is applied through the actuator point, or the actuator pair, according to the experimental procedure. In the case of an actuator pair the displacement is synchronized between the two points of loading application.

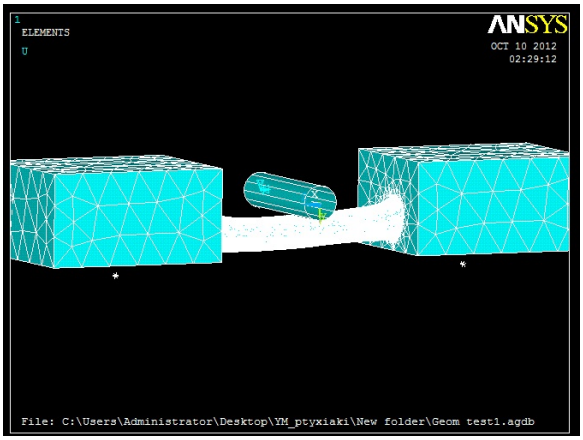


*Fig. 4.12:* Loading definition

A maximum displacement is imposed at each loading cylinder. Then, the displacement of each loading step is defined, or the number of the total steps until the maximum displacement is defined. At each step a stable displacement is imposed and the developed stress in measured after the convergence of the system.

The support system is characterized by two different constrains, which simulate spherical (pin) and roller type support. The roller support allows two degrees of freedom, a horizontal displacement and a rotation around a certain axis. The spherical support allows only one degree of freedom, the rotation around a certain axis. As a result, in the cylinder where the roller support is applied, all the degrees of freedom are constrained except from a horizontal displacement and a rotation. The constrains are represented by setting the distance between the cylinder and the specimen as stable and zero, for the degrees of freedom that are restricted. Respectively, in the cylinder where the spherical support is applied, all the degrees of freedom are constrained except from a rotation.

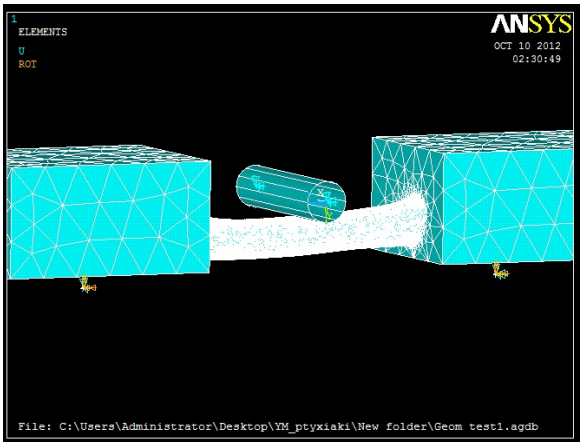


*Fig. 4.13:* Support definition

### *4.2.5 Solution and data acquisition*

Then, the computational model is completely defined. The program runs each case for the different experimental setups. A couple of parameters are defined, in order to optimize the solving procedure. For the current study, those parameters are stable for all the experimental setups. High deformations are allowed during the solution procedure, due to the complexity of the model. The number of substeps in each iteration step is selected to be adjusted at each step, in order to accelerate the solving procedure. The results are stored in each step of the procedure, after the convergence is achieved.

For the three- point bending experiment, the most important cross- section is the central cross- section. For this reason, the stress and strain values are calculated for each point of the central cross- section.

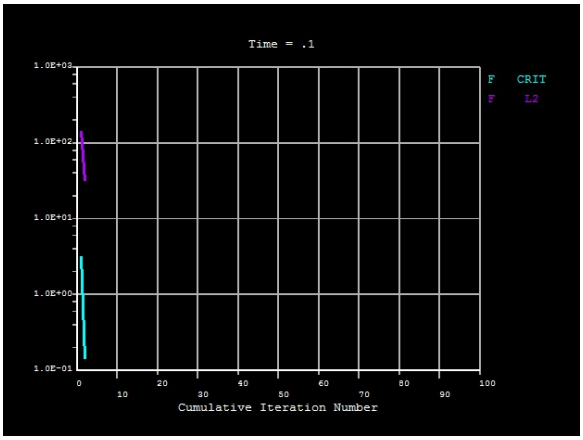


*Fig. 4.14:* Diagram of solution convergence criteria

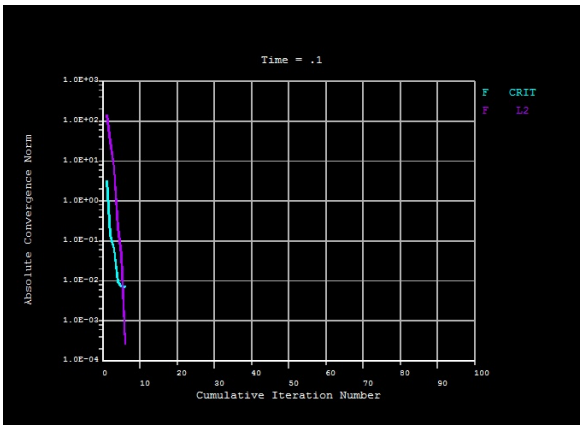


*Fig. 4.15:* Criteria of solution convergence for first step accomplished

### *4.2.6 Parametrization study*

#### *Cylinder position*

The distance of the support cylinder system from the faces of the resin parallelepipeds is a parameter that should be tested. Since, there is no optimized position for the cylinder's location, two possible positions will be compared in order to illustrate the influence of this distance to the results. The parameter of the position of the support system will be tested on the three- point bending experiment for the embedded specimen. For the exper-

imental setups used for the main part of the study, the distance of $20mm$ between the loading and the support system will be selected in order to retain consistency with the real experimental procedure.

The characteristic value that will be used for each parametrization test, is the stress distribution in the central cross- section of the diaphysis. The central cut applied in the bone volume, allows the determination of the stress distribution across the central cross- section. In the three- point bending experiment, where the load application position is stable and the fracture is expected to commence at this stable point of load application, where the maximum moment appear, the stress distribution at this point is a characteristic measurement. For the same material, the modulus of elasticity is constant, as well as the moment of inertia for stable cross- section. Also, the developed moment is stable since the maximum moment appears at the central cross- section. As a result, the stress measurement depends on the tested parameter and represents a useful comparative value. The stress distribution will be stored for each parametric case and compared for the different cases in study.

*Resin material*

The material of the resin parallelepipeds is in question, due to the possible affects in the specimen response to the experimental procedure. Because of the high practical importance of the experiment application on the embedded specimen, the result of this parametric study is significantly important. Two types of resin material will be used, in the case of the three- point bending experiment. The first type of the resin material has properties similar to the bone tissue mechanical properties. The results of the above material simulation will be compared to the results of a resin material, which corresponds to the actual material used during the experimental procedure. In the main part of the study, the resin material used during the experimental procedure will be used.

*Meshing*

As mentioned in the meshing description, the selection of the elements size is of high importance for the computational study of each mechanical procedure. For the current study, a number of different meshing selections will be used is order to test the effect of the meshing to the results. The maxi-

mum developed stress in the central cross- section will be studied respectively to the increment of the elements numbers. As the number of elements is increasing, the expected result is a stabilization of the stress distribution, which converges in a constant value. This value represents the optimized approach of the real stress value. According to the minimum acceptable deviation, the suitable meshing for the model is selected.

*Contact element parameters*

The most important factor of control at the contact element analysis, is the tangent penalty stiffness factor (FKN). For the augmented Lagrangian method, which is used at the current contact element analysis, the normal and tangential contact stiffnesses are required. The amount of penetration between contact and target surfaces depends on the normal stiffness. The amount of slip between contact surfaces depends on the tangential stiffness. Higher stiffness values decrease the amount of penetration and slip, but can lead to ill- conditioning of the global stiffness matrix and to convergence difficulties. Lower stiffness values risk to produce an inaccurate solution. Ideally, a high enough stiffness is requested for the penetration and slip to be acceptably small, and a low enough stiffness for the problem to be well-behaved in terms of convergence. The FKN factor represents a parameter which needs to be tested. In the current study a FKN parameter of 0.1 will be used at the first study and it will be progressively increased. The maximum developed stress at the central cross- section, will be compared for each FKN value and the most suitable value will be selected to be applied in the four different experimental setups.

### *4.2.7 Experimental specifications*

The two experiments are applied to both specimen types, to the embedded specimen, as well as to the free specimen. The different geometries for each case has been developed through Solid Works, as described in the previous chapter. The differences that each experimental setup introduces concerns mainly the loading and support procedure. This modification also affect the contact element definition. The element and material definition and the meshing procedure are not significantly affected.

In the case of the free specimen, there are a couple of supplementary modifications of the model. The material definition is restricted to the bone

material and the defined volumes concern merely the bone area. For this reason, the procedure of keypoint merging, described at the geometry construction, is of higher significance in the case of the free specimen, since the bone volumes should be joined consistently. The contact elements are modified so that the support system is in contact with the bone surface instead of the resin parallelepipeds.

*Three point bending details*

The three point bending is the first tested experimental setup. The parametric studies are applied in this particular experiment. As a result, the most suitable parameters are selected for the optimization of the solution. In the case of the three- point bending experiment, for the embedded specimen, the support and loading systems are constantly defined. The only parameter, which is free to be identified, is the maximum loading applied. The maximum deformation applied, which represents the maximum loading, is selected in the three- point bending procedure, so that the experimental procedure leads to a mechanical fracture. The material definition according to bibliographic data, defines the ultimate strength of the specimen. As a result, the applied deformation should be selected do that the maximum developed stress overcomes this stress value. From the solution data, the maximum moment developed in the bone is defined. The maximum moment is expected to be developed in the central cross- section, where the fracture should also appear.

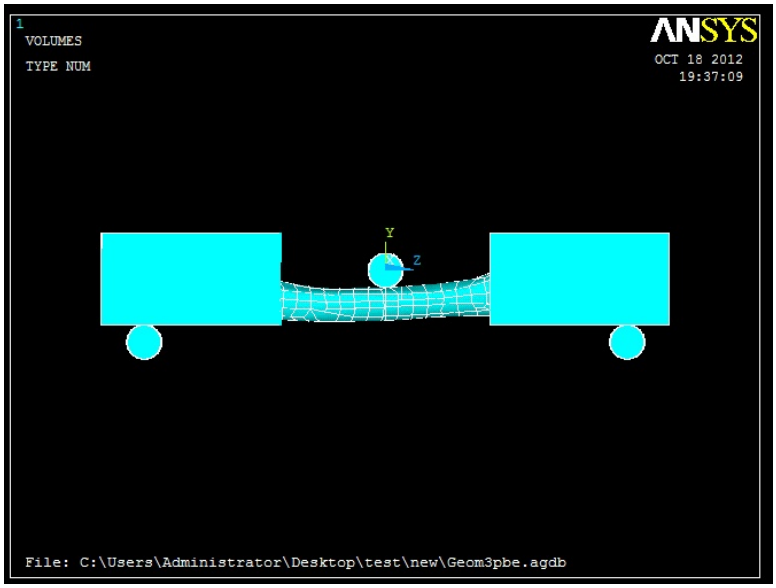


*Fig. 4.16:* Three- point bending experiment

*Four point bending details*

In the case of the four- point bending experiment, the parameters are selected to be consistent with the three- point bending experiment. The support system is constant and the maximum loading should also be identified. Since the elasticity modulus and the moment of inertia are stable, the maximum moment defines the mechanical behavior of the specimen. In order to keep the experimental procedure consistent between the different experimental setups, the maximum applied deformation will be defined from the maximum developed moment. This maximum moment should be defined from the measured maximum moment of the three- point bending experiment.

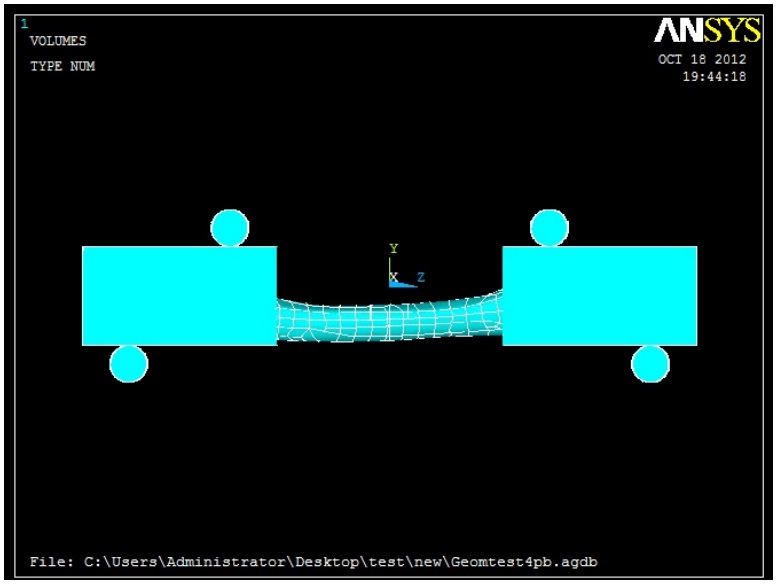


*Fig. 4.17:* Four- point bending experiment

# 5. RESULTS

## *5.1 3D reconstruction*

The geometry developed through the $3D$- DOCTOR program requires to be evaluated in order to confirm the correspondence of the model with the actual specimen. The importance of an accurate geometry is of high significance, since the results of the mechanical tests highly depend on the geometry of the bone. The first phase of the evaluation contains the regulation of the general geometrical characteristics of the specimen. The model should be consistent with the anatomy described in the first chapter.

A set of photos of the specimen, taken during the experimental procedure will be used for the first step of the evaluation process. A number of those photos are cited in the following study, in comparison with the corresponding images from the developed model. For each point of view, the photo of the model is cited along with a $3D$- DOCTOR picture and a Solid Works picture of the developed geometry. Important characteristic regions of the bone, such as the head of the femur, the condyles and the diaphysis region are cited, in order to indicate the correspondence of the model with the specimen.

The second phase of the evaluation contains the measurement of characteristic quantities of the specimen, as described in chapter 3. The geometrical features of the femur bone are calculated with two independent methods. From the computational model, the measurements of important typical quantities are obtained through the described procedure. The specimen is also measured experimentally, in consistency with the computational method. The computational results will be tested, supplementary to the image identification of important bone's regions, in order to verify the agreement with the experimental measurements.

### 5.1.1 Image verification

The first selected perspective is the anterior surface of the left femur bone. Within the first set of images, the geometry of the head, the neck, the lesser and the greater trochanter are shown. The magnitude of the images though, does not allow high precision in the comparison between the computational model and the specimen. However, the basic geometrical features indicate satisfactory agreement between the computational and the experimental features of the bone.

*Fig. 5.1:* Specimen anterior surface

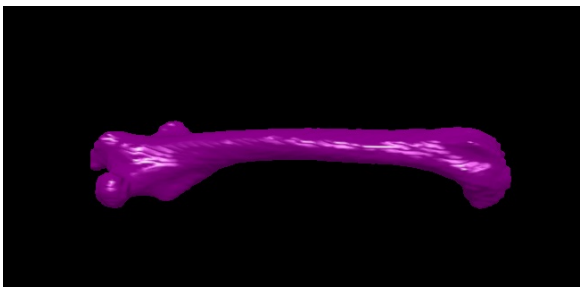

*Fig. 5.2:* 3*D*- DOCTOR anterior surface

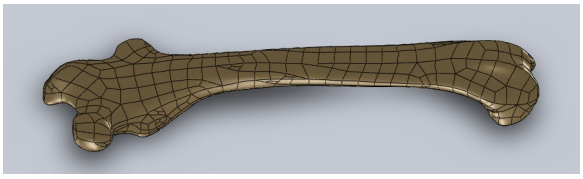

*Fig. 5.3:* Solid Works anterior surface

The second perspective also presents the anterior surface of the bone with more precision in the trochanter surfaces. This point of view allows a further study of the upper extremity. The view does not contribute much more information than the first set of images, for the evaluation process, but confirms the agreement between the computational and the experimental features of the bone.

*Fig. 5.4:* Specimen anterior surface, trochanters

*Fig. 5.5:* 3*D*- DOCTOR anterior surface, trochanters

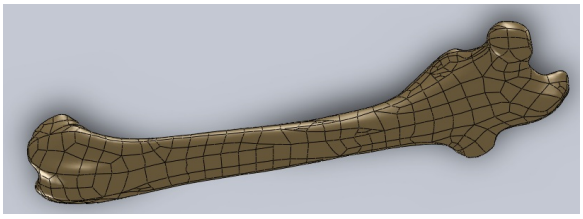

*Fig. 5.6:* Solid Works anterior surface, trochanters

The third selected perspective represents the posterior surface of the bone. The condyles are shown in detail, as well as the compartments of the upper extremity. The geometry of the lower extremity is shown in more details. There is not any observable dissimilarity between the computational model and the actual geometry. However, the agreement cannot be certified with high accuracy through image comparison.

*Fig. 5.7:* Specimen posterior surface

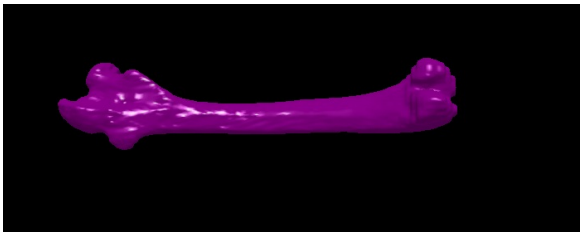

*Fig. 5.8:* 3*D*- DOCTOR posterior surface

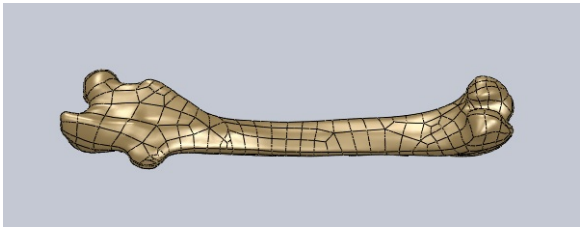

*Fig. 5.9:* Solid Works posterior surface

The next point of view, represents a lateral surface of the bone. Both extremities are shown, in low detail. The importance of this particular view concerns the curvature of the diaphysis. The diaphysis is the region of main interest for the mechanical tests applied. The curvature of the femur, at this region, is responsible for the mechanical properties that affect the bone response in different mechanical loadings. Through the lateral perspective, the agreement of the diaphysis curvature between the computational model and the specimen is confirmed.

*Fig. 5.10:* Specimen lateral surface

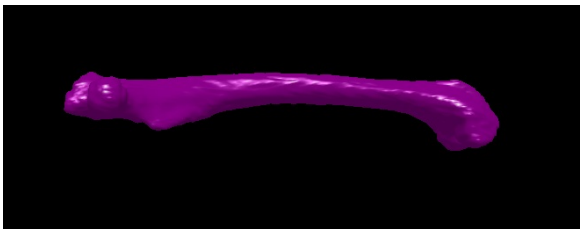

*Fig. 5.11:* 3*D*- DOCTOR lateral surface

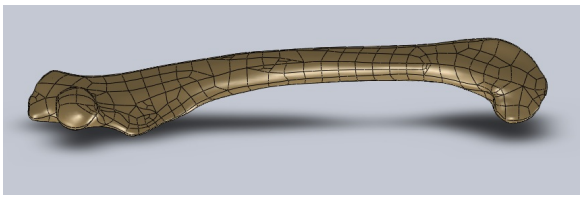

*Fig. 5.12:* Solid Works lateral surface

The next set of images, concern details of characteristic regions of the femur, that are important for the mechanical properties of the bone. The main comparable regions include the head of the femur, which is also used for the numerical measurements, and the condyles. The next images contain a more detailed view of the condyles region, for further examination.

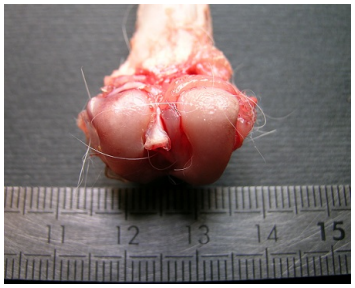


*Fig. 5.13:* Specimen condyles

*Fig. 5.14:* 3*D*- DOCTOR condyles

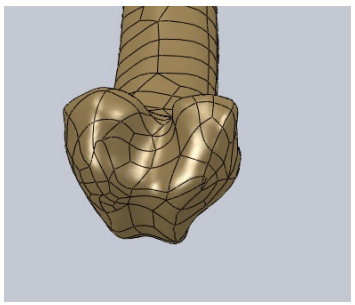

*Fig. 5.15:* Solid Works condyles

The last examined perspective represents the head of the femur. The spherical approximation of the head, performed in the measurement verification, is justified by the geometry of the head illustrated both in the specimen images and the computational model.


*Fig. 5.16:* Specimen head

*Fig. 5.17:* 3*D*- DOCTOR head

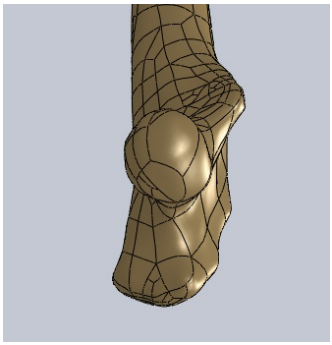

*Fig. 5.18:* Solid Works head

### *5.1.2 Characteristic measurement verification*

For the numerical evaluation of the model, the computational and the experimental measurements are compared. The evaluation procedure, described in chapter 3, results in a number of measurements for the geometric features of the bone. The conclusions of those measurements are cited in the next table. The experimental measurements along with the computational measurements for the length, the mean diameter of the bone and the diameter of the head are given in detail.

| Data | Computational | Experimental | Deviation |
|---|---|---|---|
| Specimen Length | 10.17 | 10.15 | 0.2% |
| Diaphysis Diameter- lateral- | 8.61 | 8.89 | 3% |
| Diaphysis Diameter- anteroposterior- | 8.12 | 7.88 | 3% |
| Diaphysis Thickness | 1.53 | 1.49 | 2.6% |
| Head Diameter | 5.08 | 4.94 | 2.8% |

*Tab. 5.1:* Comparison of Measurements

The above results from the comparison of the experimental data with the computational data, verify the validity of the model. The numerical deviation of the geometric measurements do not exceed the 3]%, as received from the above table. These results allow the assumption that the developed geometry is in satisfactory agreement with the actual geometry of the specimen in test.

The above statement is also supported by the comparative study of the experimental photos and the computational snapshots received during the

development of the computational model. At each point of view, for the various cited perspectives, the artificial geometries are in high accordance with the actual geometry, as permitted to be studied by the resolution of the listed images. The main geometrical features of the computational model, also tested by the more objective measurements, also seem in high accuracy with the experimental specimen. As a result, the developed geometry can be considered as a sufficiently accurate representation of the actual geometry and can be used without important limitations for the experimental simulations described.

## 5.2 Simulation of experiments

### 5.2.1 Solid Works experimental models

As described in chapter 3, the four experimental setups, utilized for the simulation of the mechanical tests are developed through the commercial program Solid Works. The geometries of the experimental setups, which contain the specimen geometry along with the auxiliary cylinders for the loading and support system, are shown in the images that are produced through the Solid Works.

The first experimental setup represents the three- point bending experiment performed at the embedded specimen. In the image below, the structure of the specimen, as well as the experimental setup, are illustrated. The central cross- section is defined by the loading point application.

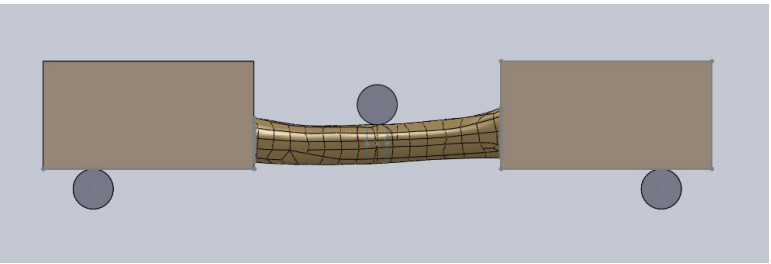

*Fig. 5.19:* Three- point bending of embedded specimen

The second experimental setup represents the four- point bending experiment performed at the embedded specimen. In the image below, the

structure of the specimen, as well as the experimental setup, are illustrated. The actuator pair is placed equilateral to the central cross- section and the loading cylinders are synchronized.

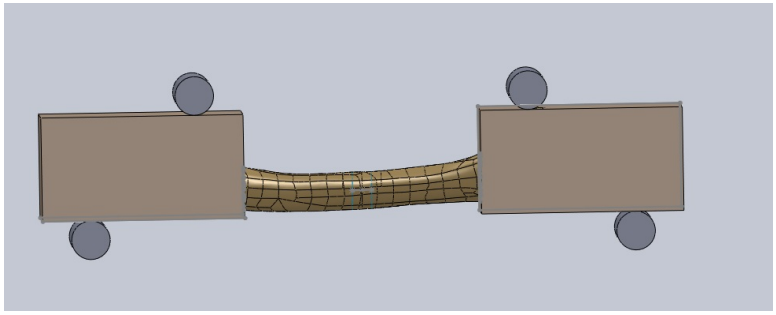

*Fig. 5.20:* Four- point bending of embedded specimen

The third experimental setup represents the three- point bending experiment performed at the free specimen. In the image below, the structure of the specimen, as well as the experimental setup, are illustrated. The loading cylinder is placed at the central cross- section, to retain consistency with the case of the embedded specimen. The support cylinders are placed so that they are equidistant from the central cross- section and at the same height level, for the free specimen to balance at the horizontal position.

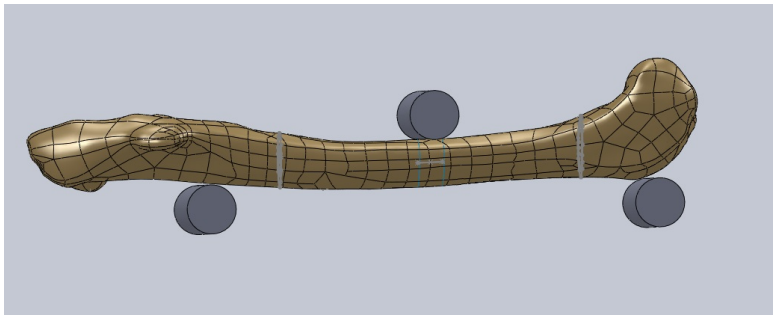

*Fig. 5.21:* Three- point bending of free specimen

The fourth experimental setup represents the four- point bending experiment performed at the free specimen. In the image below, the structure of the specimen, as well as the experimental setup, are illustrated. The support cylinders are placed according to the described procedure for the three- point

bending experiment of the free specimen. The loading cylinders must remain equidistant from the central cross- section and should be synchronized. For this reason they are selected to be almost at the same height level, depending to the complexity of the specimen geometry.

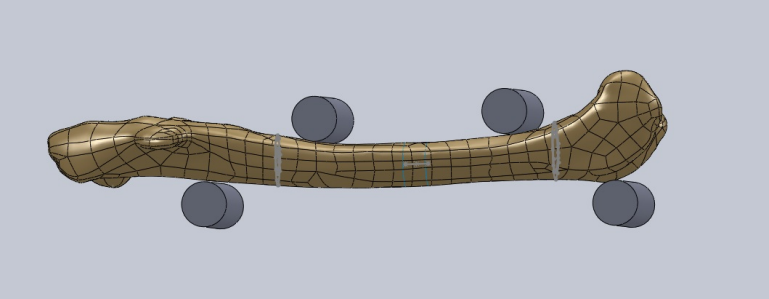

*Fig. 5.22:* Four- point bending of free specimen

### *5.2.2 ANSYS experimental models*

The described geometries are inserted into ANSYS for the simulation of each experimental procedure. Due to programming inconsistencies, related with memory and storage limitations the experimental models are simplified. The major simplification in the case of the embedded specimen is the extraction of the bone volume from the resin regions, as there is not a possible grid for the meshing of the actual model, which would lead to convergence. As a result, the resin regions are considered to be fully occupied by resin material. The four experimental setups, that will be tested, are given in the following sketches, as inserted in ANSYS.

The first experimental setup represents the three- point bending experiment performed at the embedded specimen. In the experimental setup of the following image, the parametric tests would be applied in order to verify the independence of the model from the basic computational parameters.

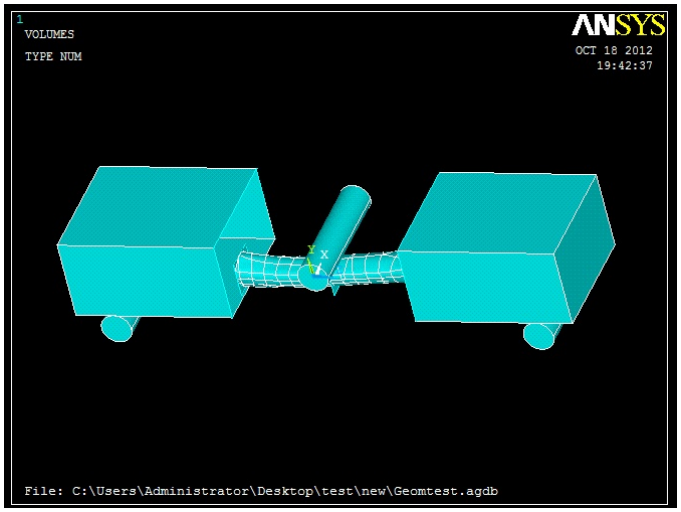


*Fig. 5.23:* Three- point bending of embedded specimen

The second experimental setup represents the four- point bending experiment also performed at the embedded specimen.

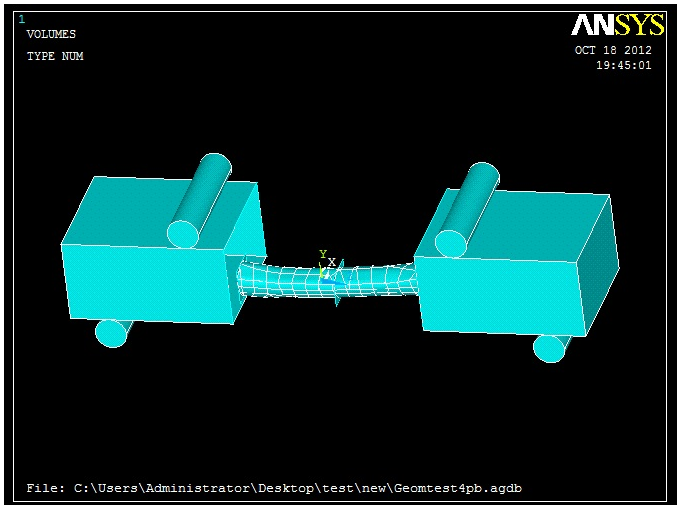


*Fig. 5.24:* Four- point bending of embedded specimen

The third experimental setup represents the three- point bending experiment performed at the free specimen.

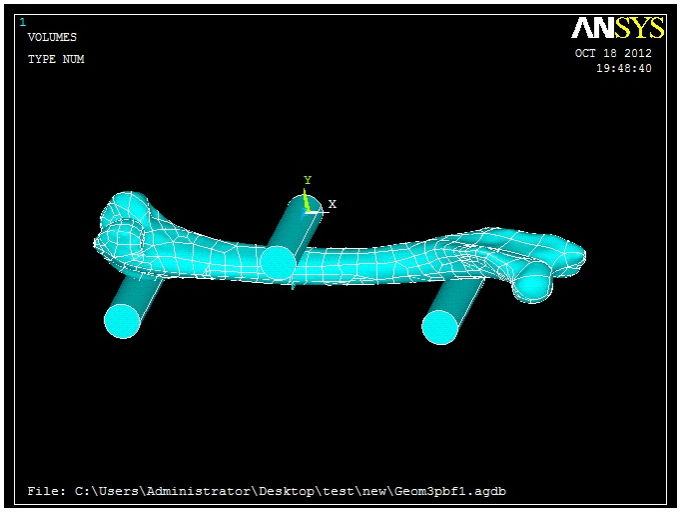


*Fig. 5.25:* Three- point bending of free specimen

The fourth experimental setup represents the four- point bending experiment performed at the free specimen.

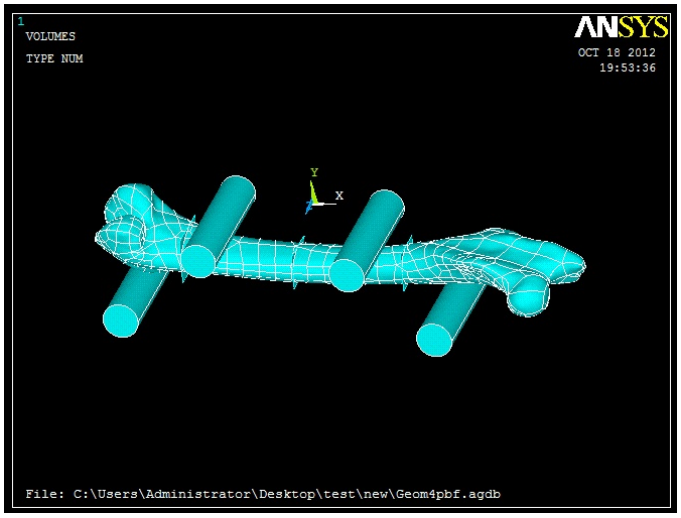


*Fig. 5.26:* Four- point bending of free specimen

### 5.2.3 ANSYS parametric study

For each case of study, the most important mechanical properties are represented by the stress distribution and the deformation of the bone beam. Those characteristics are compared between the different parametric runs, in order to verify the validity of the computational model. The first characteristic that will be tested is the dependence of the solution from the resin material. Two different materials are used. The mechanical properties of the osseus tissue are attributed to the first resin material, while the second material represents the actual material used for the experimental study of the embedded specimen.

The second parametric study concerns the position of the support and loading cylinders. In the case of the three- point bending experiment, the support cylinders will be placed in three different positions in order to identify the dependency of their position to the solution of the experimental problem. The results of the parametric study are listed below and contain the von Mises stress distribution along the bone specimen, the shear stress developed along the cross- sections of the bone, as well as the deformed shape of the bone, at the final position of the loading procedure.

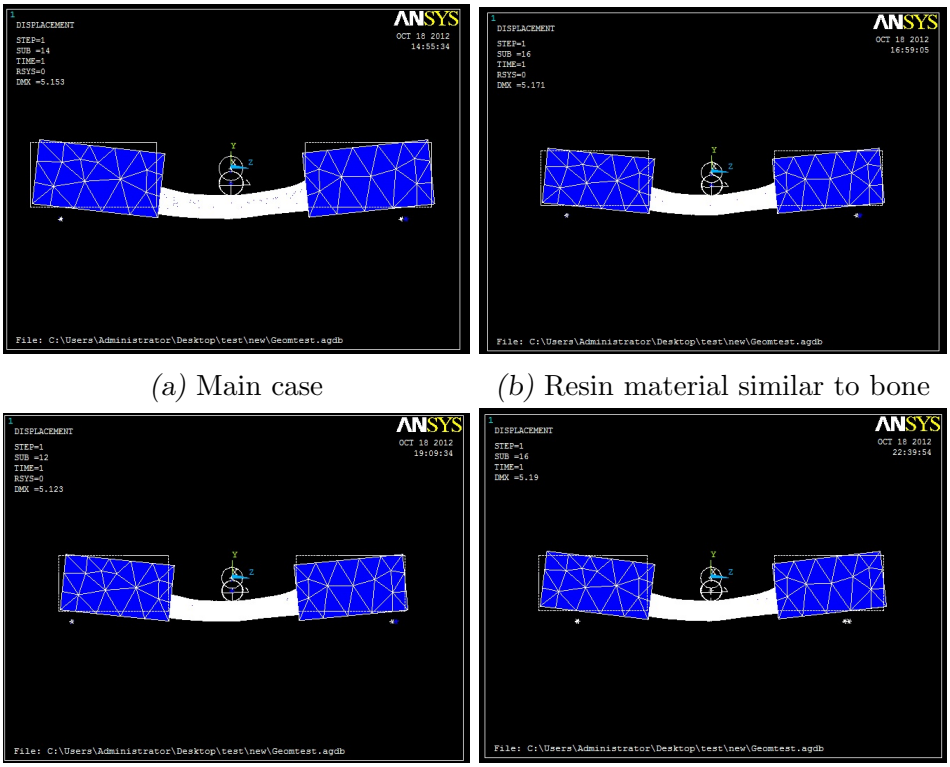


*(a)* Main case *(b)* Resin material similar to bone

*(c)* Larger distance from center *(d)* Smaller distance from center

*Fig. 5.27:* Parametric analysis: Deformation distribution

From the deformation of the beam, in the various parametric cases, significant information cannot be extracted. The curvature of the bone is almost the same for all the parametric cases and the maximum deformation does not differ significantly.

First of all, the differences between the two resin material are not distinctive. The curve of the deformation, as well as the value of the maximum deformation do not vary at a noticeable level between the two cases. This result illustrates the small effect of the resin material to the displacement of the region of interest and justifies the elimination of the bone regions within the resin regions.

The position of the support cylinders slightly affects the deformation of the beam, but important differences cannot be noticed between the different cases. A larger deviation from the central cross- section results in a restriction of the deformation and the rotation of the beam. A selection of a smaller

distance from the central cross- section results in an increment of the deformation. The maximum deformation is located at the central cross- section, where the loading is applied, for every parametric case.

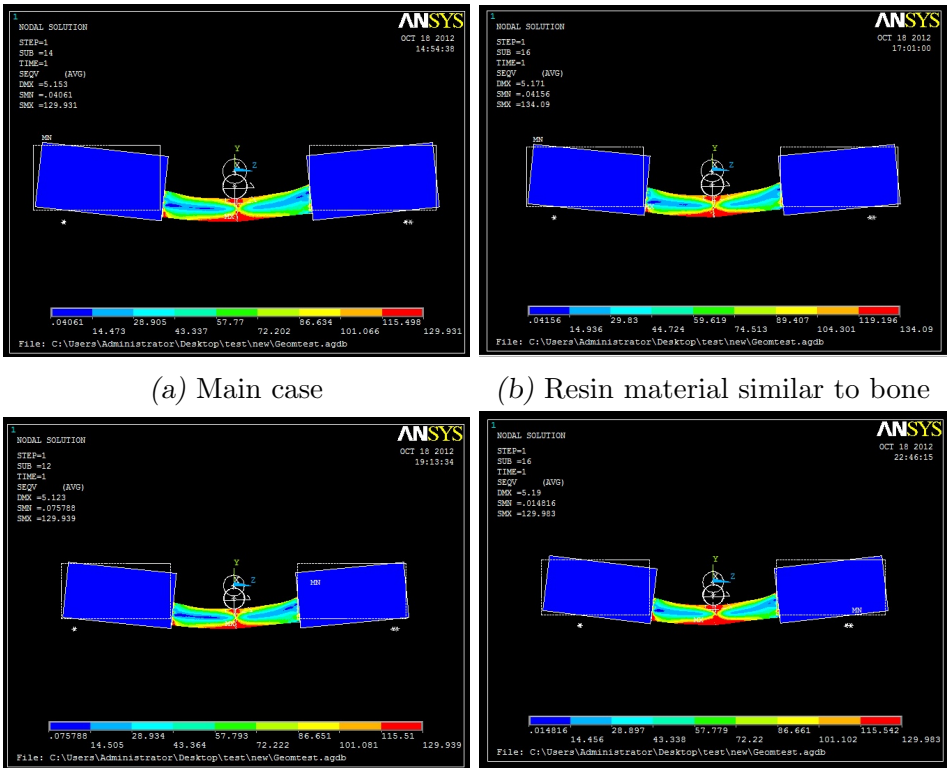


*(a)* Main case *(b)* Resin material similar to bone

*(c)* Larger distance from center *(d)* Smaller distance from center

*Fig. 5.28:* Parametric analysis: Von Mises stress distribution

As far as the stress distribution is concerned, the variation between the different cases is more distinctive. The stress distribution illustrates the regions of maximum and minimum stress. As expected, the central cross-section is the region of maximum stress for every parametric case. However, there are also several other regions where high stresses occur. For example, in the case of the actual resin material high stress occurs near the regions of contact between the bone and the resin material. Those effects are eliminated in the case where a resin material close to the bone mechanical properties is utilized. The maximum stress is higher in the later case, where the resin material's properties are similar to the bone's mechanical properties.

On the other hand, the results of the support cylinders distance from the central cross- section are negligible. The stress distribution is stable for all three cases and the maximum stress deviation is less than 0.05%, a results that illustrates the small effect of the support location from the study of the mechanical properties of the bone in the diaphysis region.

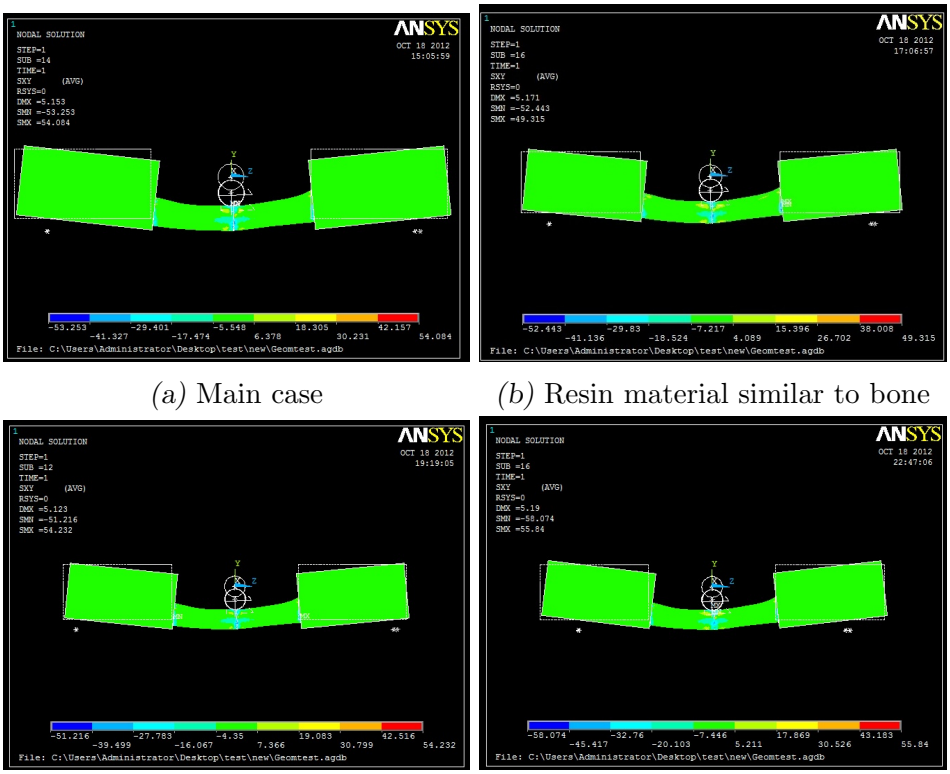


*(a)* Main case *(b)* Resin material similar to bone

*(c)* Larger distance from center *(d)* Smaller distance from center

*Fig. 5.29:* Parametric analysis: Shear stress distribution

The shear stress distribution is not highly distinctive for any case. The distribution along the bone specimen does not vary significantly at any point of the bone. However, in every case the maximum shear stress is located at the central cross- section as expected, where the famous shearing effect occurs. Important results cannot be extracted from the shear stress distribution to illustrate the differences between the studied cases.

The general conclusion of the above parametric study, is the small effect of the studied characteristics to the important mechanical properties that are

derived from the experimental procedures. The main case of study is selected to be consistent with the experimental procedure. However, important deviations do not occur between the different cases and any of those cases could be selected for the computational study of the different experimental procedures. Respectively, the meshing characteristics and the contact element factors are not significantly affecting the results of the computational study. The selected factors correspond to the optimal selection for the more rapid convergence of the computational procedure to the solution.

### 5.2.4 Experimental study

#### *Three- point bending of embedded specimen results*

The first important results concern the deformation of the beam. The first image of the results illustrates the deformation of the bone beam, from the application of $5mm$ of displacement in the central cross- section. The displacement and the rotation of the beam are also given in the following images.

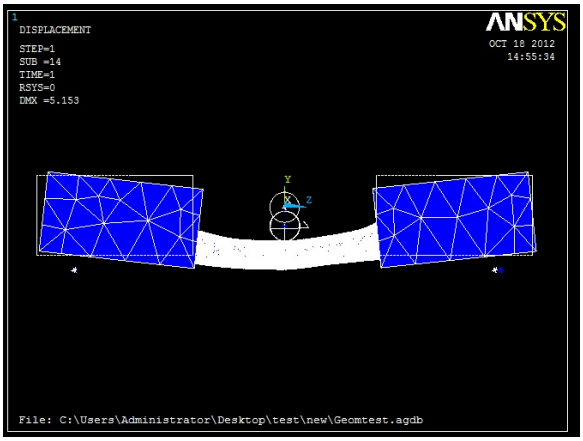


*Fig. 5.30:* Deformation occurred at the three- point bending of the embedded specimen

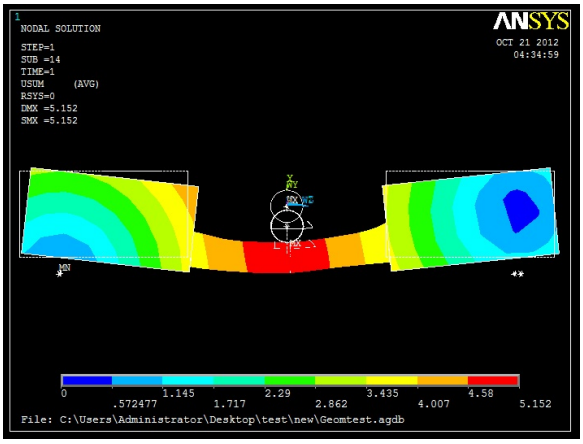


*Fig. 5.31:* Total displacement occurred at the three- point bending of the embedded specimen

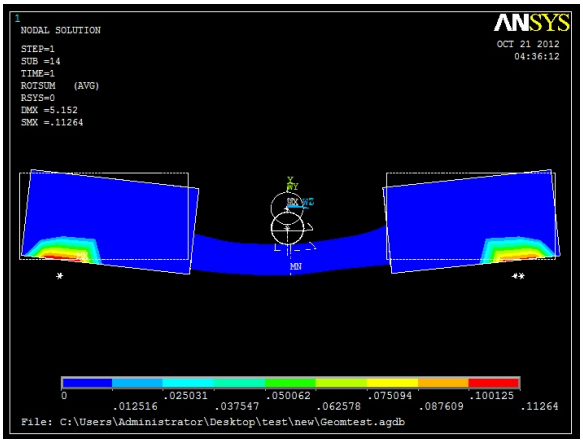


*Fig. 5.32:* Total rotation occurred at the three- point bending of the embedded specimen

Another mechanical feature of equal importance is the stress distribution along the bone beam. Different stress distributions are cited below for the case of the three- point bending procedure of the embedded specimen. The different stress distributions contain the von Mises stress, the principal stresses and the shear stresses developed in each cross- section of the specimen.

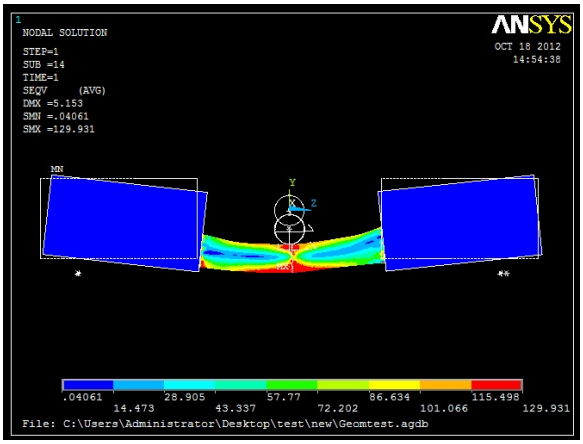


*Fig. 5.33:* Von Mises stress developed at the three- point bending of the embedded specimen

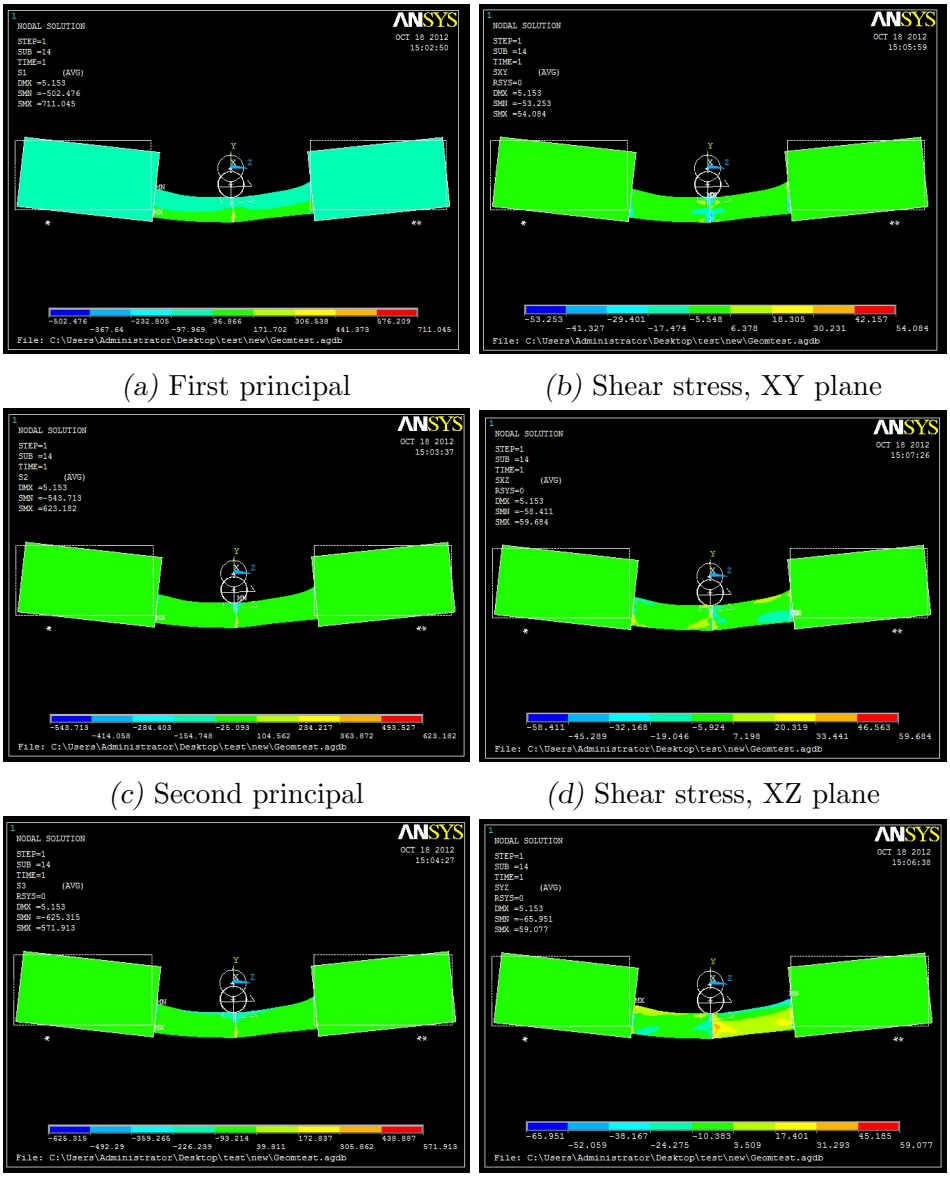


*(a)* First principal *(b)* Shear stress, XY plane

*(c)* Second principal *(d)* Shear stress, XZ plane

*(e)* Third principal *(f)* Shear stress, ZY plane

*Fig. 5.34:* Stress distribution at the three- point bending of the embedded specimen

The most important cross- section is the central cross- section, where the loading is applied. For this reason, a further study of the central cross-section is made. A more detailed distribution of the deformation and the

stress distribution is given in the images below, where the central cross-section is depicted.

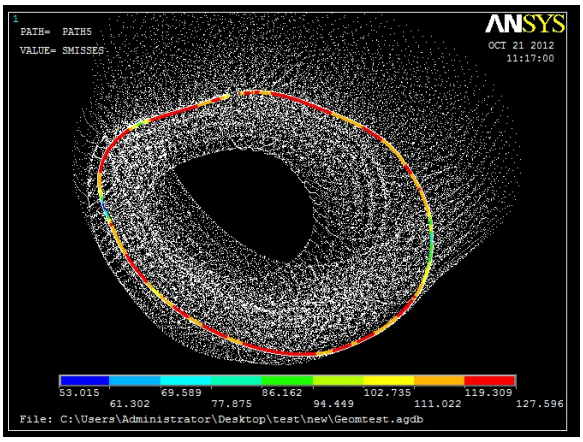


*Fig. 5.35:* Von Mises stress distribution at the central cross- section

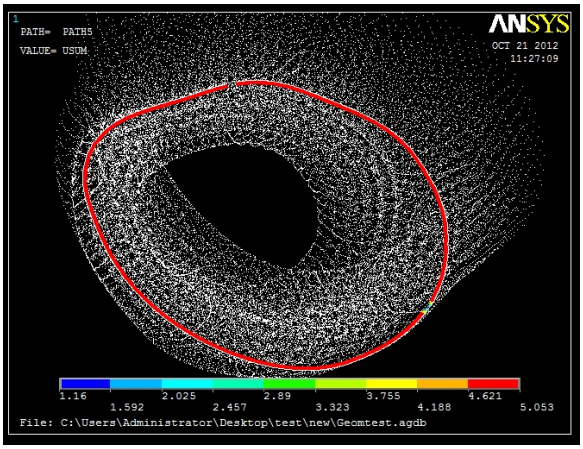


*Fig. 5.36:* Total displacement distribution at the central cross- section

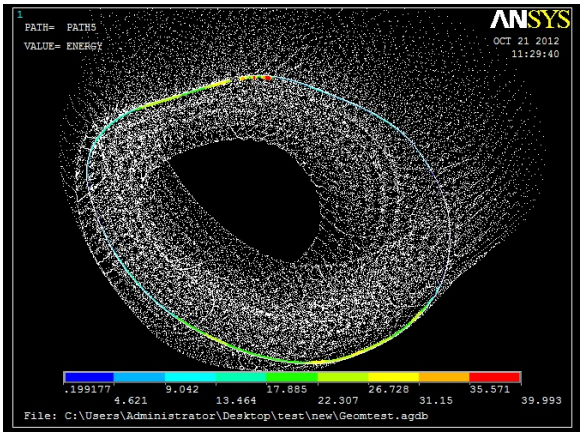


*Fig. 5.37:* Energy distribution at the central cross- section

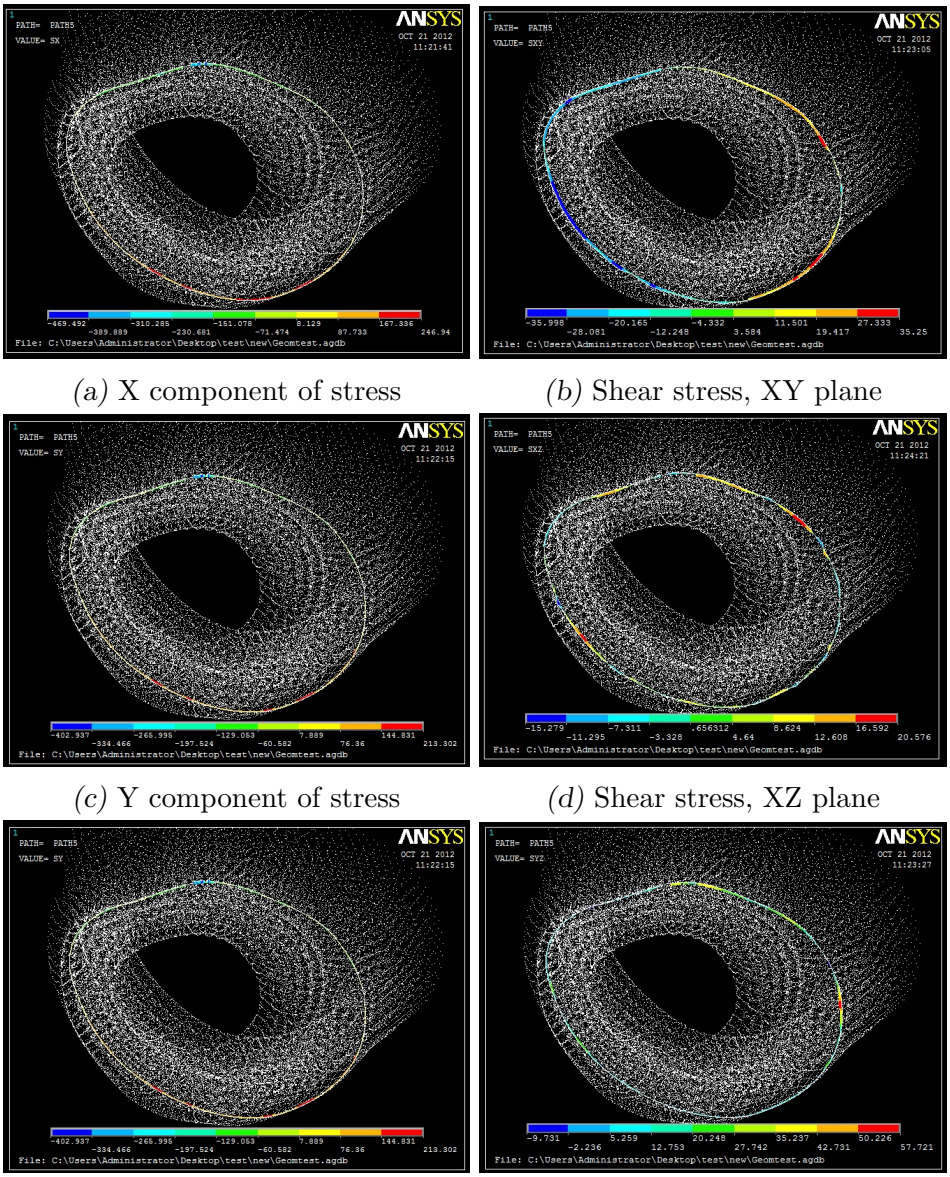


*(a)* X component of stress *(b)* Shear stress, XY plane

*(c)* Y component of stress *(d)* Shear stress, XZ plane

*(e)* Z component of stress *(f)* Shear stress, ZY plane

*Fig. 5.38:* Stress distribution at the three- point bending of the embedded specimen

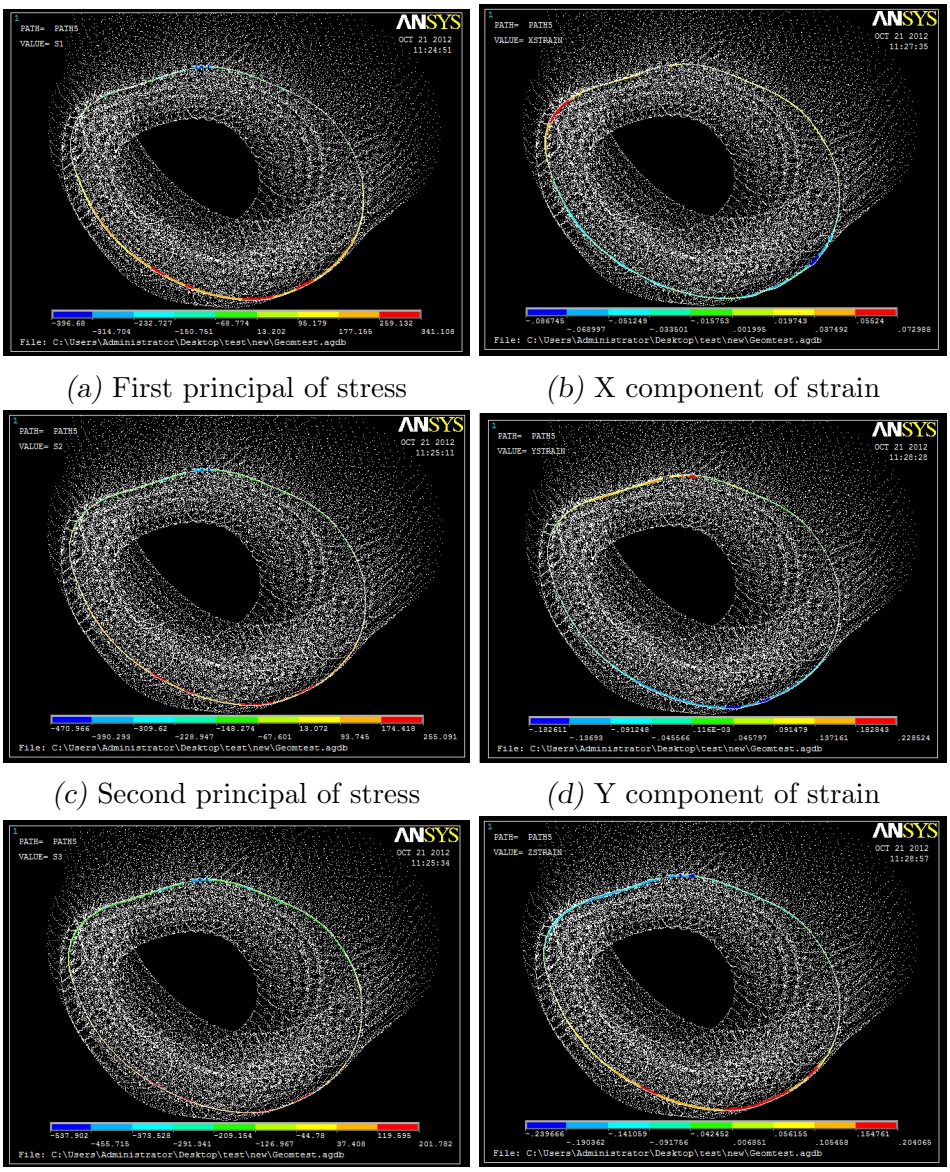


*(a)* First principal of stress *(b)* X component of strain

*(c)* Second principal of stress *(d)* Y component of strain

*(e)* Third principal of stress *(f)* Z component of strain

*Fig. 5.39:* Stress and strain distribution at the three- point bending of the embedded specimen

*Four- point bending of embedded specimen results*

The deformation of the bone beam, in the case of four point bending of the embedded specimen, is given in the next image. A displacement of $5mm$ is applied to the loading cylinders, but a fracture is observed before the total amount of the displacement is applied. The displacement and the rotation of the beam are also given in the following images.

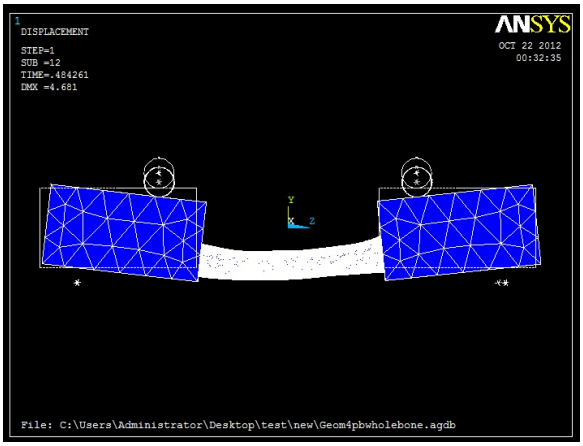


*Fig. 5.40:* Deformation occurred at the four- point bending of the embedded specimen

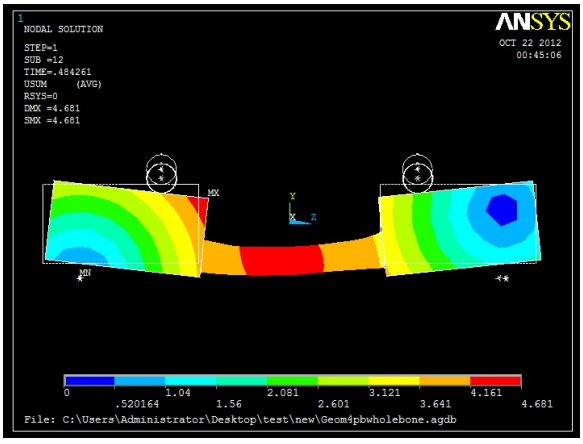


*Fig. 5.41:* Total displacement occurred at the four- point bending of the embedded specimen

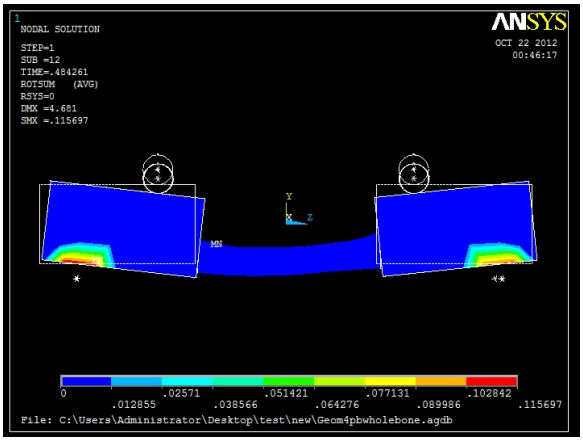


*Fig. 5.42:* Total rotation occurred at the four- point bending of the embedded specimen

The fracture is illustrated by the regions, where the von Mises equivalent stress value exceeds the ultimate stress value of the bone, as defined in the material description. Different stress distributions are cited below for the case of the four- point bending procedure of the embedded specimen. The different stress distributions contain the von Mises stress, the principal stresses and the shear stresses developed in each cross- section of the specimen. The maximum stress value is observed in the regions of the bone connection to the resin material and in the lower fiber of the bone.

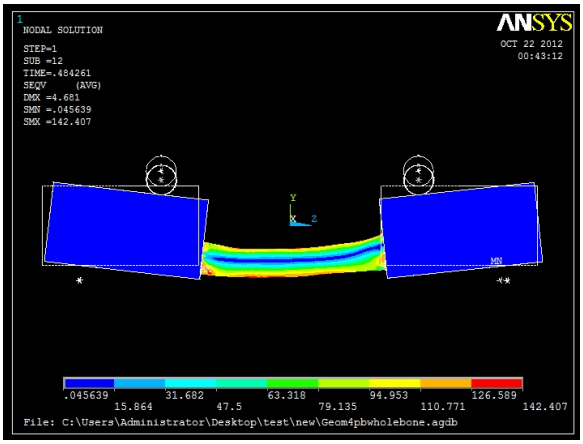


*Fig. 5.43:* Von Mises stress developed at the four- point bending of the embedded specimen

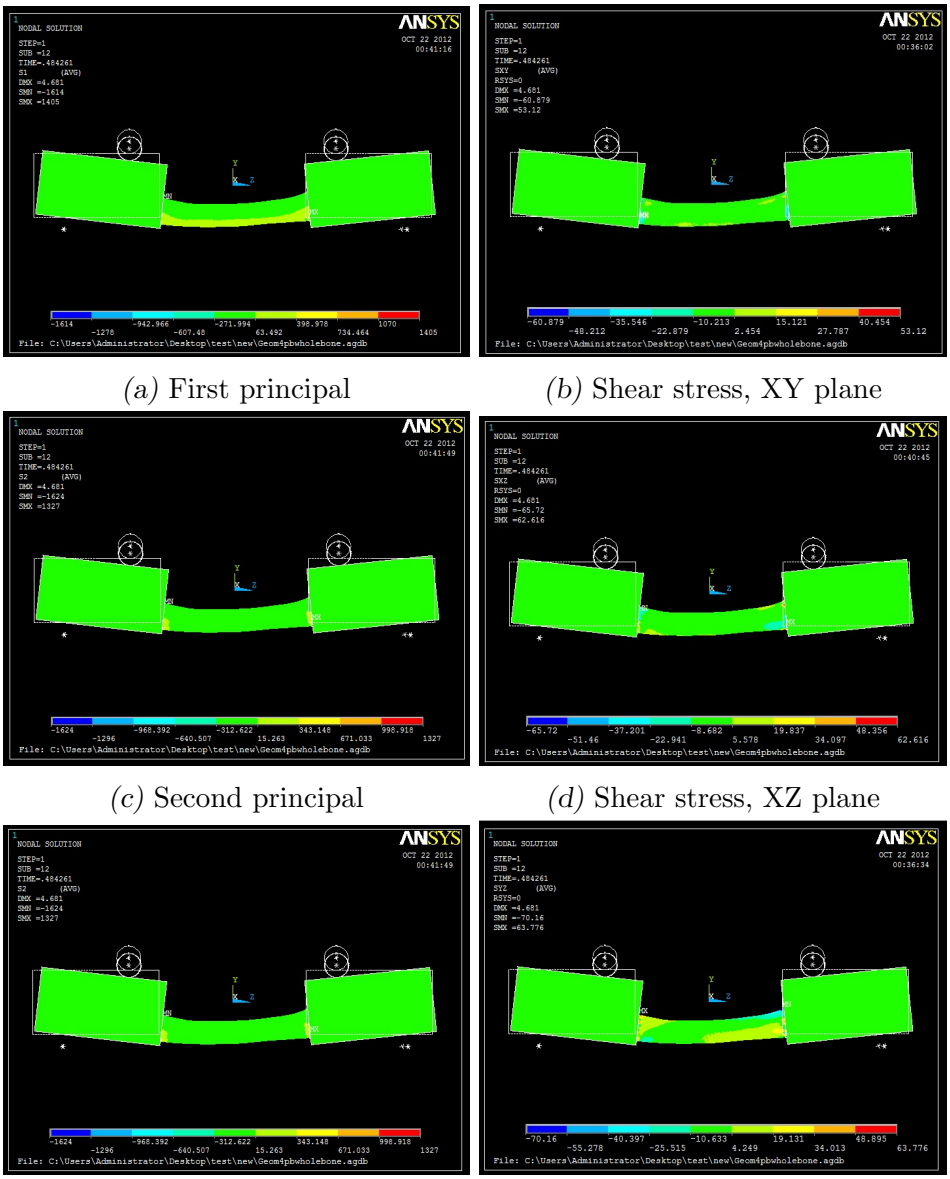


*(a)* First principal *(b)* Shear stress, XY plane

*(c)* Second principal *(d)* Shear stress, XZ plane

*(e)* Third principal *(f)* Shear stress, ZY plane

*Fig. 5.44:* Stress distribution at the four- point bending of the embedded specimen

*Three- point bending of free specimen results*

The next image illustrates the deformation of the bone beam, from the application of $1mm$ of displacement in the central cross- section. The results for the three- point bending experiment of the free specimen, concern much more smaller loading that in the case of the embedded specimen and therefore they cannot be compared.

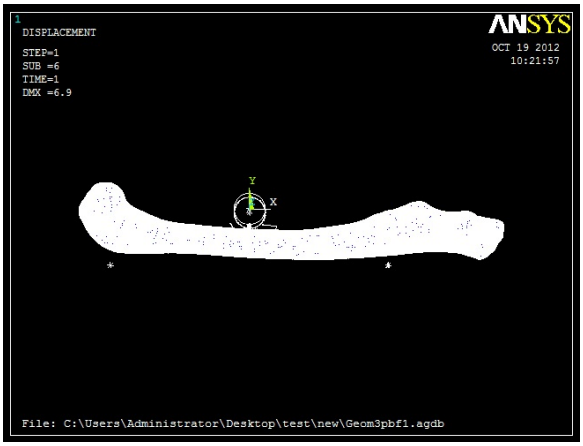


*Fig. 5.45:* Deformation occurred at the three- point bending of the free specimen

The stress distribution are also cited for the case of the three- point bending experiment of the free specimen. The different stress distributions contain the von Mises stress, the principal stresses and the shear stresses developed in each cross- section of the specimen. Due to the low loading the results of the two experimental procedures cannot be compared.

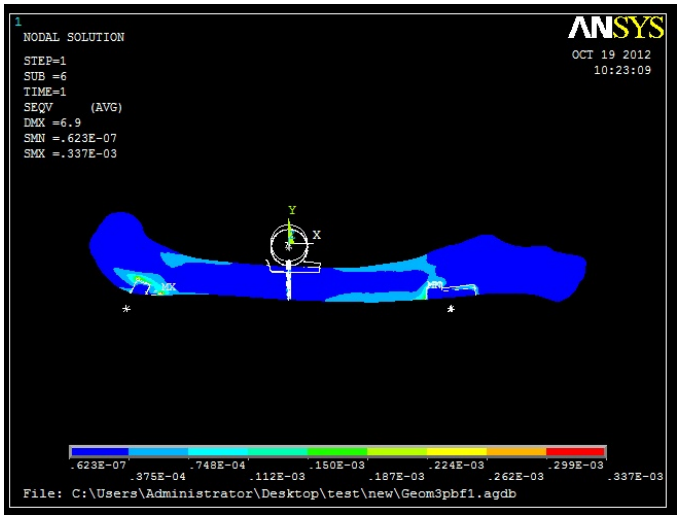


*Fig. 5.46:* Von Mises stress developed at the three- point bending of the free specimen

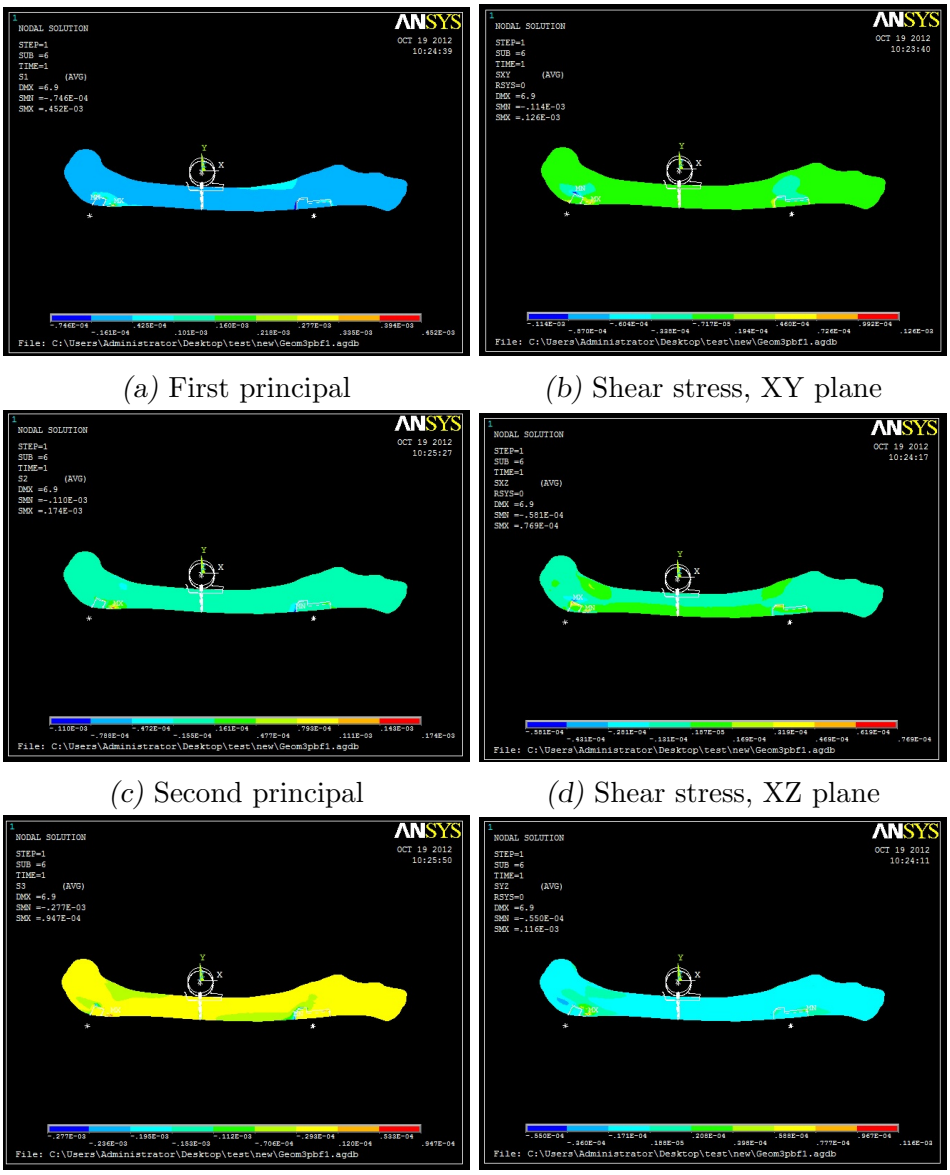


*(a)* First principal *(b)* Shear stress, XY plane

*(c)* Second principal *(d)* Shear stress, XZ plane

*(e)* Third principal *(f)* Shear stress, ZY plane

*Fig. 5.47:* Stress distribution at the three- point bending of the free specimen

For the three point bending of the free specimen two more cases are studied. In both cases a displacement of $5mm$ is applied in the central cross-section of the beam. In the first case no rotation limitations are applied

as external boundary conditions. In the second case vertical rotations are limited at the regions of contact area between the bone and the support cylinders in order to restrict the high rotation around the x- axis, which occurred during the first case of the computational simulation. The results are given below. The next images illustrates the deformation of the bone beam.

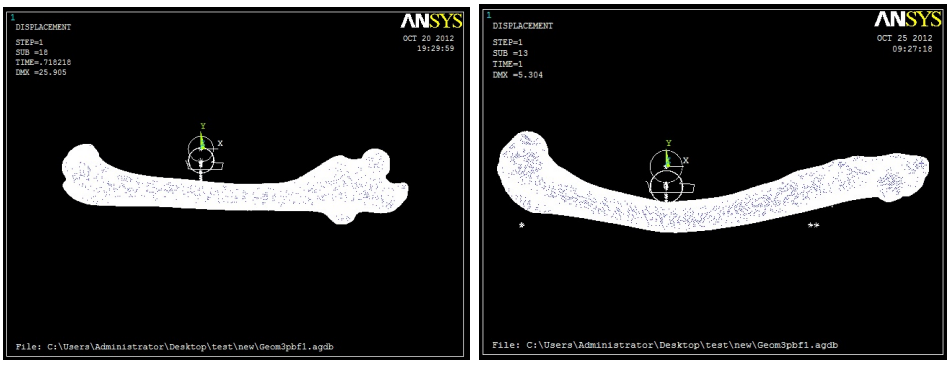


*(a)* Free specimen *(b)* Restricted rotation

*Fig. 5.48:* Deformation occurred at the three- point bending of the free specimen

The stress distribution are also cited for the two different cases of the three- point bending experiment of the free specimen. The different stress distributions contain the von Mises stress, the principal stresses and the shear stresses developed in each cross- section of the specimen. The difference of the rotation restriction is evident in the differences of the stress distribution diagram of the two cases of study.

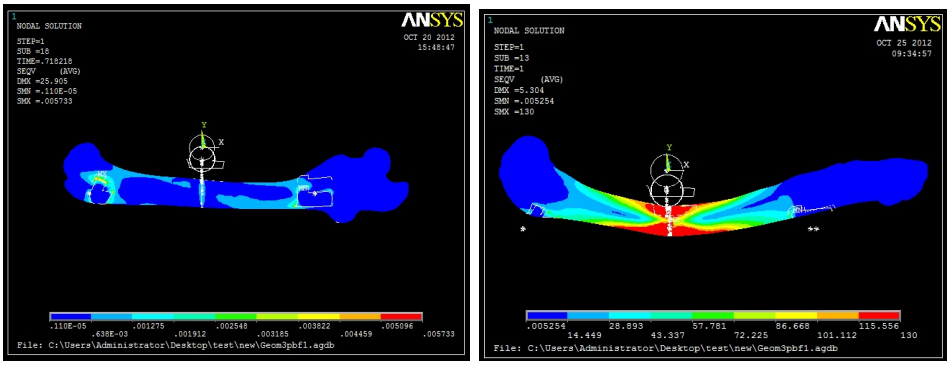


*(a)* Free specimen *(b)* Restricted rotation

*Fig. 5.49:* Von Mises stress developed at the three- point bending of the free specimen

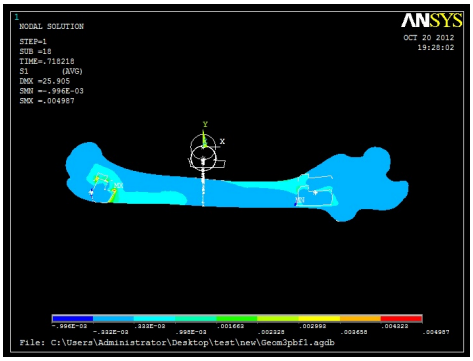


*(a)* First principal, free specimen

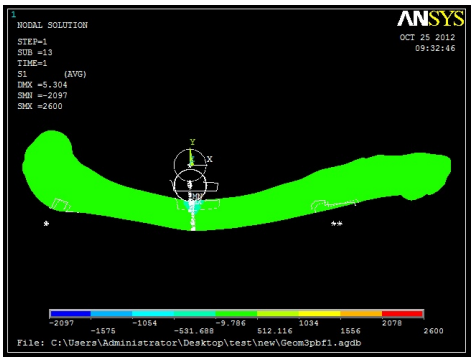


*(b)* First principal, restricted rotation

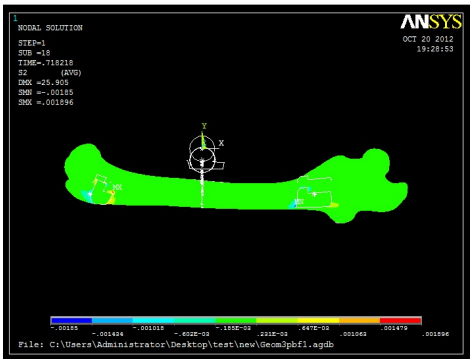


*(c)* Second principal, free specimen

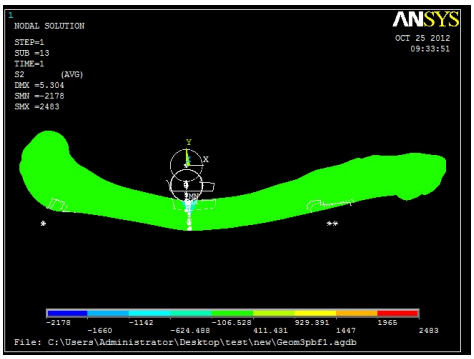


*(d)* Second principal, restricted rotation

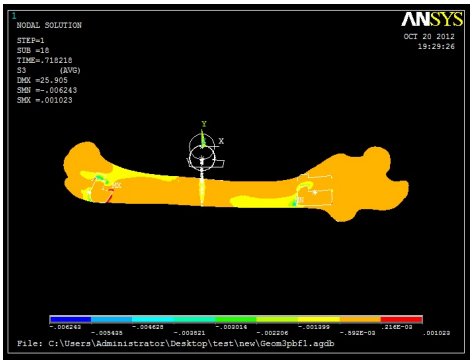


*(e)* Third principal, free specimen

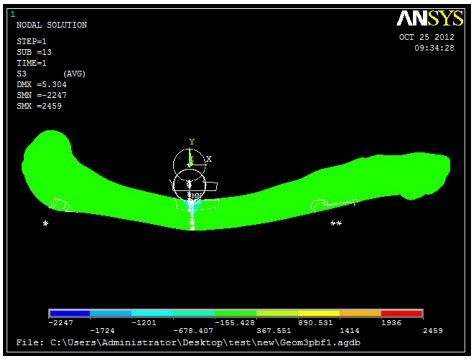


*(f)* Third principal, restricted rotation

*Fig. 5.50:* Principal stress distribution at the three- point bending of the free specimen

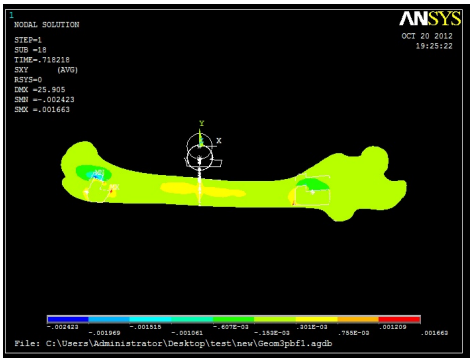


*(a)* Shear stress, XY plane, free specimen

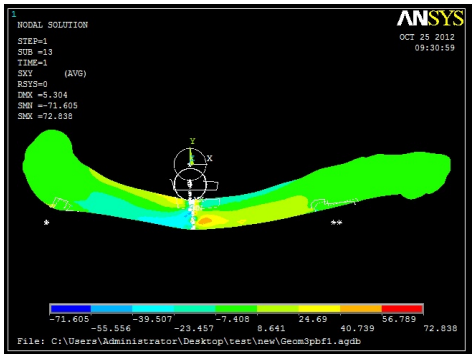


*(b)* Shear stress, XY plane, restricted rotation

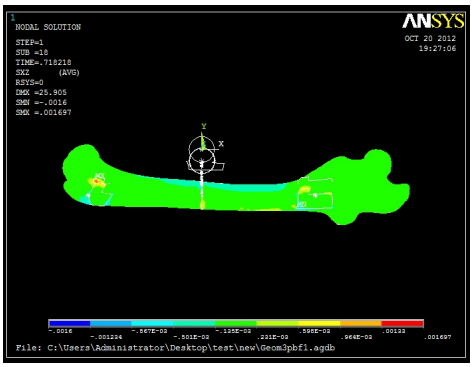


*(c)* Shear stress, XZ plane, free specimen

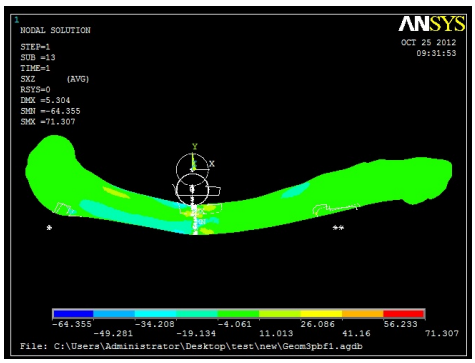


*(d)* Shear stress, XZ plane, restricted rotation

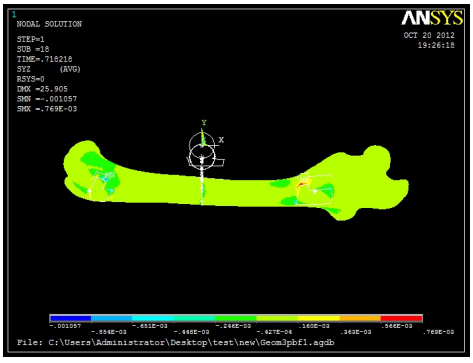


*(e)* Shear stress, ZY plane, free specimen

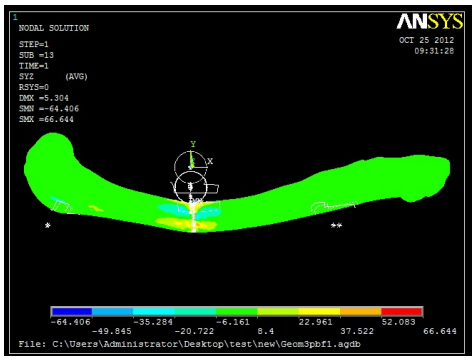


*(f)* Shear stress, ZY plane, restricted rotation

*Fig. 5.51:* Shear stress distribution at the three- point bending of the free specimen

# 6. CONCLUSIONS

The current study examines the response of a rabbit femur bone, through different loading procedures, simulating four different experimental setups of bending procedures. The most significant result of the study is the recognition of the transportation of the experimental limitations, which render the mechanical procedure difficult to be reproduced, to the computational model. The difficulties, observed during the experimental procedure, occur during the computational procedure too. At first sight, this result is negative for the generalization of the application of the computational method. However, a more meticulous study of the mentioned characteristic reveals the utility of the computational methods. The current model of a rabbit femur bone represents in fact an accurate model which can be used for further studies of mechanical response not only in bending but in other mechanical experiments too.

Through the computational procedure, a number of important problems occur. The difference from the experimental procedure, which render the computational approach significantly useful, is that those problems can be solved in their furthest extend. The computational approach gives the opportunity to deal with abnormalities, that occur during the simulations. Moreover, the solutions suggested in order to overcome the computational limitations could suggest a possible generalization to the experimental level. Since the limitations, which occur during the computational simulations, correspond to the experimental limitations, a possible solution of the first could result in the optimization of the later and an improvement of the experimental technique.

Moreover, the reproducibility of the computational method and the opportunity to simulate the same experimental procedure applied to the exact geometry, results in an opportunity of the optimization of the computational method. The improvements applied in each simulation, can be generalized in every computational model of a similar experimental simulation. The suggested solutions will also correspond to a wider category of computational

experiment. This feature of the computational methods, is the major advantage of the computational approach over the experimental procedure which lacks reproducibility and as a result cannot be easily optimized.

An important advantage of the computational method is the opportunity of post analysis of the simulation data. Important results can be extracted after the completion of the experimental simulation. For example, even though the measurements during the simulation of the experimental procedure concern merely the displacement and the developed loading, at each point of the specimen, other important information, such as the energy absorption, and stress and strain distribution along the specimen can be calculated computationally.

## 6.1 Computational improvements

Each experimental procedure has different advantages and disadvantages. From the current study, a general conclusion can be drawn: there is no optimal experimental procedure. Every case has specific limitations, that renders its application more difficult in certain situations. On the other hand, each experimental setup is superior in a different field. This is why, no optimal procedure exists. Every case should be studied by the experimental setup, which is appropriately configured to apply at the specific situation in test. However, a couple of general conclusions can be drawn for each case of study.

The material of the resin, used for the embedding of the specimen does not affect significantly the results. The displacement and stress distribution do not differ between the studied cases. However, a possible extension of the length of the resins could result in an observable effect to the solution. This is a parameter of possible further study. Respectively, the position of the support system do not affect the stress and displacement distribution either. This is the main reason for the placement of the support cylinders in the most convenient position during the experimental procedure, since the results of the central cross- section are only slightly affected, less than 1%.

In the three- point bending procedure of the free specimen, the major experimental difficulty is the rotation of the specimen, during the loading procedure. The deviation of the primal position of the specimen, causes secondary effects that cannot be easily measured experimentally and often affect the collected results. This problem causes serious inconsistencies between dif-

ferent bending experiments, that may lead to misleading results. The same problem occurs during the computational simulation. A primal rotation, however slight it is, and a possible deviation from the primal position occur during the simulation. However, the advantage of the computational method is the capability of measurement of those deviations from the primal position of the specimen. The easily identifiable variation of the specimen position in each simulation gives the opportunity of a consistent study of the procedure. The collected data correspond to the specific variation of each experiment and as a result a generalization of the mechanical results can be applied.

The major advantage of the three- point bending procedure of the free specimen is the simplicity of the experimental application and of the collection of important data. For example, the fracture point can be easily determined, since it coincides with the point of the loading application, and the deformation can be measured at the selected cross- section. The three-point bending procedure is automated to a large extent and as a result it is the mostly used experimental method with the most available experimental data to be compared and evaluated. For a determination of the ultimate strength, the three- point bending technique is currently the most commonly used and the most accurate procedure.

However, the three- point bending experimental procedure can be optimized by the embedding of the specimen, as described in the previous chapters. The embedding of the specimen offers the opportunity of a consistent method, which can be easily reproduced. The stress distribution along the specimen is stable at the region of interest, for both procedures. Consequently, the received results are consistent between the three- point bending applied in the free and the embedded specimen. A couple of restrictions should be taken into account. For example, the load intensity should be carefully chosen so that the developed moment is stable for both experimental procedures. Since the central cross- section is stable, so are the geometric properties of the specimen important for the mechanical study of the bone, such as the moment of inertia and the developed stress depends mainly on the moment developed at the diaphysis of the bone.

The disadvantage of the embedded specimen is the increment of the distance of the support and loading system from the neutral axis. This is the main reason, the procedure should be calibrated so that the developed moment should be consistent between the different experiments. The second problem is the effect of the embedding at the mechanical properties of the bone, which cannot be evaluated computationally. The embedding procedure

should be experimentally tested in order to evaluate the possible mechanical effects at the specimen, that could also affect the experimental results.

From the computational study, the variations between the free and the embedded specimen are not considered to be significantly important. Moreover, the material of the resin, used for the embedding of the specimen, does not affect the mechanical results of the experiment. Consequently, it can be assumed that around the area of interest, at the diaphysis region, the embedding regions are not affecting the independence of the mechanical results, if the mechanical characteristics of each experiment are carefully chosen. The embedding procedure can be safely applied to the experimental procedure with small influence on the results, but the features of the experimental procedure should be carefully chosen so that they retain consistency.

As far as the theoretical study is concerned, the three- point bending is difficult to be described through a complete mathematical approach. The microstructure of the bone, along with the secondary effects, which occur close to the loading region render the mathematical approach even more inaccurate. A confirmation of this observation is attributed to the punch effect, which occurs close to the loading area, at the contact area between the cylinder and the bone surface. A possible indication of the punch effect is the high deviation of the stress distribution from the symmetric distribution expected between the upper and the lower fiber at the central cross- section of the specimen. However, the punch effect cannot be easily evaluated and its contribution to the final solution cannot be quantified and eliminated.

A solution to this problem is the experimental examination of the specimen through the four point bending procedure. The advantage of the four-point bending experiment is the constant moment which is developed at the region of interest. The stability of the experimental features, allows a more generalized study that concentrates to the mechanical and geometric properties of the specimen in study.

However, the major problem of the four- point bending procedure, both in the embedded and the free specimen, is the inability of theoretical determination of the fracture point. This disadvantage is important not only for the experimental method, where the fracture point is important to be determined for the collection of the experimental results but also for the computational method, since the fracture point would also determine the cross- section from where the most important data will be stored. In the computational procedure, however, data are stored for every cross- section and the mechanical properties of the fracture cross- section are more easily

determined.

The above study cannot be considered as complete. Many supplementary parameters of the computational procedure can be tested in order to extract important information that can be utilized in the experimental procedure and improve the current methods. A more complete study, with the use of more advanced memory and storage possibilities would give the opportunity of a more in depth study of all the designed experimental setups. Many modifications can be made in the developed model in order to include more accurately the experimental details of each procedure. The advantage of the computational model is that those improvements can be easily applied in the developed model. Little modifications and improvements could lead to the development of an optimal model that would describe more accurately and consistently the experimental procedure. Numerous experimental parameter can be tested through the developed model, in order to evaluate their effect on the solution. This way, the reproducibility of the experimental procedures could be improved and the experimental data could be more consistently evaluated.

These procedure could also consist a base for a clinical application, since it is based on a non- invasive imaging technique, the CT scanning. A development of an accurate computational method that simulates with high accuracy the experimental procedure, could be applied in every geometry that would be developed through the CT scanning. The CT images could be received through a typical and simple imaging technique so that the geometry of the bane can be easily recreated and the basic mechanical properties of the bony tissue, such as bone density, can be easily measured medically. Those results could be inserted in the computational model and used for computational simulations. Through the described procedure, computational tests could result in the extraction of useful information not only for research but possibly for clinical use too and eliminate the need of experimental procedures to the basic. The current study constitutes a basis for a further study of the mechanical properties of specimen bending. The developed model could also be generalized for the application of different loading procedures or a combination of them in more complex setups.

# APPENDIX

# A. INSTRUMENTATION

The computational reproduction of the specimen's geometry and the verification of the results with the experimental data requires the utilization of a number of programs and instruments. The current study is performed under the supervision of the biomechanical laboratory of associate professor S.K. Kourkoulis, in the National Technical University of Athens. The majority of the computational programs utilized through this study, such as Solid Works and ANSYS, have been provided by the biomechanical laboratory of S.K. Kourkoulis, in the National Technical University of Athens.

The current study is performed in the framework of the experimental study of rabbit femur bones, subjected under bending experiments, carried out by the biomedical engineering company "BioHexagon", by Dr E.A. Magnissalis. The first phase of the model development requires the CT scanning of the specimen, which has been realized by "BioHexagon" company. In addition, the $3D$- DOCTOR program for the CT- images processing has also been provided by "BioHexagon" company. The experimental study evaluation also requires the measurement of the specimen, as well as the photo sampling of the specimen. The procedure of experimental verification of the model, performed through the mentioned processes, was carried out in collaboration with the "BioHexagon" company. The camera and the microscope instruments for the specimen study has been provided by "BioHexagon" company.

In detail, a list of the instruments and programs used, throughout the current study, is outlined below.

- **Digital Camera NIKON Coolpix** 5400, provided by "BioHexagon" company, used for still picture and video capture, during biomechanical testing and microscope application.
- **3D- DOCTOR**, developed by Able Software Corp., provided by "BioHexagon" company, is an advanced 3D image rendering, processing, and analysis software. $3D$- DOCTOR was developed to provide a

complete set of tools for visualizing 3D volume image data, such as Computed Tomography data (CT).

- **Solid Works**, Office Premium 2010 × 64 Edition, developed by Dassault Systemes S.A., provided by National Technical University of Athens, is a $3D$ CAD Design software developed for the simulation of mechanical systems and applications.
- **ANSYS 2012**, release 12.0.1, provided by National Technical University of Athens, is a simulation software developed for the simulation of structural aspect of mechanical products.

# BIBLIOGRAPHY


[1] Henry Gray, *Anatomy of the human body*, Longmans, Green and Co. Ltd., 1968

[2] Matthew Landrigan, Charles Penninger, Marissa J. Post, *Experimental and computational investigations in bone structure and adaptation*, Multi-Scale Modeling, Fall 2006

[3] Michael Locke, *Structure of Long Bones in Mammals*, Department of Biology, University of Western Ontario, Canada

[4] Αναστασόπουλος Θ. Γεώργιος, *Μεθοδολογίες ελέγχου δομικής ακεραιότητας σπογγώδων οστών*, Διδακτορική διατριβή, Τμήμα Μηχανολόγων Μηχανικών και Αεροναυπηγών, Εργαστήριο στοιχείων μηχανών, Πάτρα 2008

[5] Δήμητρα- Αγγελική Βαβλαδέλη, *Ανάλυση του σπογγώδους οστού για μεγάλες παραμορφώσεις*, Διπλωματική εργασία, Τμήμα Εφαρμοσμένων Μαθηματικών και Φυσικών Επιστημών, Εθνικό Μετσόβιο Πολυτεχνείο, Αθήνα 2011

[6] S. Timoshenko and J.N. Goodier, *Theory of elasticity*, McGraw-Hill book company Inc.New York, Toronto, London 1951

[7] Yuehuei H. An, M.D. Robert A. Draughn, *Mechanical Testing of Bone and the Bone, Implant Interface*, D.Sc. CRC PRESS, United states of America 2000

[8] Uemuet Goerguelue, *The difference between Euler-Bernoulli and Timoschenko*,

[9] M. Huurman and A.C. Pronk, *Theoretical Analysis of the 4 point bend test*, Deft University of Technology, Netherlands, 2009

[10] Reinhold G. Erben, *Embedding of Bone Samples in Methylmethacrylate: An Improved Method Suitable for Bone Histomorphometry, Histochemistry, and Immunohistochemistry*, Institute of Physiology, Physiological Chemistry, and Animal Nutrition, University of Munich, Munich, Germany, 1997

[11] Adela Hervas Garcia, Miguel Angel Martinez Lozano, Jose Cabanes Vila, Amaya Barjau Escribano, Pablo Fos Galve, *Composite resins. A review of the materials and clinical indications*, Lecturers in Dental Pathology and Therapeutics, Cardenal Herrera-CEU University, Moncada, Valencia

[12] T. A. Stolarski, Y. Nakasone and S. Yoshimoto , *Engineering Analysis With ANSYS Software*, MPG Books Ltd., Bodmin, Cornwall 2006

[13] Saeed Moaveni, *Finite element analysis, theory and application with ANSYS*, Minnesota State University, Mankato Prentice Hall, Upper Saddle River, New Jersey 1999

[14] Terry Peters *CT Image Reconstruction*, Robarts Research Institute, London, Canada

[15] Wilbur L. Reddinger, *CT Instrumentation and Physics*, OutSource, Inc., 1997

[16] Sergey Bezryadin, Pavel Bourov, Dmitry Ilinih, *Brightness Calculation in Digital Image Processing*, KWE Int.Inc., San Francisco, CA, USA; UniqueIC"s, Saratov, Russia

[17] Johan Sunnegardh *Combining Analytical and Iterative Reconstruction in Helical Cone-Beam CT*, Department of Electrical Engineering, Linkopings universitet, Sweden, Linkoping, February 2007

[18] Ανδρέας Γ. Μπουντουβής, *Υπολογιστική Ανάλυση με την μέθοδο των πεπερασμένων στοιχείων, Εισαγωγικές σημειώσεις*, Αθήνα 1992